

**Design and Implementation of On-board
Electrical Power Supply of Student Nanosatellite
OUFTI-1 of University of Liège.**

Pierre THIRION

Thesis submitted in partial fulfillment of the requirements for the degree of

Master in Electrical Engineering

at the Applied Science Faculty of the University of Liège.

Advisor: Prof. Jacques Verly
Industrial advisor: Alain Gruwé and Grégory Dewilde (Thales)

Academic Year 2008-2009

Acknowledgements

I want to thank the Professor Jacques Verly for launching this wonderful project and his support to the whole team.

I also thank Gregory Dewilde, Alain Gruw  , my industrial supervisors at Thales Alenia Space of Mont sur Marchienne, for all their advices, and giving me the opportunity to work in an industrial environment.

I wish to thank the monitoring students, Amandine Denis and Jonathan Pisane, for the time they devoted to manage the team, and also to Luc Hallbach for his help and advice to the team.

Thanks to all the students I had the pleasure to work with during this project for their useful cooperation and for the good time we had together.

I finally thank my parents, for their continuous support during my thesis and throughout whole studies.

Pierre Thirion



Abstract

OUFTI-1 is a picosatellite developed by students at the University of Liège (ULg). The goal of the OUFTI project is to provide a hands-on satellite experience to students. The subject of the present thesis is the design and implementation of the electrical power system (EPS) of OUFTI-1. The EPS role is to supply other systems of the satellite with appropriate electrical power. First, the requirements of the EPS are defined. The architecture of the EPS is then designed. When the architecture is known, we verify that the consumed power on board does not exceed the produced power. The electrical design of the different modules of the EPS is carried out. Finally, the prototypes of the EPS are presented.

Keywords: OUFTI-1, CubeSat, LEODIUM, Electrical power system.

Contents

1	Introduction	9
1.1	Cubesat Concept	9
1.2	Mission Objectives of OUFTI-1	9
1.2.1	D-STAR	10
1.2.2	The Experimental Electrical Power System (EPS2)	10
1.2.3	New generation solar cells	10
1.3	Role of Electrical Power System	10
2	Requirements of the EPS	12
2.1	Introduction	12
2.2	Constraints	13
2.2.1	Space Environment	13
2.2.2	Launch	15
2.2.3	Mechanical architecture of OUFTI-1	16
2.3	Functionalities	17
2.3.1	Power source	17
2.3.2	Power storage	17
2.3.3	Power conditionning	18
2.3.4	Housekeeping parameters	19
2.3.5	Antennas Deployment System	19
3	Design of EPS architecture	20
3.1	Introduction	20
3.2	Solar Cells	20
3.2.1	Theory	20
3.2.2	Azurspace's solar cells	22

3.2.3	Simple model	23
3.2.4	Matlab model	24
3.2.5	Solar panels	25
3.3	Batteries	29
3.3.1	Technology	29
3.3.2	Architecture	29
3.3.3	Capacity	30
3.3.4	Redundancy	31
3.3.5	KOKAM batteries	31
3.4	Battery protection circuits	34
3.4.1	Electrical characteristic	34
3.4.2	Over charge protection (i.e. over-voltage protection)	35
3.4.3	Over discharge protection (i.e. under-voltage protection)	35
3.4.4	Over current protection	35
3.5	Dissipation system (Shunt regulator)	36
3.6	Battery heater	36
3.6.1	Control	36
3.6.2	Supply voltage	37
3.7	USB battery charger	37
3.8	Power conditioning unit	38
3.9	Protection circuits	38
3.10	Measurement system (Housekeeping parameters measurements)	38
3.11	Antennas deployment circuit	39
3.12	About the experimental EPS	39
4	The Power Budget	40
4.1	Introduction	40
4.2	Estimation of input power	40
4.3	Estimation of consumed power	41
4.3.1	Operation modes of subsystems and corresponding power needs	42
4.3.2	Efficiency of converters	44
4.4	Discussion	44
4.4.1	Cold case	44

4.4.2	Mean case	45
4.4.3	Hot case	46
5	Electrical Design of EPS	48
5.1	Introduction	48
5.2	Design of Converters	48
5.2.1	Theory	48
5.2.2	Design of 7.2V converter	56
5.2.3	Design of 5V converter	61
5.2.4	Design of 3.3V converter	65
5.2.5	Remarks	68
5.3	Design of input filters	70
5.3.1	Type of filter	70
5.3.2	Stability problem	70
5.3.3	Middlebrook's criterion	71
5.3.4	Comparison between Middlebrook's criterion ($Z_D(s)$ and $Z_N(s)$) and measured $Z_{in}(s)$	72
5.3.5	Measurements of the input impedance of the converters	73
5.3.6	Frequency design of the filters	76
5.4	Design of the dissipation system (shunt regulator)	78
5.4.1	Choice of Design	78
5.4.2	First version	79
5.4.3	Second version	80
5.4.4	Components design	81
5.5	Design of the protection circuits	83
5.5.1	Description	83
5.5.2	Components	83
5.6	Design of the antennas deployment circuit	84
5.6.1	Functionality	84
5.6.2	Implementation	84
5.6.3	Location	85
5.6.4	Components	85
5.7	Design of the battery heater	86
5.7.1	Control by the OBC	86

5.7.2	Independent control	86
5.8	Design of the measurement system	88
5.9	Components selection	89
5.9.1	Formats	89
5.9.2	Capacitors	89
5.9.3	Dielectric	89
5.9.4	Rated voltage	90
5.9.5	Bending strength	90
5.10	Schematics of the EPS	90
6	Prototypes of the EPS	91
6.1	Introduction	91
6.2	The breadboards model	91
6.2.1	The second dissipation system	92
6.2.2	The protection circuit	92
6.3	The engineering model	93
6.3.1	Included systems and interfaces	93
6.3.2	Implementation	95
6.3.3	Tests	96
7	Miscellaneous activities, presentations and publications	97
7.1	Publications	97
7.2	Presentations	97
7.3	Activities	98
8	Conclusions	99
8.1	Accomplished work	99
8.1.1	Architecture	99
8.1.2	Design	100
8.1.3	Implementation and tests	100
8.2	Future work	100
A	Matlab code for the I-V curves of solar panels	103

B Power budget worksheet	106
C Pictures of the prototypes	110
D Schematics of the engineering model of the EPS	112

Chapter 1

Introduction

1.1 Cubesat Concept

A CubeSat is a picosatellite with standardized dimension and weight. It is a small cube of 10cm x 10cm x10 cm. The mass must be inferior to 1kg. The commonly used slogan for CubeSats is "One litter, one kilogram, one watt". The standard has been developed in the U.S.A. by California Polytechnic State University, San Luis Obispo, L.A., and Stanford University's Space Systems Development Lab, Stanford, L.A.

The concept provides a low-cost and reliable way to send payloads in orbit and opens an access to space for universities and private companies. Dozens of universities and high schools are participating in the CubeSat program. Resources and information are shared within the community, through direct communication between developers and through CubeSat workshops.

The educational benefits are huge. Students have the opportunity to develop skill and experience in real space applications.

The features provided by the CubeSat program are [11]:

- A standard physical layout and design guidelines.
- A standard, flight-proven deployment system (P-POD).
- Coordination of required documents and export licenses.
- Integration and acceptance testing facilities with formalized schedules.
- Shipment of flight hardware to the launch site and integration to launch vehicle.
- Confirmation of successful deployment and telemetry information.

1.2 Mission Objectives of OUFTI-1

OUFTI-1 is developed at the University of Liège (ULg) and is the first Belgian picosatellite. The goal of the OUFTI project is to provide a hands-on satellite experience to students. The

design and the tests are delegated to students. OUFTI may be interpreted as for Orbital Utility For Telecommunication Innovation. It is also a typical interjection from Liege related to astonishment. OUFTI-1 will carry several innovative equipments.

1.2.1 D-STAR

The main mission of OUFTI-1 is to test the use of D-STAR in space. D-STAR is a new communication protocol. It has been developed by the Japanese amateur-radio league (JARL) for the ham-radio community. It can be used on UHF, VHF, and microwave amateur-radio bands. D-STAR is a fully digital protocol. It allows simultaneous data and voice transmission. It also specifies a network connection method. With D-STAR, a user can contact another user within range. He also can pass through a D-STAR repeater station and contact a user in the range of the station. Some D-STAR repeaters also have an access to the internet. A user can thus "enter" in the network through a repeater, and contact a user who is in the range of another relay station.

OUFTI-1 will be the first picosatellite to use the D-STAR protocol in space. The satellite will act as an extension of the D-STAR repeater of the University of Liège (ON0ULG).

1.2.2 The Experimental Electrical Power System (EPS2)

OUFTI-1 will also test an Experimental Electrical Power System, developed in cooperation with Thales Alenia Space ETCA. The Experimental EPS is a digitally-controlled flyback converter. This system will be redundant with a function of the main Electrical Power System (EPS). The Experimental EPS will provide a 3.3V power output for other electrical systems.

1.2.3 New generation solar cells

The satellite will be equipped with last-generation triple-junction solar cells from AzurSpace with an efficiency of 30%.

1.3 Role of Electrical Power System

The primary role of the Electrical Power System (EPS), which is the subject of this report, is to supply other systems of the CubeSat with appropriate electrical power.

This power is collected from the solar panels. Solar cells produce power when they are exposed to direct solar radiations or to indirect radiations from albedo.

In orbit, the satellite regularly passes through the shadow of the earth. There, the radiations caught by the solar cells are not sufficient to generate enough electrical power. Furthermore, even in daylight, D-STAR communications may need more power than the output of the solar panels. The EPS thus needs batteries to store enough energy for the eclipses and peak demands.

The collected and stored power must then be distributed to other systems. On OUFTI-1,

subsystems must be supplied with 3.3V, 5V, and/or 7.2V. The EPS has a power conditioning unit, able to deliver the required amount of electrical power at these voltages.

The EPS secondary functions.

Some important voltages, currents, and temperatures (they are called the "Housekeeping Parameters") are measured, scaled, converted from analogical to digital, and transferred to an I^2C bus. The EPS gathers measurements of its own parameters, but also the temperature of the external faces of the CubeSat.

The switches controlling the current for the antenna's deployment are on the EPS.

Heavy radiations can cause "single event latch-up" in the semiconductor devices on the satellite. This can burn the component if the power is not turned off quickly enough. Protecting the power outputs against over-currents was initially one of the secondary functions of the EPS. The choice has been made to place such protection circuits on other cards, on the power input of each system. So, the power can be turned on and off for each system independently.

In short, the primary functions of the EPS are:

- Power source
- Power storage
- Power conditioning and distribution.

The secondary functions of the EPS are:

- Telemetry measurements and conditioning
- Power control of the antenna's deployment system
- Over-current protection (located on user's cards).

Chapter 2

Requirements of the EPS

2.1 Introduction

The first step before beginning the design of the EPS is to know exactly what our goals and our constraints are. This is the subject of this chapter.

There are constraints due to space environment. The EPS must withstand vacuum and wide ranges of temperatures and radiations. There are constraints linked to the launch, like accelerations, vibrations, and rules for the CubeSats in the Vega launch vehicle. Finally, there are constraints due to the construction of OUFTI-1. The dimensions of the electronic cards and available volumes are specified.

The desired functionalities also guide the design. The EPS must produce enough energy to supply the CubeSat. Enough energy has to be stored to supply the satellite during the period of eclipse. The EPS must provide several power outputs with stabilized voltages.

The constraints will also guide the validation tests applied to the prototypes. Most of electrical and temperature tests were done on the engineering model this year. Batteries were tested under vacuum. Complete vibration tests and maybe radiation tests will be carried out next year.

Most functionalities and constraints were known as soon as the project started. But there were also functionalities and constraints that came from an iterative work. From the first requirements, design choices were made. These choices brought new constraints and a new iteration began. At each development step, interaction with other teams also had a huge influence on the design and requirements. Reporting here all iterations and each new development would lead to write a long document. As a consequence, this report is most of time focused on the last iteration in the development process.

2.2 Constraints

2.2.1 Space Environment

Vacuum

The satellite is expected to be released in an elliptical orbit with an altitude between 350 and 1,200km [4]. At such altitudes, the atmosphere pressure can be neglected and considered as vacuum. Therefore, all components used in the satellite must withstand vacuum. The two threats of vacuum are:

- Deformations due to mechanical constraint of vacuum
- Out gassing.

The most sensitive component of the EPS is the batteries.

Radiations

Charged particles of solar wind, electrons, and protons, are captured by the earth magnetic field. They form the radiations belts, also known as the Van-Allen belts. There are two belts:

- The inner belt, between 1,000 and 15,000 km, containing high concentrations of energetic protons with energies exceeding 100 MeV and electrons in the range of hundreds of keV.
- The outer belt, extending till 50,000km, and consisting mainly of high energy electrons (from 0.1 to 10 MeV).

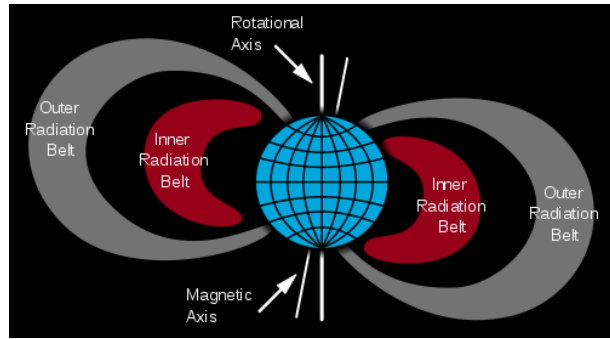


Figure 2.1: Van Allen Belts.

The apogee of OUFTI-1 is in the inner belt.

Spacecrafts need to be protected against radiations, especially if they go through the radiation belts. Trapped particles in the radiation belts and cosmic rays can cause “Single Event Phenomena” (SEP) within semiconductor devices. There are three different types of SEP:

- The Single-Event Upset (SEU)

This is when a high energy particle hits a logic device and changes digitally stored data or causes a gate to open or close at the wrong time.

- The Single-Event Latch up (SEL)

The SEL is when a high energy particle directly damages the device. It can, however, be corrected if the SEL is detected and the power to the device quickly turned off, then turned back on.

- The Single-Event Burnout (SEB)

This is the case where the device is destroyed.

The radiation dose is estimated to more than $10^5[\text{rad}]$. A protection against SEL can be provided to the subsystems with current-limiter circuits. There is no particular protection against SEU and SEB except reducing the effect of the radiations inside the satellite with a layer of shielding aluminium (less than $2.10^4[\text{rad}]$ with 2mm of aluminium) [6]. There are components designed and/or tested to be more resistant to radiations. Such components should be used in the more critical systems of the EPS.

Temperatures

The temperatures in space, when the satellite is turned on, will essentially depend of the thermal design. The temperature ranges are not the same everywhere in the satellite. Thermal simulations give an idea of the temperature at different points of the CubeSat. Following the latest simulations [7], the external temperature will vary the most (from -33°C to $+40^\circ\text{C}$), the temperature of the EPS card will stay between -22°C and $+37^\circ\text{C}$, and the temperature of batteries card between -22°C and $+37^\circ\text{C}$. The EPS must thus be able to work within these ranges.

- Solar cells must be selected so that they are able to work in the predicted range of -33°C to $+40^\circ\text{C}$.
- The electronics on the EPS card must be designed to be able to operate from -22°C to $+37^\circ\text{C}$ (PCB T°). Wider ranges were given by the first simulations. We decided to use components with an operating temperature range of at least -40°C to $+85^\circ\text{C}$ as "absolute maximum rating". The temperature tests have been done at -30°C and $+70^\circ\text{C}$.
- Lithium-Polymer batteries can withstand 0 to $+45^\circ\text{C}$ during charge and -20 to $+60^\circ\text{C}$ during discharge (but with a significant loss of capacity under 0°C) [20]. A solution must be found to maintain the batteries card in these ranges of temperature.

2.2.2 Launch

Vibrations and accelerations

The payload of Vega will be subjected to vibrations during the launch. The maximum amplitude and the frequency of the vibrations at the base of the launcher are characterized in figure 2.2.

DIRECTION	LONGITUDINAL		LATERAL	
Frequency Band (Hz)	5 - 45	45 - 100	5 - 25	25 - 100
Sine Amplitude (g)	≤ 0.8	≤ 1.0	≤ 0.8	≤ 0.5

Figure 2.2: Sine excitation at spacecraft base [14].

The effects of acceleration during launch are not to be underestimated. The payload of Vega has to be able to withstand an acceleration of 15g [14], even if it will probably be lower in reality.

Special attention must be paid to the fixation of heavy components. Also, components could be damaged by the bending of the PCB under vibrations and accelerations. Automotive components will be chosen whenever possible.

Temperatures

The launch vehicle will pass through several atmospheric layers with specific temperatures. Inside Vega LV, the CubeSat will endure temperatures of -40°C to 80° during launch [13]. Components of the EPS have to be able to withstand such temperatures during storage (the CubeSat is inactive during launch). Components with a working temperature range of -40°C to 85°C should not have any problems.

The batteries are still the most sensible component. Their storage temperature should stay between -20°C and 60°C [20]. A passive solution must be found to protect them during launch. Thermal insulation and thermal inertia will certainly help.

Regulations for CubeSats

Following articles are extracted from the document "CubeSat Design Specifications" [12]:

3.3.1 No electronics shall be active during launch to prevent any electrical or RF interference with the launch vehicle and primary payloads. CubeSats with rechargeable batteries shall be fully deactivated during launch or launched with discharged batteries.

3.3.2 One deployment switch is required (two are recommended) for each CubeSat. The deployment switch should be located at designated points (Appendix A).

3.3.5 A remove before flight (RBF) pin is required to deactivate the CubeSats during integration outside the P-POD. The pin will be removed once the CubeSats are integrated into

the P-POD. RBF pins must fit within the designated data ports (Appendix A). RBF pins should not protrude more than 6.5 mm from the rails when fully inserted.

2.2.3 Mechanical architecture of OUFTI-1

We use the CubeSat kit developed by Pumpkin (figure 2.3). It includes the structure and the FM430 flight module (OBC1). The subsystems cards must be compatible with these components. There are five subsystems cards (figure 2.4); they all have to respect the PC104 standard. The EPS card carries a smaller card for the batteries (“batteries card”).



Figure 2.3: Pumpkin’s structure.

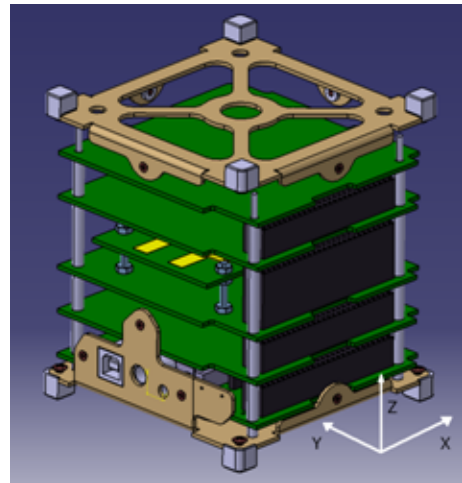


Figure 2.4: OUFTI-1 cards [5].

Maximum height

The spacing between the structure and the cards and between successive cards is shown in Fig. 2.5. The spacing between subsystems card determines the maximum height of components. The standard space between two cards on OUFTI-1 is 15mm. 10mm are reserved for the components on the top side. We wish to keep 1mm of margin between the components of two successive cards. There are 4mm left for the components or structures under the card.

The space between the EPS card and the EPS2 (Experimental EPS) is 25mm because of the batteries card. There are two areas on the EPS card:

- The surface under the batteries

There, the maximum allowed height for components is there reduced. In agreement with the "Structure" (STRU) team, this height has been fixed to 4.8mm.

- The remnant space (not under the batteries)

The available height for components is around 20mm. Tall components will though be avoided because of vibrations during launch.

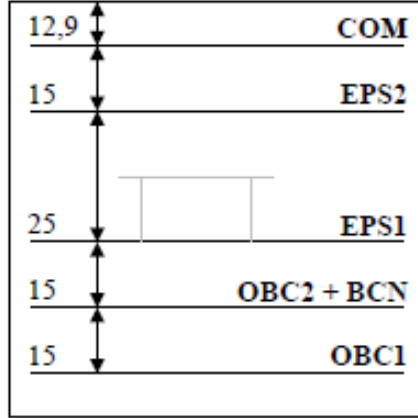


Figure 2.5: Distance between cards in OUFTI-1 [5].

Surface

The figure 2.6 is the top view of a PC104 card. The available surface on a PC104 PBC, after the space taken by main connector and fixation holes have been removed, is around 62.5cm^2 [5]. The total surface taken by all components, secondary connectors and particular mechanical structures must thus be less than 62.5cm^2 . It is useful to be able to estimate the surface occupied by electronics before drawing the PCB layout. A practical rule, used at Thales Alenia Space ETCA, is to compute the area of each single component, add up the various areas, and multiply the result by 1.6. It is wise to be careful with this rule. Thales Alenia Space only works with space certified components. They are generally bigger than commercial components. On the EPS, some commercial components with very small footprint will be used. As a result, the factor of 1.6 was replaced by a factor of 2. The EPS card has four extra holes for the fixation of the batteries card. They must be taken into account when estimating the occupied surface.

2.3 Functionalities

2.3.1 Power source

The OBC, the EPS, and the beacon should never be shut down. We also wish the radio reception for D-STAR and AX.25 to be always active. The radio transmission for D-STAR and AX.25 will be active only a fraction of time. The solar cells must provide enough energy to supply all subsystems. This is verified with the power budget, which is the subject of Chapter 4.

2.3.2 Power storage

The batteries have to store enough energy to supply the whole satellite during the periods of eclipse. This is also verified in Chapter 4.

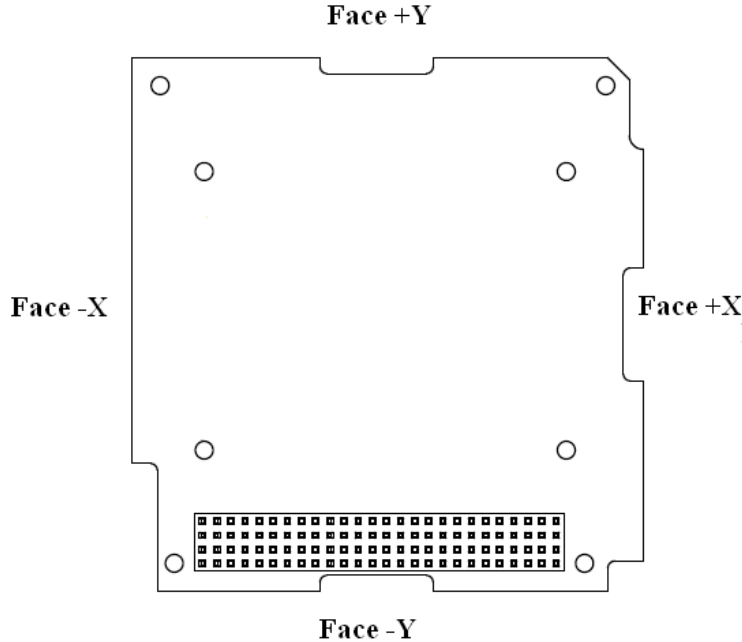


Figure 2.6: Top view of the PC104 card for the EPS [5].

2.3.3 Power conditionning

The EPS has to provide several stabilized voltage power outputs. Figure 2.7 shows the different power buses and the subsystems. The maximum current from each output has to be known before we can design the power conditioning unit. The exact consumptions of subsystems were not available during the work on this thesis, so that the following estimations were made:

- The OBC1 consumes 10mW at 5V. The current is thus 2mA [22].
- The OBC2 consumes 10mW at 3.3V. The current is thus 3mA.
- The Beacon uses one ADF7021, supplied in 3.3V. The maximum current consumed by an ADF is 25mA [8].
- The COM can use two ADF at a time. The maximum consumption is 50mA with 3.5V [8].
- Measurement systems are supplied with 3.3V. It is reasonable to think that the consumption will stay under 50mA.
- There will be one or two amplifier(s) for radio transmission, supplied with 7.2V. The desired RF power transmitted by the Beacon is 100mW. The desired RF power emitted by D-STAR and AX.25 is around 750mW. Assuming the amplifier has an efficiency of 30% (it should be higher), the maximum consumed power would be close to 3000mW. This corresponds to a current of 417mA [8].

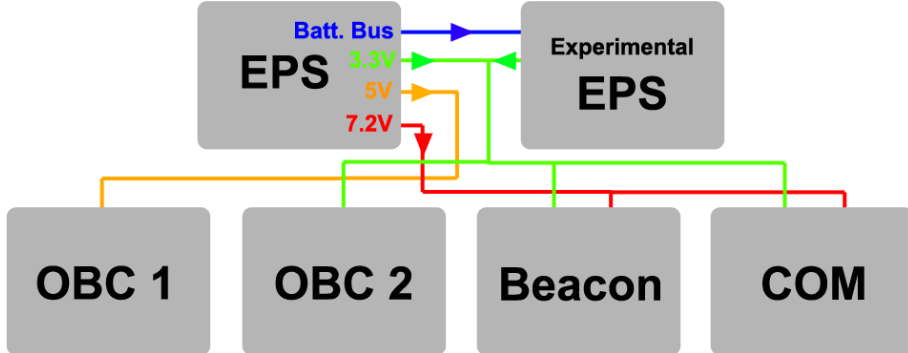


Figure 2.7: OUFTI-1 subsystems and power buses.

The requirements for the power conditioning unit are based on the above assumptions. The maximum current of the 3.3V and 5V outputs is higher than computed above, to let some flexibility.

Requirements for the power conditioning unit:

- One output at 3.3V with un maximum current of 200mA.
- One output at 5V with un maximum current of 200mA.
- One output at 7.2V with un maximum current of 420mA.

These requirements should be reviewed each time changes are made to the architecture of the cubesat.

2.3.4 Housekeeping parameters

There are important values on the EPS, like solar panels currents, batteries voltages, batteries temperature, and power bus voltage, that must be measured and transmitted to the ground, to know the state of the CubeSat and to verify that everything works fine. The EPS will include the measurement circuits, sensors, and ADC's. There must be an interface with the OBC to command the measurement circuits and to transmit data. An I^2C bus has been chosen as an interface.

A current-limiting protection circuit must also be included on the EPS for the measurement circuits.

2.3.5 Antennas Deployment System

During the launch, antennas are wound. They are held back by a string. To release the antennas, the string is cut by a thermal cutter. It is a resistor crossed by an important current (the exact current value is still unknown but its order of magnitude is around 1A). The antenna deployment is controlled by the OBC, but the OBC cannot deliver such a current. A power switch will be used and it will be located on the EPS card. The switch will be designed to withstand a current of 3A.

Chapter 3

Design of EPS architecture

3.1 Introduction

From the analysis of the EPS architecture of other CubeSats by Philippe Ledent, two decisions were taken [3]:

- The main power bus is not regulated.
- There is no Maximum Power Point Tracking.

In this chapter, the design of the Electrical Power System (EPS) of OUFTI-1 is built step-by-step. The solar cells and the batteries are analyzed first, because their characteristics determine the design of the architecture. The batteries have to be protected against over-discharge and over-charge. It is the role of the battery protection circuits and the dissipation system. A battery heater circuit is also inserted in the design because the temperature of the batteries must be kept over 0°C. There is an USB battery charger to charge the batteries as necessary before launch. The power conditioning unit provides three stabilized voltages to supply the subsystems of OUFTI-1. It is composed of three DC/DC converters. The EPS also includes several circuits for housekeeping parameters measurements and a circuit for the deployment of the antennas. The current architecture of the EPS is illustrated in figure 3.1.

3.2 Solar Cells

The first element of an EPS is the power source. The more practical power source for satellites is without contestation a set of solar cells.

3.2.1 Theory

A solar cell is a semiconductor device that converts sunlight energy into electric energy by the photovoltaic effect. A basic solar cell consists of a large-area silicon (Si) P-N junction. All solar cells are characterized by their current versus voltage curve (I-V curve). In the dark,

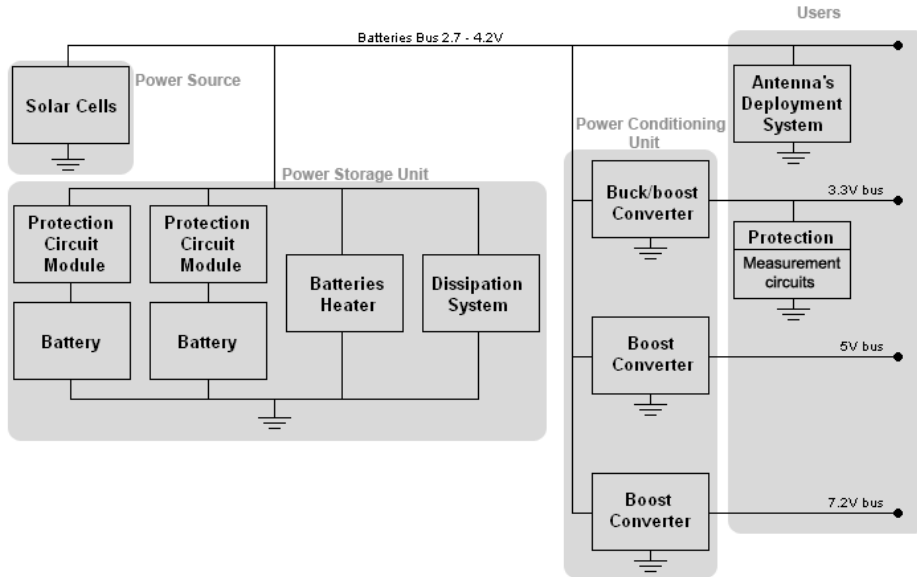


Figure 3.1: Block diagram of EPS.

the I-V curve of a solar cell is the same as that of a reverse-biased diode (Fig. 3.2). When photons with enough energy (higher than the silicon band gap value) penetrate the solar cell and hit the semiconductor material, the density of mobile electron-hole pairs is increased. The I-V curve is then moved upward (Fig. 3.3). More advanced solar cells can be made of other semiconductors, like gallium arsenide (GaAs), and have several junctions.

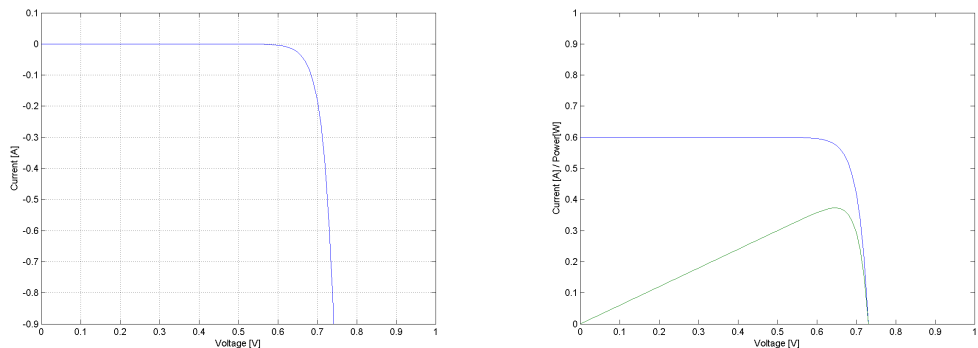


Figure 3.2: I-V curve of Si cell in the dark. Figure 3.3: I-V curve of Si cell in the light.

A power versus voltage curve (P-V curve) can be derived from the I-V curve. The P-V curve has a maximum, called the Maximum Power Point (MPP). Manufacturers rarely provide the I-V curve of their solar cells, but some important values (Fig. 3.4):

- The open-circuit voltage (1) on Figure 3.4
- The short-circuit current (2) on Figure 3.4

- Voltage (4) and current (5) at maximum power point (3) on Figure 3.4.

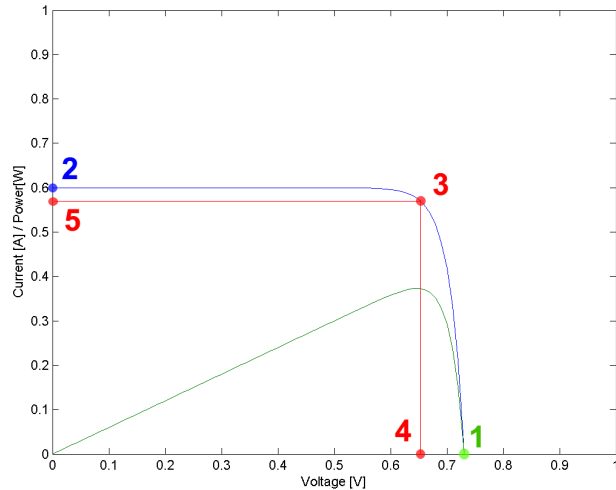


Figure 3.4: I-V curve of Si solar cell in sunlight.

The I-V curve is dependant upon several environmental parameters. The most important are:

- The temperature.

The short-circuit current is slightly increased with temperature while the open-circuit voltage is decreased. In usual temperature ranges, the efficiency of solar cells decreases with temperature.

- The light exposure.

The current increases with light intensity. The wavelength of the light has an influence. I-V curves are generally given for a particular spectrum. “Air Mass Zero (AM0)” is the spectrum of the sunlight in space, at the sun-earth distance. AM1.5 is the spectrum on earth.

- The age.

Radiations tend to decrease the efficiency over time. Commonly used terms to define the age of a solar cell are “Begin Of Life” (BOL) and “End Of Life” (EOL).

3.2.2 Azurspace's solar cells

AzurSpace is a German company that produces solar cells for space application since 1969. More than 340 satellites have been equipped with their products. The company contributes to our project by providing the solar cells for OUFTI-1. They are triple-junction GaAs solar cells. This kind of solar cell has a high efficiency and is commonly used in space application.

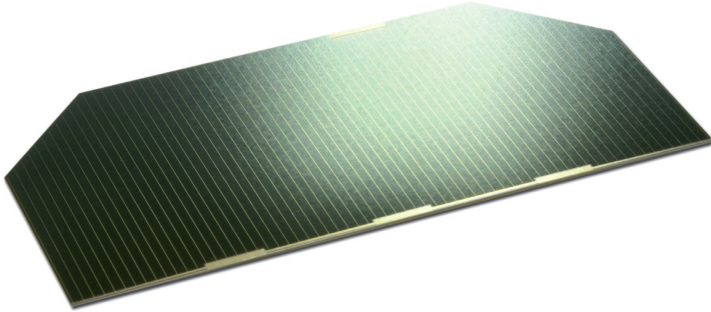


Figure 3.5: 3G - 28% solar cell from AzurSpace.

The last commercialized model, the “3G - 28%” (figure 3.5), has an efficiency of 28% at Begin Of Life (BOL), but a new model with 30% efficiency at BOL will be tested on OUFTI-1.

The dimensions of the solar cells are 80mm x 40mm with cropped corners, for a total surface of 30.18cm^2 .

Azurspace provided a document with electrical data for the 30% cells (table 3.1). The short circuit current is thus 528.15 mA for one cell, and the current at max. power is 513.06mA.

Open Circuit Voltage $V_{OC}[\text{mV}]$	2,716
Short Circuit Current $J_{SC}[\text{mA/cm}^2]$	17.5
Voltage at max. Power $V_{pmax}[\text{mV}]$	2,427
Current at max. Power $J_{pmax}[\text{mA/cm}^2]$	17.0
Maximum Power $P_{pmax}[\text{mW/cm}^2]$	41
Average Efficiency $\eta_{bare}[\%]$	30.1

Table 3.1: Electrical characteristics of Azurspace 3G - 30% solar cells at 28°C and for the AM0 spectrum [23].

3.2.3 Simple model

An ideal solar cell can be modelled by a reverse-biased diode (PN junction) in parallel with a current source (photovoltaic effect). A more practical model includes a shunt resistor and a series resistor. The equivalent circuit is shown on Fig.3.6, where R_{sh} is the shunt resistance and R_s the series resistance.

The R_{sh} resistance has generally a value of several hundreds Ohm. The current in R_{sh} is very small compared to the other currents, and the effect of R_{sh} can thus be neglected [17]. Solar cell models without R_{sh} give satisfactory results.

Thus, ignoring the shunt resistor, the equations giving the relation between V and I are then

$$V = V_j - IR_s$$

$$I = I_L - I_D$$

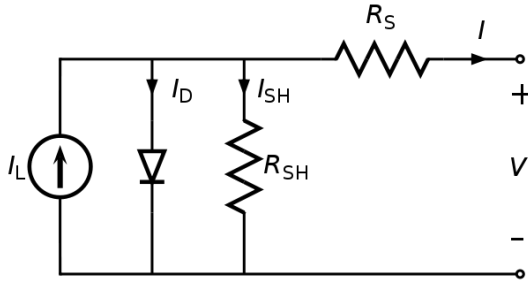


Figure 3.6: The equivalent circuit of a solar cell (Picture from Wikipedia).

$$I_D = I_0 \left(\exp \left[\frac{qV_j}{nkT} \right] - 1 \right)$$

$$I_0 = K_1 T^3 \exp \left(\frac{-E_g}{kT} \right)$$

With,

V	$[V]$:	Output voltage
I	$[A]$:	Output current
I_L	$[A]$:	Photogenerated current
I_D	$[A]$:	Diode current
I_0	$[A]$:	Reverse saturation current
V_j	$[V]$:	Voltage across diode
q	$[As]$:	Electric charge
k	$[J/K]$:	Boltzmann constant
T	$[K]$:	Temperature
n	-	:	Diode ideality factor
K_1	$[A/(cm^2 K^3)]$:	Manufacturer's thermal constant
E_g	$[J]$:	Forbidden band energy

The third equation is the Shockley ideal diode equation.

3.2.4 Matlab model

Based on this model, the SwissCube team has written a Matlab program to compute the I-V curve of a 26.6% efficiency solar cell, as a function of temperature and insolation [15]. With the help of parameters given by AzurSpace, this code has been adapted to the 3G 30% solar cells in [3]. Some minor mistakes were corrected (i.e. value of the short circuit current) and now the code can be used to obtain and display an approximation of the I-V curve of our solar cells. Figures 3.7 and 3.8 show I-V and P-V curves for temperatures from -35°C to $+45^\circ\text{C}$ (minimum and maximum temperatures on solar panels according to thermal simulations), under a full insolation ($G = G_{\text{nom}} = 1,350\text{W/m}^2$)

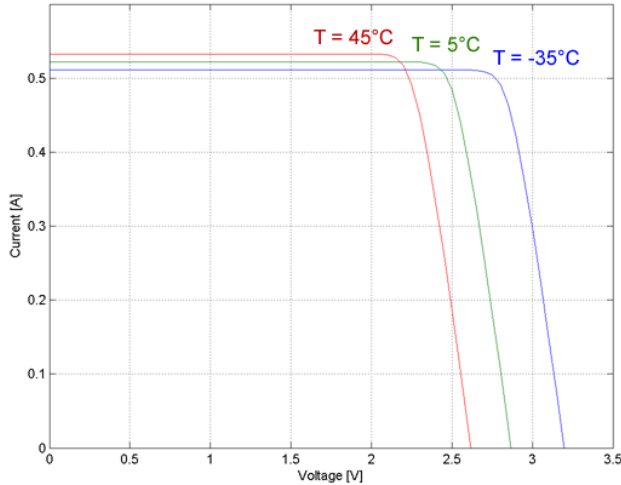


Figure 3.7: Matlab simulation of the I-V curve as a function of temperature.

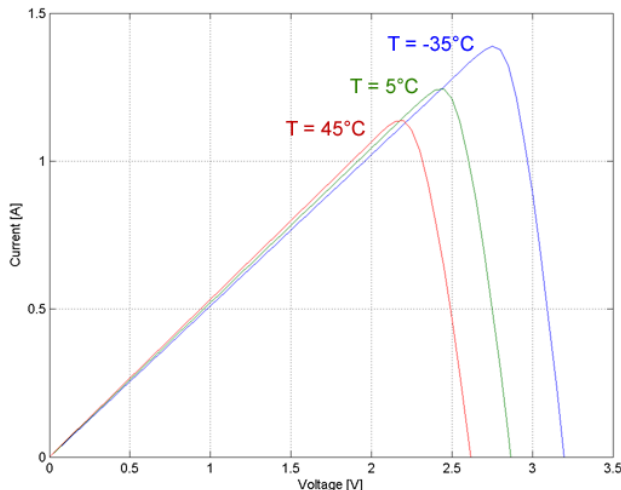


Figure 3.8: Matlab simulation of the P-V curve as a function of temperature.

3.2.5 Solar panels

There will be two solar cells per face, on five faces. The last face is occupied by the antennas and communication ports.

A non-regulated power bus has been chosen for the EPS of OUFTI-1. The solar cells and the batteries are connected to this bus. As a consequence, its voltage is determined by the batteries (the bus is called the “batteries bus”). The next section will show that the voltage

of our Lithium-Polymer batteries varies between 2.7V and 4.2V, depending on the state of charge/discharge.

The solar cells of one face will be connected in series. This forms a “solar panel”. Connecting two cells in series does not pose any problem. The current in each cell will be the same as for one cell alone.

Five solar panels are connected in parallel on the batteries bus. If a solar panel does not produce enough power, it will be crossed by a negative current. This current is lost for the CubeSat and could even damage the solar cells.

Therefore, solar panels have to be protected by a diode. To minimize the power loss on the diode, a Schottky rectifier is used. The voltage at the terminals of the used Schottky rectifier is between 0.5V and 0.6V. Figure 3.9 shows the electrical schematics of a solar panel. The voltage at the terminal of a solar panel will be the voltage of two solar cells minus the voltage of the diode.

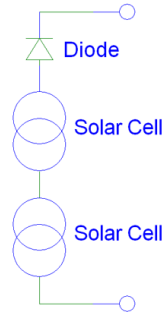


Figure 3.9: Components and schematics of a solar panel.

It is interesting to plot the I-V and P-V curves of a solar panel. The curve of one solar cell is already known. A model of Schottky rectifier has been chosen. The I-V curve of a Schottky rectifier has been measured and integrated to Matlab. The Matlab code used to plot the I-V and P-V curves of the solar panels is shown in the Appendix A. Figures 3.10 and 3.11 show the characteristics of the solar panel for temperatures of -35°C, 5°C, and 45°C, with full insolation ($G_{nom} = 1350W/m^2$). Figures 3.10 and 3.11 show the I-V and P-V curves for insolation of $0.25G_{nom}$, $0.5 G_{nom}$, $0.75 G_{nom}$, and G_{nom} , when the temperature is 5°C.

The voltage applied on a solar panel is the voltage of the batteries (V_{batt}). The power output of a solar panel is thus dependent of the state of the batteries. In other words, the figure 3.11 can be interpreted as the power output of a solar panel under full insolation as a function of the batteries voltage.

The following statements can be deduced from figure 3.11.

- The maximum amount of power lost because $V_{batt} > V_{mpp}$ is around 0.35W. This occurs when $V_{batt} = 4.2V$ and $T = 45^\circ C$. The output power is then around 1.65W.
- The maximum amount of power lost because $V_{batt} < V_{mpp}$ is around 1.2W. This occurs when $V_{batt} = 2.6V$ and $T = -35^\circ C$. The output power is then around 1.3W.

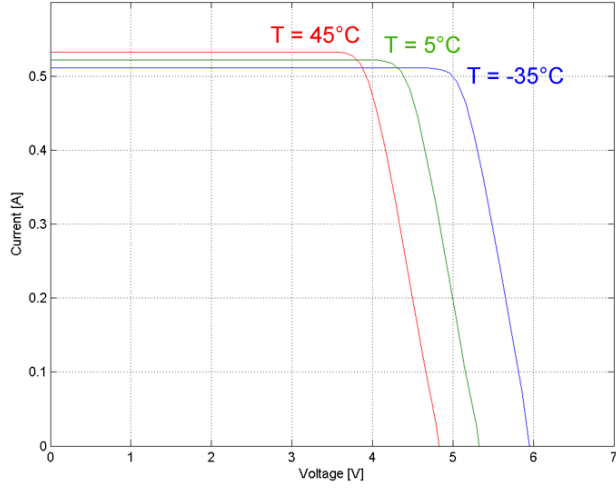


Figure 3.10: I-V curve of a solar panel for tree temperatures and under a full insolation (G_{nom}).

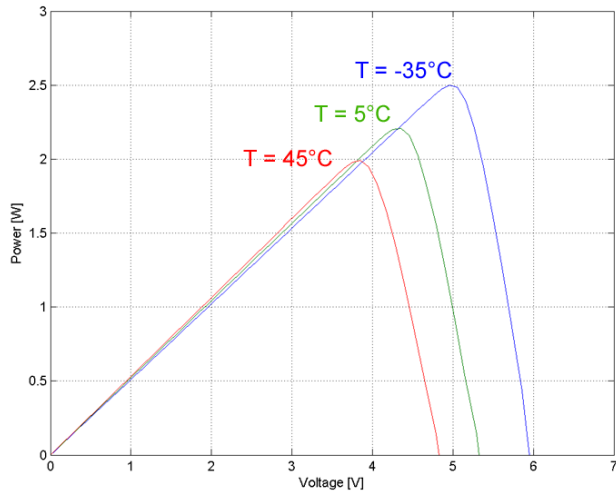


Figure 3.11: P-V curve of a solar panel for tree temperatures and under a full insolation (G_{nom}).

- The MMP cannot be reached when the temperature is under around 10°C.
- The maximum reachable output power is around 2.2W. V_{batt} must be maximum (4.2V) and the temperature must be under around 10°C.
- For $V_{batt} \cong 4V$ and a temperature between 5°C and 35°C (most of time the case for a panel exposed to sun), the operating point is close to the MPP.

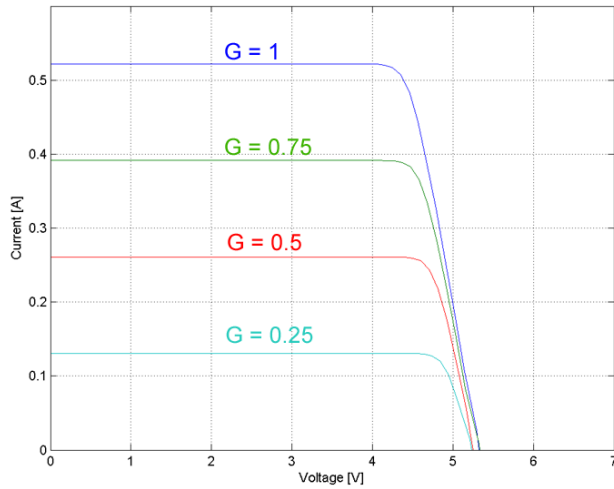


Figure 3.12: I-V curve of a solar panel for several insolation values (expressed in units of G_{nom}) and at $T = 5^\circ\text{C}$.

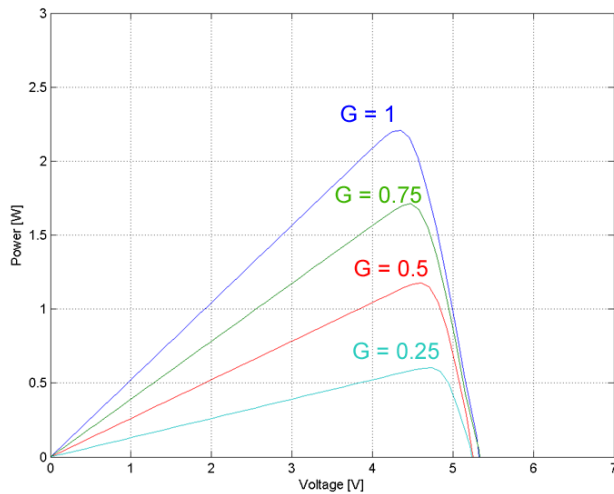


Figure 3.13: P-V curve of a solar panel for several insolation values (expressed in units of G_{nom}) and at $T = 5^\circ\text{C}$.

- The available power will nearly always be better if the batteries are in a good state of charge.

3.3 Batteries

In a CubeSat of one kilogram and one liter, the batteries have high chances to be the biggest and heaviest component. They are very sensible to temperature, and vacuum can have disastrous effects on them. Without them, the CubeSat would be completely shut down during each eclipse. The subsystem could never consume more power than produced by the solar panels at a given moment.

The batteries are obviously a critical component of the CubeSat. It is wise to choose a model of batteries that has already been used in several successful missions. In spite of this, they have to be tested under all possible operating conditions.

3.3.1 Technology

Figure 3.14 from Varta [19] shows the gravimetric and volumetric energy density for several battery technologies. The best choices would be Lithium-Ion (Li-Ion) or Lithium-Polymer (Li-Po) batteries. The Li-Po technology offers several advantages:

- Better energy density than Li-Ion because they do not need a metal packaging.
- Less hazardous because the solid polymer is not flammable, unlike the organic solvent of Li-Ion batteries.
- The technology has been successfully tested and used in CubeSats (e.g. in Clyde Space, Compass-1, and AAU).

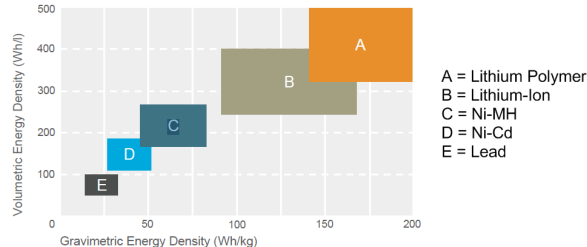


Figure 3.14: Energy density of several types of battery [19].

3.3.2 Architecture

The battery will be connected to the main power bus. There is no voltage conversion between the battery and the power bus. The equivalent schematics of a Li-Ion battery is a capacitor with a very low series resistance (when the voltage is above the minimum voltage of the battery). As a consequence, the voltage of the main power bus will be determined by the state of charge/discharge of the battery.

3.3.3 Capacity

A important value to know is the required minimum capacity of the battery for our CubeSat. The battery must provide enough energy to allow the CubeSat to be operational during each eclipse. The consumed power during an an eclipse can be computed with the power budget worksheet (Appendix).

Assumptions:

- Cold case (max. eclipse duration, heater on 24% of time).
- D-STAR or AX-25 transmission turned on 25% of time.
- 3.3V provided by EPS2.

The power consumed during eclipse is around 1.2Wh (= 324 mAh at 3.7V). A capacity of 324 mAh is the strict minimum for the batteries.

The capacity of Li-Pol batteries slightly decreases at each charge and discharge cycle. A good practice to limit this effect is to chose a low Depth of Discharge (DoD). A DoD of 30% means that a battery is discharged of 30% of its capacity before being charged again. The effect of DoD is shown in Fig. 3.15 and 3.16 [25]. Several batteries (C - Nominal capacity = 0.80 Ah, D - Nominal capacity = 1.45 Ah and F - Nominal capacity = 1.05 Ah) are compared, first with a DoD of 30%, and then with a DoD of 80%, at atmospheric pressure and in vacuum. The loss of capacity with a DoD of 30% is about the same than with a DoD of 80% after three times as many cycles. During the test, the charge rate is “C” and the discharge rate is “C/2” (3.2). “C” is the nominal capacity of the battery. For a battery with a nominal capacity of 0.80 Ah, a discharge rate of C/2 means that the discharge current is equal to 400 mA.

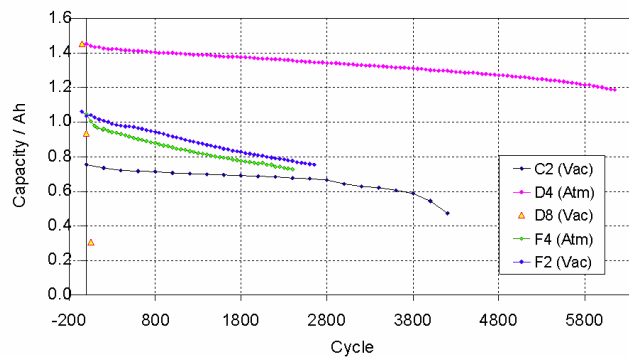


Figure 3.15: Capacity vs. number of cycles (cycling to 30% DoD).

Discharge rate	C
Charge rate	C/2 + tapering
Temperature	20°C

Table 3.2: Test conditions

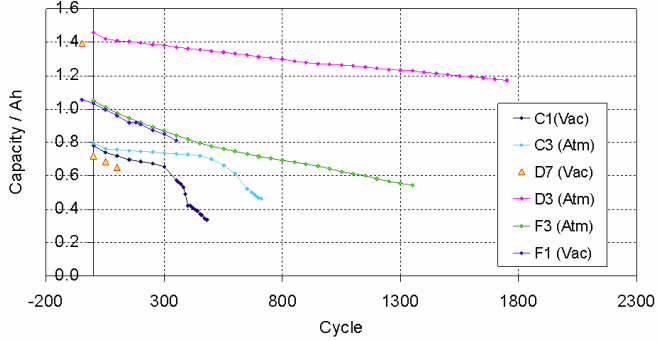


Figure 3.16: Capacity vs. number of cycles (cycling to 80% DoD).

The orbit of OUFTI-1 will have a duration of around 103 minutes. This corresponds to 5,103 cycles in one year. A DoD of 30% or less is recommended for this kind of application. The ideal capacity for our battery is thus at least $\frac{324mAh}{0.3} = 1,070mAh$.

3.3.4 Redundancy

Since the battery is a critical and sensible component, it is wise to add redundancy. There will be two batteries in parallel, connected to the main power bus (the main power bus can be called “the batteries bus”). Using two batteries for redundancy means that the CubeSat must be operational with only one battery. A second benefit of having two batteries is the reduction of the DoD. The DoD will be reduced to 15% or less, which will increase the lifespan of the batteries.

3.3.5 KOKAM batteries

The choice of batteries is discussed in [3]. A very interesting model was the Varta Poliflex Li-Pol cells. They are no longer being produced, and the SwissCube team strongly recommends not using Varta batteries that are more than two years old. Contacts have been taken (by Philippe Ledent) with several battery manufacturers, and KOKAM accepted to provide the batteries for OUFTI-1.

Two models of KOKAM batteries were purchased, the SLPB554374H and the SLPB723870H4, the characteristics of which are compared in Table 3.3.

From an electrical point of view, the SLPB723870H4 (1,500 mAh) was more interesting than the SLPB554374H (1,250 mAh) since it has a better capacity and a lower impedance. However, the second model (i.e. SLPB554374H) was chosen for mechanical reasons. The thickness of the SLPB723870H4 was too important to place two batteries on the batteries card.

The SLPB554374H cell has a nominal capacity of 1,250mAh. The depth of discharge will be 26% for one cell and thus 13% for two cells. The voltage range of the batteries, and thus of the batteries bus, will be 2.7V to 4.2V. The maximum consumed power has been estimated

Parameter		SLPB723870H4	SLPB554374H
Nominal Capacity		TYP 1,500 mAh	TYP 1,250 mAh
Nominal Voltage		3.7V	3.7V
Charge Condition	Max. Current Voltage	1C(1,500mAh) 4.20 ± 0.03V	1C(1,250mAh) 4.20 ± 0.03V
Discharge Condition	Max. Current Cut-Off Voltage	20C(30,000mAh) 2.7V	15C(18,750mA) 2.7V
AC-Impedance.($m\Omega$)		MAX. 9.0 (1kHz)	MAX. 16.0 (1kHz)
Operating T°	Charge Discharge	0°C to 45°C -20°C to 60°C	0°C to 45°C -20°C to 60°C
Weight(Max.)		41.0 g	34.0 g
Energy Density	Volumetric Gravimetric	278 Wh/l 145 Wh/kg	287 Wh/l 152 Wh/kg

Table 3.3: Characteristics of two candidate KOKAM batteries [20].

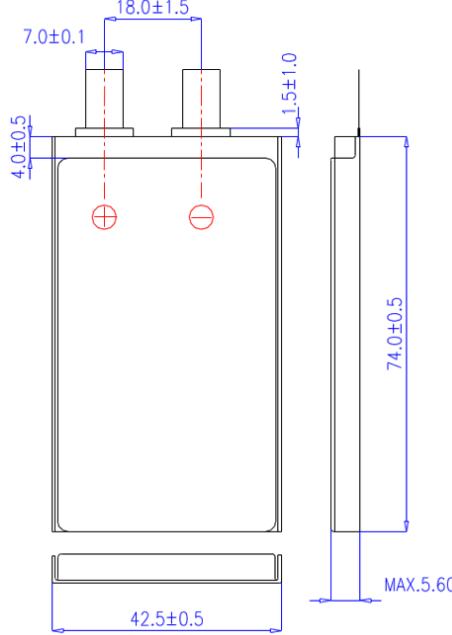


Figure 3.17: Dimensions of the KOKAM SLPB554374H battery [20].

to 4,720mW with the power budget worksheet (Chapter 4). The corresponding maximum consumed current is 1.75A at 2.7V and 1.12A at 4.2V. This corresponds respectively to discharge rates of 1.4C and 0.9C. Figure 3.18 shows the charge characteristics of KOKAM batteries. Figure 3.19 and 3.20 show their discharge characteristics.

Figure 3.18 shows that the batteries are not fully charged when their voltage reaches 4.2V. The dissipation system on the EPS is a shunt regulator (Chapter 5). Another system could be to disconnect the batteries when their voltage reaches 4.2V. The use of a shunt regulator will allow the batteries to reach the full charge. This is still to be confirmed by tests.

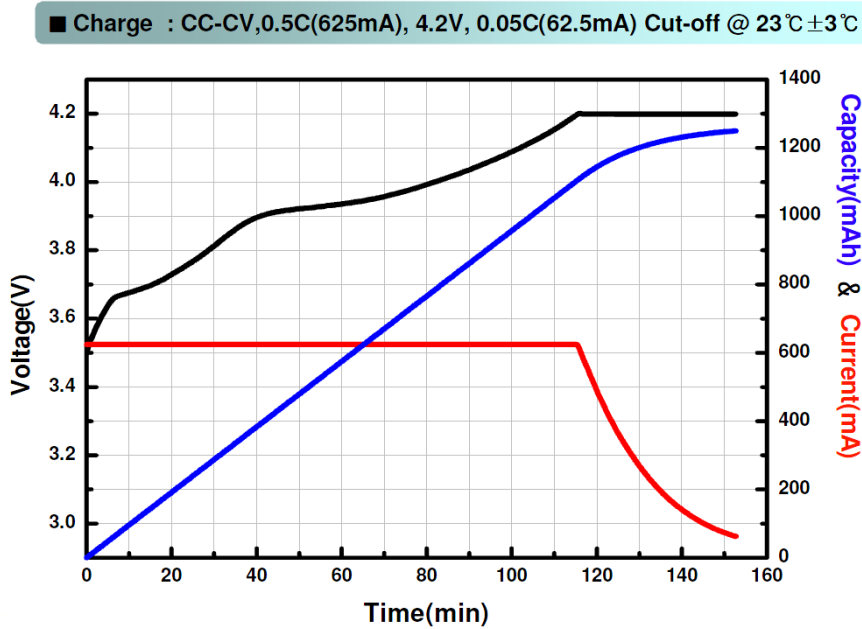


Figure 3.18: Charge characteristics of KOKAM SLPB554374H (KOKAM Datasheet).

Figure 3.19 shows that, for a DoD of 13% (which corresponds to 162 mAh) and a discharge rate under 1C, the voltage should stay between 4V and 4.2V (at 23°C and begin of life).

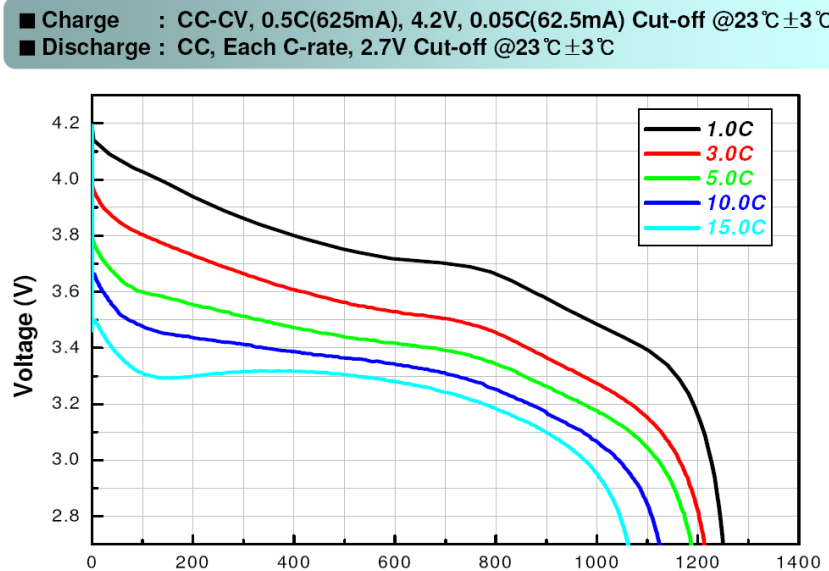


Figure 3.19: Variation of voltage of KOKAM SLPB554374H during discharge for several discharge rates [20].

The temperature of the batteries during charge must be between 0°C and 45°C or they could suffer permanent damages. The spacers between the batteries card and the EPS card will have a high thermal resistance. Simulations show that, with this solution, the temperature

of the batteries is kept between -22°C and +37°C [7]. The batteries will be maintained above 0°C by a 500mW heater. According to Fig. 3.20, a beneficial side effect of the heater is to keep the batteries capacity beyond 1,100mAh.

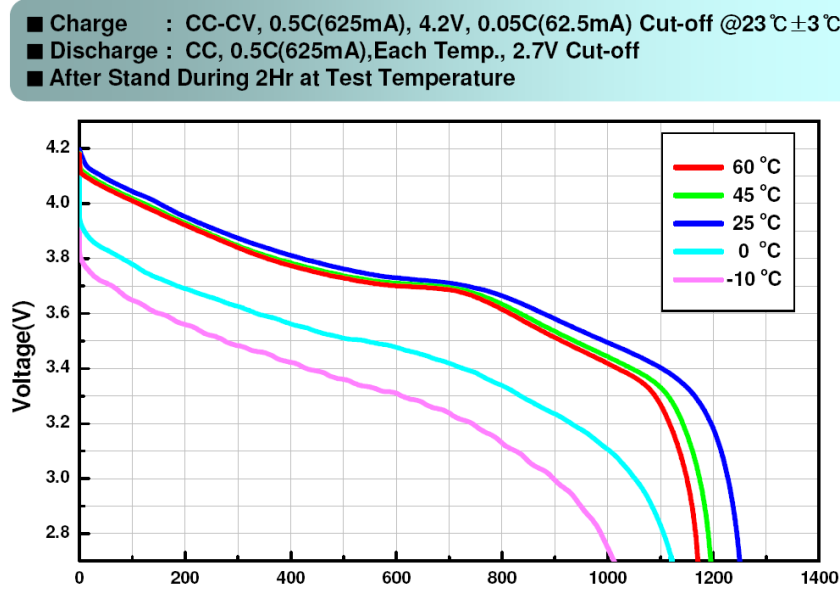


Figure 3.20: Variation of voltage of KOKAM SLPB554374H during discharge for several temperatures [20].

The batteries have been successfully tested in vacuum by Philippe Ledent.

3.4 Battery protection circuits

The KOKAM batteries are delivered with a protection circuit module (PCM). The role of the PCM is to protect the batteries against over-charge, over-discharge and over-currents. These modules are directly soldered on the batteries terminals. Each battery has its own PCM.

The choice can be made to keep that circuit or to make our own. Our first choice was to use the protection circuits of the manufacturer (KOKAM).

The operating temperature range of the KOKAM PCM is -10°C to 50°C and the storage temperature range of the KOKAM PCM is -20°C to 60°C. Given that the PCM is in direct contact with the batteries, and that the temperature of the batteries is maintained between 0°C and 45°C, the temperature of the PCM is expected to stay in a good range.

The schematics of the KOKAM PCM is shown on figure 3.21.

3.4.1 Electrical characteristic

The electrical characteristics are shown in the table 3.4.

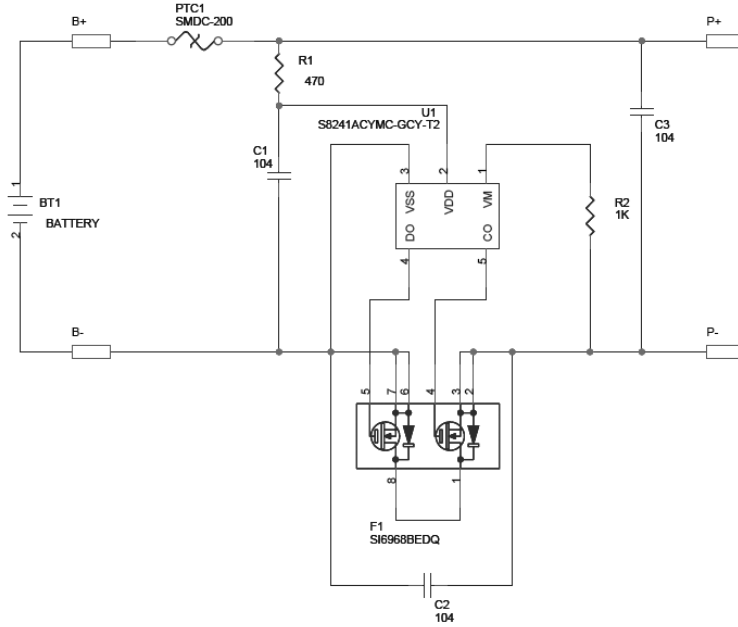


Figure 3.21: Schematics of the KOKAM PCM [21].

3.4.2 Over charge protection (i.e. over-voltage protection)

The PCM disconnects the battery when the voltage reaches 4.275V. The connection is established again when the voltage drops to 4.075V. This prevents the battery from being damaged by an over charge. However, to operate in optimal condition, the battery voltage should not rise over 4.2V. Another circuit, the dissipation system, will be designed to prevent the batteries voltage to get over 4.2V.

3.4.3 Over discharge protection (i.e. under-voltage protection)

The PCM disconnects the battery if the voltage drops to 2.6V. The connection is established again when the voltage is higher than 2.9V.

3.4.4 Over current protection

The over-current protection is a fuse. The fuse melts with a current between 2A and 4A (depending upon voltage). There will be two batteries in parallel, so that the current in each battery should not be higher than half of the current consumed in the CubeSat. Nevertheless, the CubeSat is supposed to be functional with only one battery. Then, the total current consumed in the satellite must be kept under 2A during eclipse.

Over Charge	Prohibition Release Delay Time	$4.275 \pm 0.025V/Cell$ $4.075 \pm 0.050V/Cell$ $1.0sec \pm 300msec$
Over Discharge	Prohibition Release Delay Time	$2.600 \pm 0.080V/Cell$ $2.900 \pm 0.100V/Cell$ $125 \pm 37msec$
Over Current	Prohibition Release Delay Time	$3A \pm 1A$ (Depend on cell voltage) by Charging $8 \pm 4msec$
Current Consumption	Operation	Max. $5\mu[A]$
	Power down	Max. $0.1\mu[A]$

Table 3.4: Electric Characteristic of KOKAM Protection Circuit Module [20].

3.5 Dissipation system (Shunt regulator)

The role of the dissipation system is to prevent the voltage of the batteries to get over 4.2V by dissipating the exceeding power. There will be one dissipation system, connected to the batteries bus. The reliability of this system is thus critical. Its failure would result in the loss of the whole mission.

The worst case is when solar panels output is maximum and no power is consumed in the CubeSat. We can show that the instantaneous power produced by our five solar panels will never be higher than 5.5W. This value of 5.5W corresponds to an optimal exposure to sun, an albedo of 30%, operation at MPP [6]. The dissipation system must thus be able to dissipate a current of up to 1.31A (5.5W / 4.2V).

3.6 Battery heater

Thermal simulations were done by the THER team [7]. Results are shown in Fig. 3.22. They predict that, in absence of any temperature control measure, the temperature of the batteries will fall to -21.4°C in a cold case, and rise to 36.3°C in a hot case. However, the recommended operating temperature of the batteries is between 0°C and 45°C. Therefore, a heater will be directly placed on the batteries to keep their temperature above 0°C.

3.6.1 Control

There are two possible solutions to control the heater. The heater could be controlled by the OBC, or could have an independent control. Table 3.5 shows conveniences and drawbacks of each solution.

It was difficult to decide between these two solutions. After discussion with the OBC team, the solution of the independent control was selected. The control will take the temperature of the batteries and let the current flow in the heater when the temperature falls below some predetermined threshold.

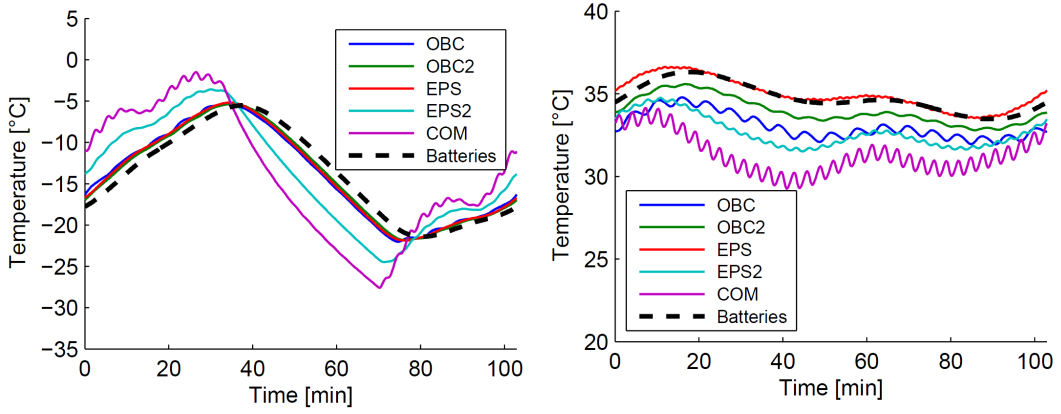


Figure 3.22: Temperatures of cards in OUFTI-1, in the cold case (left) and hot case (right), during one orbit time [7].

Control by OBC	Independent control
Uses less components. Less reliable (depends of OBC). The heater can be controlled by an algorithm. Needs a pin in the PC104 port.	Uses more components. Independent of OBC and measurement system (more reliable). The control is “dumb”. One pin of the PC104 port is spared.

Table 3.5: Comparisons of solutions to control the batteries heater.

3.6.2 Supply voltage

The chosen solution is to supply the heater directly from the batteries. The reasons are:

- The heater does not really need a regulated voltage.
- The heater is independent of the power conditioning unit, which improves reliability.
- The electrical supply is near, so that there is no need to have a wire connecting the heater to a voltage regulated output.

3.7 USB battery charger

The sixth face of OUFTI-1 contains an USB port. This is the only interface with the satellite when the faces are closed. One of the functions of the USB port will be to allow the charge of the batteries when the CubeSat is sealed. A current of 100mA can be delivered through the USB port, with a voltage of 5V.

The USB battery charger is a circuit that manages the charge of batteries when it is

supplied in 5V. The circuit will be located on the batteries card. This is not a critical component since it will not be used in space.

3.8 Power conditioning unit

Most subsystems have to be supplied with a regulated voltage. The power conditioning unit provides the required voltages by converting power from the batteries bus. The list of required voltages and corresponding maximum currents is given in chapter 2.

	Output 1	Output 2	Output 3
Voltage [V]	3.3	5	7.2
Max. Current[mA]	200	200	420
Max. Power [mW]	660	1,000	3,024

Table 3.6: Specifications for the power conditioning unit in term of output voltage, max.current, and max. power.

Early in the project [3], it was decided to use three DC/DC converters to produce the desired voltages. The batteries bus voltage will be converted to 5V and 7.2V by two "boost" DC/DC converters, and to 3.3V by one "buck/boost" converter.

3.9 Protection circuits

The protection of subsystems against over-current was in the initial objectives of the EPS. A current-limiting circuit was chosen in [3]. This circuit prevents the current at its output to get over a chosen threshold. The circuit has a "FAULT" logical output that will be used to indicate to the OBC when a protection circuit detected an over-current. It also has a ON/OFF input, that allows to turn on and off the power on the output of the current-limiting circuit.

If such a circuit is located on the EPS, it can protect each power bus (3.3V, 5V, and 7.2V), but not each subsystem individually (there is a limited number of power busses in the PC104 port). With the OUFTI-1 team, we took the decision to use a current-limiting circuit on each subsystem. The protection circuit will be located on the user's cards. Doing so, a lot of space is saved on the EPS card. There will be only one protection circuit on the EPS card: the protection circuit of the measurement circuits. Another advantage of this structure is that the OBC can turn the power on and off for each subsystem individually.

3.10 Measurement system (Housekeeping parameters measurements)

There are several measurement circuits on the EPS. Current sense IC's, temperature probe, and voltage scalers (two resistors) are connected to analogic-to-digital converters. All the corresponding circuits must be supplied with 3.3V. Like other subsystems, measurement circuits have to be protected against over-current. The corresponding protection circuit is placed

on the EPS. The protected 3.3V bus will be connected to a pin of the PC104 port. All measurement circuits in the satellite will be supplied from this bus.

3.11 Antennas deployment circuit

The antennas deployment circuit is a switch controlling whether the current flows or not in a thermo-cutter. It is used only one time, around 30 minutes after the insertion into orbit. The amount of current was unknown when the architecture of the EPS was designed. It was then decided to design a circuit able to deliver up to 10W of power in the resistor. Since then, the required power was determined. The thermo-cutter will have a resistance of around 10Ω , which corresponds to a maximum power of 1.76W if the batteries voltage is 4.2V.

There is no DC/DC converter able to deliver 10W on the EPS. Therefore, the circuit will be supplied directly from the batteries bus. Even if a converter was able to deliver enough power, there would be no real convenience to supply the antennas deployment circuit by means of this converter. A failure of the converter would cause the antennas not to deploy, and as a consequence the failure of the whole mission.

3.12 About the experimental EPS

The Experimental Electrical Power Supply, or EPS2, is a digitally controlled flyback converter. Its power input is connected to the batteries bus and it provides a stabilized 3.3V output. The EPS2 is designed to be able to supply the 3.3V bus of the CubeSat.

The EPS2 will be connected in parallel with the 3.3V converter of the EPS. A switch will allow the OBC to chose whether the output of EPS2 is connected to the 3.3V bus or to a test load. The exact means of connecting the output of the EPS2 with the output of the 3.3V regulator of the main EPS remains to be determined. A Schottky rectifier can be inserted on the output of the 3.3V converter (before the feed-back loop) if needed. The behaviour of this parallel connection will need to be investigated in tests.

We chose to let the EPS2 supply the 3.3V most of time. The 3.3V converter of the EPS will be a back-up solution. Since the efficiency of the EPS2 is very low compared to the 3.3V converter, this must be taken into account in the power budget.

Chapter 4

The Power Budget

4.1 Introduction

The goal of the power budget is to verify that the consumed power on board does not exceed the produced power. The power budget is defined on a time interval. In our case, the chosen interval is one orbit. The power input over one orbit is computed for several scenarios (cold case, mean case, and hot case). Then, the consumed power is estimated for several operation modes of the CubeSat and the time sharing of these modes is discussed.

4.2 Estimation of input power

The maximum instantaneous electrical power that can be captured by solar cells is given by:

$$P = \eta A_{eff} C_s$$

where

- η is the efficiency of the solar cells. It is expected to be 30% at BOL (Begin Of Life) and to drop to 23% at EOL (End Of Life).
- A_{eff} is the effective area of the solar cells. The effective area is the area of the projection of the solar panels onto a plane perpendicular to the direction of the solar rays. The maximum value is 104.55cm^2 , and the mean value has been estimated to be 76.6cm^2 by simulations [6].
- C_s is the solar constant, with a minimum value of $1,321\text{W/m}^2$, a mean value of $1,358\text{W/m}^2$, and a maximum value of $1,413\text{W/m}^2$ [6].

This formula would be useful if the extracted power from the solar cells was always the maximum power. With an MPPT system, the input power would be given by $P = \eta_{conv}\eta A_{eff} C_s$ where η_{conv} is the efficiency of the MPPT converter.

As no MPPT system is used in our architecture, the input power must be estimated in a different way.

The P-V curves of each solar panel were computed in Chapter 3 from the corresponding Matlab model. The power produced by a solar cell is mainly dependent on three parameters:

- The insolation.
- The applied voltage at its terminals.
- The temperature.

When these parameters are known, the input power from one solar panel can be deduced from the Matlab model.

In real operating conditions, the power is most of time provided not by a single solar panel, but by three of them. The mean effective area of solar panels $A_{effMean}$ is calculated in [6]. Knowing the batteries voltage, can the mean input power be estimated by taking the input power of one solar panel and multiply it by the effective areas ratio $\frac{A_{effMean}}{A_{panel}}$ where A_{panel} is the area of one panel?

$$P_{mean}(V_{batt}) \cong \frac{A_{effMean}}{A_{panel}} P_{panel}(V_{batt}) \quad (4.1)$$

Figure 4.1 shows that the power produced by one panel is essentially proportional to the received light power for all voltages up to the MPP voltage (corresponds to the maximum of the P-V curve of the solar panel) at G_{nom} . The figure also shows that the MPP voltage is higher in the case of a less exposed panel. Equation 4.1 is thus true for all voltage up to the MPP voltage at G_{nom} .

Figure 4.2 shows that the MPP voltage is above 4.2V when the temperature is between -35°C and 15°C. Equation 4.1 is thus true for all voltage in the batteries voltage range (2.6V to 4.2V) if the temperature is under 15°C.

The produced power for a given effective area can thus be expressed as the power produced by one panel multiplied by the areas ratios when the temperature is under 15°C.

4.3 Estimation of consumed power

The consumed power in the CubeSat depends on the operating state of the electrical subsystems. For each subsystem, the operation modes and the corresponding consumptions on the different power busses are listed in a worksheet (given in Appendix B). During the first steps of the project, the consumptions were estimated from datasheets and simulations, but these consumptions should be determined by direct measurements on prototypes as soon as such prototypes become available. It will be important to keep an eye on any change in consumptions resulting from changes in design and construction.

A fraction of the power delivered on each power bus is lost in the power conditioning unit. The real amount of consumed power can then be computed using

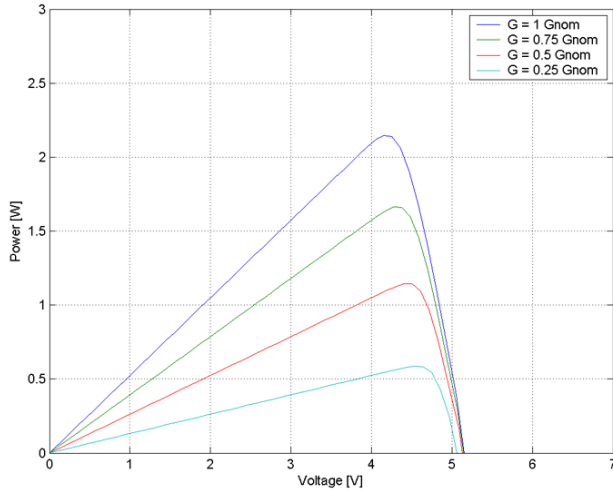


Figure 4.1: P-V curve of a solar panel for several insolation values (expressed in units of G_{nom}) and at $T = 15^\circ\text{C}$.

$$P_{out} = \eta^{-1} P_{in} \quad (4.2)$$

where η is the efficiency of the corresponding converter. The efficiency of a converter depends on the output current. However, for simplicity, we assume that this efficiency is constant. The converters are indeed used in a limited range of output currents.

Finally, percentages of utilization are attributed to each operation mode and the consumed power is integrated on one orbit.

4.3.1 Operation modes of subsystems and corresponding power needs

- EPS

EPS has two modes:

1. ON: EPS is always active and 5mA are consumed (on batteries bus).
2. ON+Heater: When active, the heater consumes around 500mW on the batteries bus. This must be added to the consumption of EPS.

- OBC

OBC1 and OBC2 are always active and consume 10mW each. The OBC1 consumption is 2mA on the 5V bus. The OBC2 consumption is 3.3mA on the 3.3V bus.

- EPS2 (Experimental EPS)

EPS2 has three modes:

1. OFF: EPS2 consumes no power.

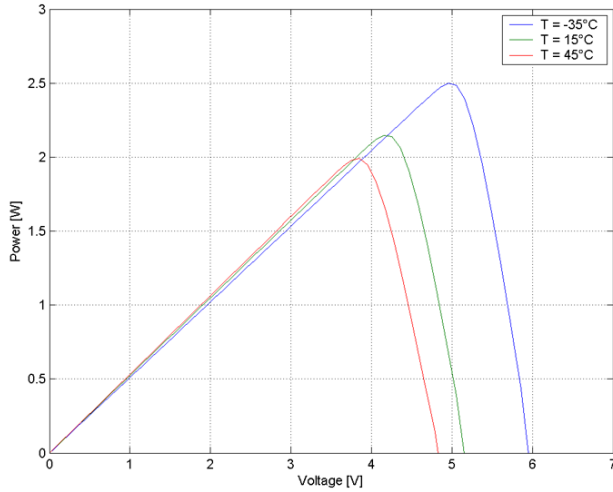


Figure 4.2: P-V curve of a solar panel for tree temperatures and under a full insolation (G_{nom}).

2. Supply: it supplies the 3.3V bus, with an efficiency of at most 50% (for 100mA). In this case, the 3.3V converter of EPS lets EPS2 supply the subsystems. The efficiency of EPS2 quickly decreases as the output current decreases. As a consequence, rather than setting an efficiency of 50% for the 3.3V bus when EPS2 is active, we assume that a constant power of 300mW is consumed.
3. Test: EPS2 supplies a load in which 100mA are dissipated, the efficiency is 50% (total 660mW consumed), and this lasts only a few seconds.

- COM

COM has two modes:

1. Rx only: COM is always “listenning” on the D-STAR and AX.25 receive (Rx) channel. Corresponding consumption is at most 20mA on the 3.3V bus.
2. Rx + Tx (receive and transmit): When a D-STAR signal or AX.25 signal is transmitted, the COM consumption is 35 mA on the 3.3V bus and 208 to 347mA on the 7.2V bus, these currents corresponding to Tx RF signal power of 750mW and an amplifier efficiency ranging from 30% to 50%.

- Beacon

Beacon is always active. Its consumption is 15mA on the 3.3V bus and 28 to 46mA on the 7.2V bus, these currents corresponding to a Tx RF signal power of 100mW and an amplifier efficiency ranging from 30% to 50%.

4.3.2 Efficiency of converters

To attribute a constant efficiency to a converter, we first have to know in which output current range it will work.

Based on the analysis of section 4.3.1, the range of consumed current on each power bus can be computed:

- On 3.3V bus: 45 to 80mA.
- On 5V bus: 2mA.
- On 7.2V bus: 28 to 400mA.

The efficiency of the converters was measured on the engineering model for several output current values [1]. On this basis, a realistic, conservative efficiency for the above ranges of output current is chosen for each converter:

- Efficiency of 3.3V converter: 90%.
- Efficiency of 5V converter: 70%.
- Efficiency of 7.2V converter: 85%.

The efficiencies are inserted in the worksheet. The equation 4.2 is applied on the consumption of each system to obtain the real consumption, which take the losses in the converters into account.

At this stage, the maximum consumed instantaneous power can be computed. This of course correspond to the case where all subsystems are in their most consuming mode. The maximum consumed instantanous power is found to be of 4,720mW.

4.4 Discussion

The energy provided by solar panels is computed from the P-V curve for the batteries voltages of 2.7V, 3.7V and 4.2V. The portion of time per orbit during which the D-STAR and AX.25 transmitter (Tx) can be turned on is then calculated for an amplifier efficiency η_{ampl} of 30% and 50%. The worksheet gives the following results:

4.4.1 Cold case

EPS2 in “supply” mode

Assumptions:

- Longest eclipse, i.e. 35.9% of orbit duration [6].

- Solar panels temperature of 5°C.
- Battery heater turned on for 35 min per orbit [7].
- 3.3V supplied by EPS2.

Batteries voltage	[V]	3	3.7	4.2
Power input per orbit	[mWh]	2,100.3	2,660.4	3,080.4
Tx usage ($\eta_{ampl} = 30\%$)	%	5	16	24
Tx usage ($\eta_{ampl} = 50\%$)	%	17	35	49

EPS2 turned Off

Assumptions:

- Longest eclipse, i.e. 35.9% of orbit duration [6].
- Solar panels temperature of 5°C.
- Battery heater turned on for 35 min per orbit [7].
- 3.3V supplied by EPS1.

Batteries voltage	[V]	3	3.7	4.2
Power input per orbit	[mWh]	2,100.3	2,660.4	3,080.4
Tx usage ($\eta_{ampl} = 30\%$)	%	15	26	34
Tx usage ($\eta_{ampl} = 50\%$)	%	34	51	65

4.4.2 Mean case

Assumptions:

- Mean eclipse, i.e. 24.2% of orbit duration [6].
- Solar panels temperature of 15°C.
- Battery Heater turned on for 10% of time.
- 3.3V supplied by EPS2.

Batteries voltage	[V]	3	3.7	4.2
Power input per orbit	[mWh]	2,566.5	3,228.8	3,559.9
Tx usage ($\eta_{ampl} = 30\%$)	%	18	31	37
Tx usage ($\eta_{ampl} = 50\%$)	%	38	59	70

Figure 4.3 shows the consumptions of the OUFTI-1 subsystems in the mean case.

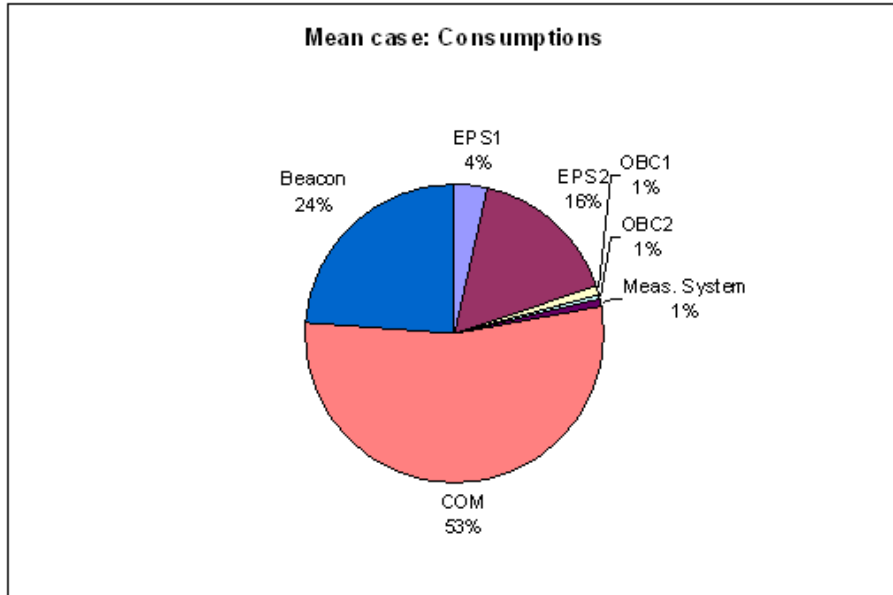


Figure 4.3: Consumptions in % in mean case, with $V_{batt} = 3.7V$, $\eta_{ampl} = 30\%$, and a Tx usage of 31%.

4.4.3 Hot case

Assumptions:

- No eclipse.
- Solar panels temperature of 45°C.
- Battery Heater turned off.
- 3.3V supplied by EPS2.
- The mean power produced by an effective surface of one A_{panel} at 4.2V is 1.9W.

We stated that the produced power at a given voltage was proportional to A_{eff} when the batteries voltage was under the MPP voltage. This condition was true for voltage between 2.6V and 4.2V when the temperature was under 15°C. This is thus not true anymore in the hot case.

Figure 4.4 shows the P-V curve of one solar panel at a temperature of 45°C facing the sun and the cumulated P-V curve of three solar panels at a temperature of 45°C when a corner of the CubeSat is oriented toward the sun (then $A_{eff} = \sqrt{3}A_{panel}$). In the first case, the produced power is around 1.7W at 4.2V while in the second case the produced power is around 3.5W at 4.2V (which corresponds to 2W per A_{panel}). In the second case, the MPP voltage is higher. This is due to the fact that when a face receives less insolation, its MPP voltage is higher.

In either case, the MPP voltages is higher than 3.7V. For voltage of 3V and 3.7V, the produced power is thus still proportional to A_{eff} .

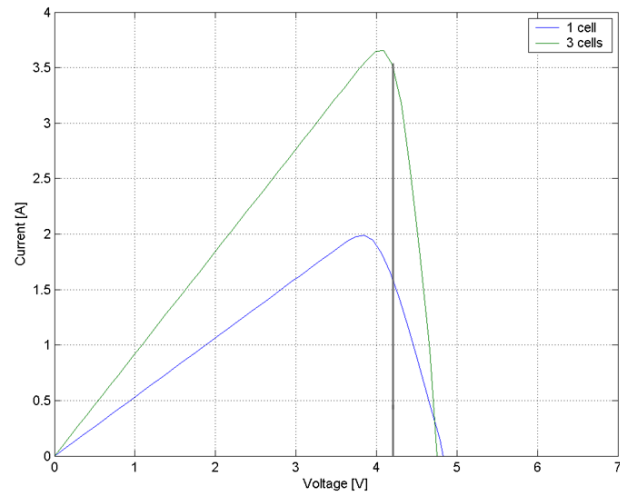


Figure 4.4: P-V curve of one solar panel facing the sun, and of three solar panels when the corresponding corner is oriented toward the sun, at $T = 45^\circ\text{C}$.

Batteries voltage	[V]	3	3.7	4.2
Power input per orbit	[mWh]	2,566.5	3,228.8	3,559.9
Tx usage ($\eta_{ampl} = 30\%$)	%	34	51	55
Tx usage ($\eta_{ampl} = 50\%$)	%	64	92	99

Chapter 5

Electrical Design of EPS

5.1 Introduction

In this chapter, the electrical design of each module of the EPS is explained. The first and second sections deal with the design of the power conditioning unit. Some theory is given about converters and input filters. The design of the dissipation system, the antennas deployment system, the protection circuit, and the batteries heater is discussed in subsequent sections. Finally, the complete electrical schematics of the EPS is given.

5.2 Design of Converters

This section describes the design of the three DC/DC converters. The 7.2V and 5V converters are "boost" or "step-up" converters. The 3.3V converter is an hybrid "buck/boost" converter. This last converter can pass from one operating mode to another depending upon the input voltage. First, the theory about switching DC/DC converters is explained (for Buck and Boost) and design rules are deduced. The electrical design of each converter is then presented. Finally, we indicate how the design of the converters could be updated.

A first design of the converters was made by Philippe Ledent [3]. The prototypes of these converters have been tested [1]. Based on the lessons learned with the tests of the first design, and based on the upgraded requirements of the power conditioning unit, a new design is proposed in this section. Compared to the first design, the control circuits remained the same, but the passive components were modified.

5.2.1 Theory

The converters of the EPS are output-voltage controled converters. A converter is composed of a power stage and a control (Fig. 5.1). The power stage performs the voltage conversion. We will see below that the power stage contains a switch and that the portion of time during which this switch is closed determines the voltage conversion ratio. The portion of time during which the switch is closed is called the duty cycle (D). The duty cycle is set by the control. By adjusting the duty cycle, the control can maintain an electrical value constant. Here, the

duty cycle is determined by the output voltage. In other kinds of converters, the duty cycle can be determined by the input voltage if a stabilized input voltage is needed, by the input current, or by the output current.

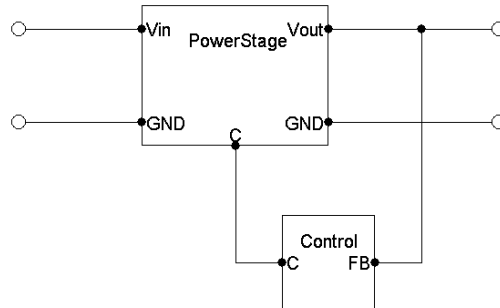


Figure 5.1: Block diagram of an output voltage controlled converter.

"Buck" converter [16]

Principle

The power stage of the buck converter is composed of a switch, an inductor, and a capacitor (Fig. 5.2). The switch is in position 1 during a time interval DT_s (phase 1), and in position 2 during an interval $D'T_s$, with $D' = 1 - D$. D is called the duty cycle. T_s is the switching period, and $f_s = 1/T_s$ is the switching frequency. The voltage V_s is equal to the input voltage V_{in} when the switch is in position 1 and equal to zero when the switch is in position 2.

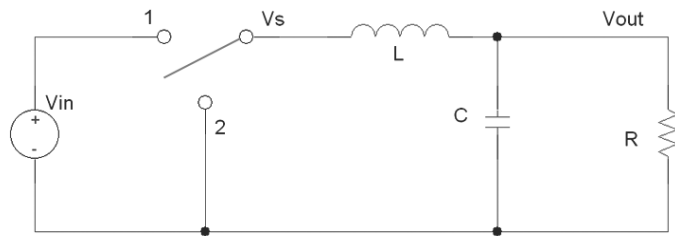


Figure 5.2: Power stage of a buck converter.

The DC component of V_s is equal to DV_{in} . The inductor and the capacitor form a low-pass filter. As a consequence, the DC voltage V_{out} on the load R is equal to DV_{in} . The Buck converter is able to convert a voltage to a lower voltage, with a better efficiency than linear converters, especially if the difference between V_{in} and V_{out} is important. The ratio between the output voltage and the input voltage is

$$\frac{V_{out}}{V_{in}} = D. \quad (5.1)$$

Since $D \leq 1$, this formula confirms the fact that a buck converter can only lower or maintain equal the input voltage. This is actually reflected by the name of the converter which is related to the verb “to buck”.

This formula is true assuming that all components are ideal. In practice, the switch is composed of semiconductor devices, i.e. a transistor and a diode, which implies switching losses. Furthermore, the inductor and the capacitor have a series resistance. To take losses into account, a coefficient is introduced in the formula. This coefficient is the efficiency η of the converter,

$$\frac{V_{out}}{V_{in}} = \eta D. \quad (5.2)$$

Inductor design

The three main criteria to choose the inductor are:

- The current ripple in the inductor is inversely proportional to the inductance. A good practical rule is to keep the ripple below 20% of the maximum inductor DC current.
- The saturation current of the inductor must be higher than the inductor peak current I_{max} .
- The equivalent series resistance of the inductor must be low, to avoid power losses.

The voltage across the inductor, $v_L(t)$, is equal to $V_s(t) - V_{out}(t)$. The inductance and the capacitor form a second-order low-pass filter. This filter attenuates the high frequencies components of V_s . If the filter is well designed, the variation of V_{out} can be neglected. We have $v_L(t) = V_{in} - V_{out}$ when the switch is in position 1, and $v_L(t) = -V_{out}$ when it is in position 2.

The relation between v_L and i_L is $v_L(t) = L \frac{di_L(t)}{dt}$. Thus, the slope of the inductor current is

$$\frac{di_L(t)}{dt} = \frac{V_{in} - V_{out}}{L} \text{ during phase 1.} \quad (5.3)$$

$$\frac{di_L(t)}{dt} = \frac{-V_{out}}{L} \text{ during phase 2.} \quad (5.4)$$

The inductor current is illustrated in Fig. 5.3 (third curve).

The maximum current in the inductor, I_{max} is equal to I_{av} , the average current in L plus half the current ripple Δi_L (peak to peak). The average current I_{av} is equal to the current I_{out} flowing in the load. We can thus write

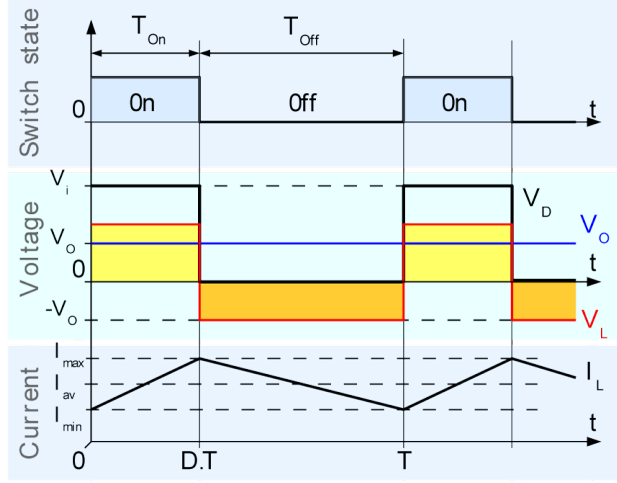


Figure 5.3: Evolution of voltages and currents in a buck converter (from Wikipedia).

$$I_{max} = I_{out} + \frac{\Delta i_L}{2}, \quad (5.5)$$

where the ripple Δi_L is given by the slope of i_L times the phase 1 interval, i.e. DT_s . As a result, we get

$$\Delta i_L = DT_s \frac{V_{in} - V_{out}}{L}. \quad (5.6)$$

$$I_{max} = I_{out} + \frac{V_{out}(V_{in} - V_{out})}{V_{in} 2\eta f_s L}. \quad (5.7)$$

The literature recommends to have a value of Δi_L which lie in the range of 0.2 to 0.4 I_{out} (with maximum load) [16]. We write the constraint as

$$\Delta i_L < k I_{out}, \quad (5.8)$$

where $k \in [0.2; 0.4]$.

Using the above equation, we get

$$L > \frac{V_{out}(V_{in} - V_{out})}{V_{in} \eta k f_s I_{out}}. \quad (5.9)$$

which provides the minimum value for the inductance.

The power losses in the inductor are equal to $I_{av}^2 R_L$, where R_L is the series resistance of the inductor. They represent a loss of 1% efficiency if

$$R_L < 0.01 \frac{V_{out}}{I_{out}} = 0.01R. \quad (5.10)$$

We now have all the elements necessary to design the inductor. The procedure is as follows:

- The inductance is given by Eq. 5.9, with maximum V_{in} and maximum I_{out} .
- The peak current in the inductor is given by Eq. 5.7, with maximum V_{in} and maximum I_{out} .
- An acceptable inductor series resistance is given by Eq. 5.10.

Capacitor design

From the integration of $i_C = C \frac{dv_C}{dt}$ and Fig. 5.3, the voltage ripple on the capacitor Δv_C is found to be

$$\Delta v_C = \frac{\Delta i_L T_s}{8C}. \quad (5.11)$$

Using the value of Δi_L given by Eq. 5.6, we have

$$\Delta v_C = \frac{V_{out}}{\eta V_{in}} \frac{V_{in} - V_{out}}{8f_s^2 LC}, \quad (5.12)$$

$$C = \frac{V_{out}}{\eta V_{in}} \frac{V_{in} - V_{out}}{8f_s^2 L \Delta v_C}. \quad (5.13)$$

This formula gives the value of the capacitor C corresponding to a chosen voltage ripple Δv_C .

"Boost" converter [16]

Principle

The power stage of a boost converter includes the same components than a Buck converter, but the position of the switch and the inductor are inverted (Fig. 5.4). The switch is in position 1 during a time interval DT_s (phase 1) and in position 2 during an interval $D'T_s$ (phase 2), with $D' = 1 - D$.

In phase 1, the voltage v_L across the inductor is equal to the input voltage V_{in} . The inductor is being charged of magnetic energy. The current in the inductor is increasing and the slope of the waveform is given by $v_L(t) = L \frac{di_L(t)}{dt}$. The variation of i_L over the phase 1 is

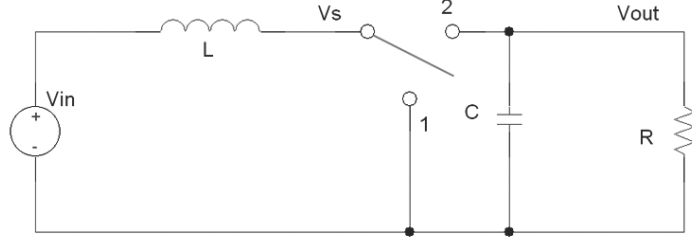


Figure 5.4: Power stage of a boost converter.

$$\Delta i_{L,1} = \frac{V_{in}DT_s}{L}. \quad (5.14)$$

In the phase 2, the magnetic energy of the inductor is released. The voltage across the inductor is inverted. $V_s = V_{in} + v_L$ and $V_{out} = V_s$. As a result, C is charged at a voltage higher than V_{in} . The current in the inductor i_L is decreasing and the variation over the phase 2 is

$$\Delta i_{L,2} = \frac{(V_{in} - V_{out})D'T_s}{L}. \quad (5.15)$$

In steady-state (Fig. 5.5), the net variation of i_L equals zero.

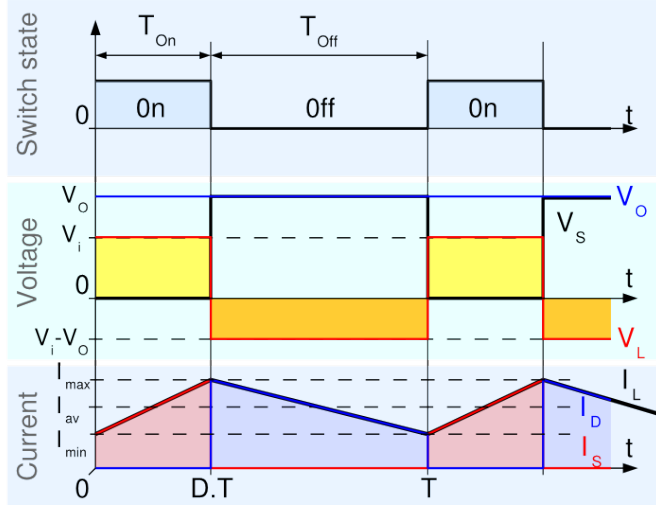


Figure 5.5: Evolution of voltages and currents in a boost converter (from Wikipedia).

As a consequence, from Eq. 5.14 and Eq. 5.15, we have

$$\Delta i_{L,1} + \Delta i_{L,2} = 0, \quad (5.16)$$

$$V_{in}D + (V_{in} - V_{out})D' = 0, \quad (5.17)$$

$$V_{in} = V_{out}D', \quad (5.18)$$

$$\frac{V_{out}}{V_{in}} = \frac{1}{D'}. \quad (5.19)$$

Since $D' \leq 1$, this formula confirms the fact that a boost converter can only raise or maintain equal the input voltage. This is actually reflected by the name of the converter which is related to the verb “to boost”.

Introducing the losses, the expression becomes

$$\frac{V_{out}}{V_{in}} = \frac{\eta}{D'}. \quad (5.20)$$

Inductor design

In steady state, the net change in the capacitor charge over one switching period must be equal to zero. During phase 1, the capacitor supplies the load. During phase 2, the current from the inductor recharges the capacitor and supplies the load. The charge balance equation is thus

$$-I_{out}DT_s + (I_{av} - I_{out})D'T_s = 0 \quad (5.21)$$

where I_{av} is the average current in the inductor. This leads to

$$I_{av} = \frac{I_{out}}{D'} \quad (5.22)$$

The literature recommends to have a value of Δi_L which lie in the range of 0.2 to 0.4 I_{out} (with maximum load) [16]. We write the constraint as

$$\Delta i_L < kI_{av}, \quad (5.23)$$

where $k \in [0.2; 0.4]$.

Using the above equation, we get

$$\frac{V_{in}D}{f_s L} < k \frac{I_{out}}{D'}, \quad (5.24)$$

$$\frac{V_{in}(1 - \frac{\eta V_{in}}{V_{out}})}{f_s L} < k \frac{I_{out}V_{out}}{\eta V_{in}}, \quad (5.25)$$

$$L > \frac{V_{in}^2 \eta (V_{out} - \eta V_{in})}{V_{out}^2 I_{out} k f_s}. \quad (5.26)$$

which provides the minimum value for the inductance.

To find the largest possible value of the RHS of Eq. 5.26, we take the derivative of the numerator $N = V_{in}^2 V_{out} - \eta V_{in}^3$, i.e.

$$\frac{dN}{dV_{in}} = 2V_{in}V_{out} - 3\eta V_{in}^2. \quad (5.27)$$

This gives

$$V_{in} = \frac{2V_{out}}{3\eta} \quad (5.28)$$

This value of V_{in} is used if it is in the range of possible V_{in} for the converter. Otherwise the closed V_{in} within the range of possible V_{in} is used.

The peak current in the inductor is thus successively given by

$$I_{max} = \max \left\{ I_{av} + \frac{\Delta i_L}{2} \right\} \quad (5.29)$$

$$I_{max} = \max \left\{ \frac{I_{out}}{D'} + \frac{V_{in}D}{2Lf_s} \right\} \quad (5.30)$$

$$I_{max} = \max \left\{ \frac{I_{out}V_{out}}{\eta V_{in}} + \frac{V_{in}(V_{out} - \eta V_{in})}{2Lf_s V_{out}} \right\} \quad (5.31)$$

The power losses in the inductor are equal to $I_{av}^2 R_L$, where R_L is the series resistance of the inductor. They represent a loss of 1% efficiency if

$$R_L < 0.01 \frac{V_{out} D'^2}{I_{out}} = 0.01 D'^2 R. \quad (5.32)$$

We now have all the elements necessary to design the inductor. The procedure is as follows:

- The inductance is given by Eq. 5.26, where V_{in} is given by Eq. 5.28 and at maximum I_{out} .
- The peak current in the inductor is given by Eq. 5.31, with maximum V_{in} and maximum I_{out} .
- An acceptable inductor series resistance is given by Eq. 5.32.

Capacitor design

During phase 1, $\frac{dv_C}{dt} = \frac{i_C}{C} = \frac{-I_{out}}{C}$, and during phase 2, $\frac{dv_C}{dt} = \frac{i_C}{C} = \frac{I_{av} - I_{out}}{C}$.

If the slope of v_C during one phase is known, the voltage ripple on the capacitor Δv_C can be obtained as follows:

$$\Delta v_C = \frac{I_{out}D}{C f_s} \quad (5.33)$$

Using the value of Δi_L given by Eq. 5.14, we have

$$C = \frac{I_{out}D}{\Delta v_C f_s} \quad (5.34)$$

This formula gives the value of the capacitor C corresponding to a chosen voltage ripple Δv_C .

5.2.2 Design of 7.2V converter

Specifications

- Input voltage: 2.7V to 4.2V.
- Output voltage: 7.2V.
- Maximum output current: 420 mA.

The output voltage is higher than the input voltage. A boost converter will be used.

Choice control IC

The converter is designed around the control integrated circuit (IC) TPS61087 from Texas Instruments. This IC includes the controller and the switch of the converter. An external rectifier diode must however be used. Fig. 5.6 shows the role of the TPS61087.

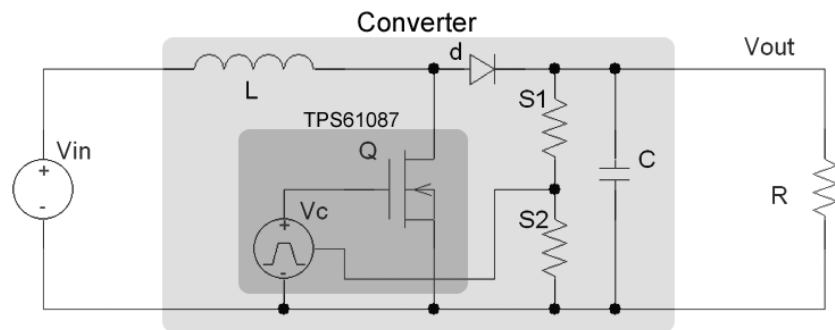


Figure 5.6: Simplified schematics of the 7.2V converter.

The advantages of TPS61087 control IC are:

1. Very small size (3×3 mm).

2. The switch is included.
3. High expected efficiency (85% to 90%).
4. Power PAD and thermal shutdown (the power PAD is a metallic area under the IC, that is soldered on the PCB for a better power dissipation).
5. There is a soft-start (this avoids a peak current call when the converter starts).

The choice of the control IC mainly depends on the properties of its internal switch. This switch must be able to:

1. withstand a current equal to I_{max} (when the switch is closed, the current is the same as in the inductor).
2. withstand a voltage of $V_{out} + V_{diode}$.
3. dissipate the heat due to switching losses and ohmic resistance.

This is verified below.

Maximum current in the switch

The maximum current will be determined during the inductor design. The switch is able to withstand 3.2A.

Maximum voltage on the switch

The TPS61087 can be used for an output voltage up to 18.5V.

Heat dissipation

The first version of the converter was designed with a slightly different model of control IC: the TPS61085 [3]. The internal circuitries of the TPS61087 and the TPS61085 are practically identical but the package (or case) is different. The TPS61085 has a 8-pin TSSOP package while the TPS61087 has a 10-pin QFN package.

With an output able to deliver 420mA at 7.2V, the 7.2V converter deals with quite important amounts of power for its size. An important part of the losses in the converter are localized in the semiconductor devices. For $V_{in} = 3V$ and maximum load, the losses in the whole converter were measured at 550mW (first prototype) [1]. The losses in the diode alone can easily be estimated once the average current in the inductor is known, i.e. $P = I_{av}V_{diode,2}D'$ (where I_{av} is the average current in the inductor, $V_{diode,2}$ is the voltage across the diode when it is forward biased, and D' is the complement of the duty cycle). For more precision, $V_{diode}(t)$ was measured and integrated to a Matlab code written to compute the ohmic diode losses. The above formula for P gives an ohmic loss of 225mW, which represents about 40% of the total losses. There are still about 330mW that are potentially dissipated in the control IC.

There is no data about the case to PBC thermal resistance in the datasheet of the TPS61085. Only the case to air thermal resistance is available but it is useless in vacuum. With no certitude about its capacity to dissipate the produced heat, it was decided to choose another IC, i.e. the TPS61087.

The TPS61087 is equipped with a “Power PAD”, which allow a good thermal contact between the case and the PCB. The junction-air thermal resistance is $30^{\circ}\text{C}/\text{W}$ when the Power PAD is soldered to the PCB. As the low thermal resistance is essentially due to the junction-PCB resistance, the thermal resistance will be close to $30^{\circ}\text{C}/\text{W}$ in vacuum.

From “Absolute Maximum Ratings”, the maximum operating junction temperature is 150°C . A margin of 25°C is taken. The converter is designed to work with a PCB temperature of -40°C to 85°C . The maximum dissipated power is

$$P_D = \frac{T_J - T_A}{R_{\vartheta JA}} = \frac{125 - 85}{30} = 1.33\text{W},$$

where T_J is the junction temperature, T_A the air (or PCB) temperature, and $R_{\vartheta JA}$ the thermal resistance between junction and air.

Switching frequency

The switching frequency f_s on the TPS61087 can be chosen to be 650kHz or 1200kHz. The efficiency can be improved by choosing a f_s of 650kHz but the ripple will be more important. The breadboard prototype was designed with $f_s = 650\text{kHz}$ while the engineering model uses a f_s of 1.2MHz. The tests show that the efficiency is practically the same with 1.2MHz as it is with 650kHz.

Design of inductor and capacitor

A worksheet was written to help with the design of the converters. The inputs are the minimum input voltage $V_{in,Min}$, the maximum input voltage $V_{in,Max}$, the output voltage V_{out} , the maximum output current $I_{out,Max}$, the expected efficiency η , the switching frequency f_s , the maximum ratio between the current ripple and the average current in the inductor k ($\Delta i_L/I_{av}$ max), and the maximum output voltage ripple Δv_{max} .

There are two steps.

In the step 1, the inductance is determined using Eqs. 5.26 and 5.28. The peak inductor current is found with Eq. 5.31 (it is computed for several values of V_{in} in a table and the maximum is kept). The desired series resistance and the output capacitor are also determined.

Results for $k = 0.3$, $\Delta v_{max} = 10\text{mV}$, and $\eta = 0.85$ are presented in Fig. 5.7. On the basis of these results, an inductor and a capacitor are selected. The inductance and the capacitance will not exactly correspond to the computed values (real components have standardized values).

In the second step, the worksheet is filled up with the values of real components (figure 5.9). We obtain the real values of the maximum current in the inductor and of Δv_{max} .

Forced values		
Name	Value	Unity
V_in_min	2,7000	[V]
V_in_max	4,2000	[V]
V_out	7,2000	[V]
I_out_max	0,4200	[A]
Efficiency	0,8500	[%]
Sw Frequ	1,20E+06	[Hz]
k	0,3000	no
DeltaV max	0,0100	[V]
Computed values		
Maximum Load	17,1429	[ohm]
Duty cycle max	0,6813	no
Duty cycle min	0,5042	no
Minimum L		
V_in (L_max)	5,6471	[V]
kept V_in (L_max)	4,2000	[V]
Duty cycle (L_max)	0,5042	no
L	6,94E-06	[H]
I_max	1,53	[A]
P_out	3,024	[W]
P_in	3,56	[W]
R_L (1%)	0,017417411	[ohm]
Minimum C		
C	2,38E-05	[F]

Figure 5.7: Worksheet for 7.2V converter, step 1.

Inductor selection

The chosen inductor is the EPCOS B82464Z4682M. A picture of the inductor is shown on Fig. 5.8. Its characteristics are given in table below.



Figure 5.8: Inductor EPCOS B82464Z4682.

Characteristics
Size: $10.4 \times 10.4 \times 4.8$ (mm)
$L = 6.8\mu H$
Magnetically shielded
Temperature range: up to $125^\circ C$
$R_{max} = 20m\Omega$
Rated current: 4.3A

Capacitor selection

Four $10\mu F$ ceramic capacitors in parallel are used at the output.

Forced values		
Name	Value	Unity
V_in_min	2,7000	[V]
V_in_max	4,2000	[V]
V_out	7,2000	[V]
I_out_max	0,4200	[A]
Efficiency	0,8500	[%]
Sw Frequ	1,20E+06	[Hz]
k	0,3062	no
DeltaV max	0,0060	[V]
Computed values		
Maximum Load	17,1429	[ohm]
Duty cycle max	0,6813	no
Duty cycle min	0,5042	no
Minimum L		
V_in (L_max)	5,6471	[V]
kept V_in (L_max)	4,2000	[V]
Duty cycle (L_max)	0,5042	no
L	6,80E-06	[H]
I_max	1,53	[A]
P_out	3,024	[W]
P_in	3,56	[W]
R_L (1%)	0,017417411	[ohm]
Minimum C		
C	4,00E-05	[F]

Figure 5.9: Worksheet for 7.2V converter, step 2.

From the second step, the value of the maximum inductor current is found to be 1.53A. This current is acceptable for the switch.

Design of other components

R_{comp} and C_{comp} :

Using $V_{in} = 3.7, C_{out} = 40\mu F, L = 6.8\mu H, I_{outMax} = 0.42A$. in the formulas from the TPS61087 datasheet, we find

$$R_{comp} = \frac{110V_{in}V_{out}C_{out}}{LI_{outMax}} = 41k\Omega,$$

$$C_{comp} = \frac{V_{out}C_{out}}{7.5I_{outMax}R_{comp}} = 2.126nF.$$

The real components chosen have the values $C_{comp} = 2.2nF$ and $R_{comp} = 41k\Omega$.

C_{ss}

A capacitor of 100nF is chosen, following the datasheet.

Schottky diode

The maximum operating junction temperature is 175°C. The junction to case resistance is 30°C/W.

For a PCB temperature of 85°C,

$$P_{diss} = \frac{175 - 85}{30} = 3W.$$

Feedback scaler (RFBA and RFBB)

For the output voltage regulation, the control IC measures the output voltage. The output voltage is too high to be directly used by the control IC, a voltage scaler must be used. It is composed on two resistors.

The internal reference of the control is 1.238V. The ratio RFBB / RFBA is thus 0.2076. If the resistances are too high, the feedback input bias current ($I_{FB} < 1.00E - 07A$) could influence the output voltage.

The real components chosen have the values RFBA = 86.6kΩ and RFBB = 18kΩ.

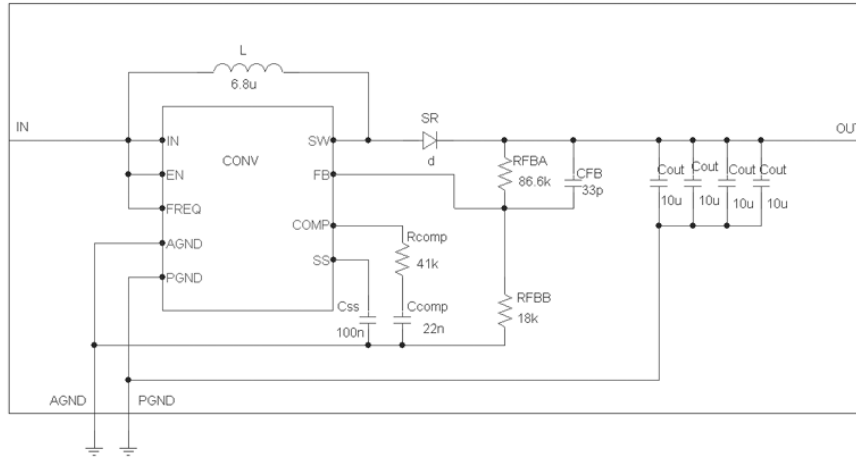


Figure 5.10: Schematics of 7.2V converter.

5.2.3 Design of 5V converter

Specifications

- Input voltage: 2.7V to 4.2V.

- Output voltage: 5V.
- Maximum output current: 200mA.

The output voltage is higher than the input voltage. A boost converter will be used.

Choice control IC

The LTC3528 from Linear Technology was chosen for the control IC. The device includes the control and the switch. There is no need of external rectifier diode (an internal FET takes the place of the diode).

The advantages of the LTC3528 model are:

1. Very small size.
2. High expected efficiency (90% to 95%).
3. A special mode improves efficiency at light load.
4. Power PAD and thermal shutdown.
5. There is a soft-start.
6. Low start-up voltage (700mV).

The choice of the control IC mainly depends on the properties of its internal switch. This switch must be able to:

1. withstand a current equal to I_{max} .
2. withstand a voltage of $V_{out} + V_{diode}$.
3. dissipate the heat due to switching losses and ohmic resistance.

This is verified below.

Maximum current in the switch

The switch is able to withstand 1A.

Maximum voltage on the switch:

The LTC3528 can be used for an output voltage from 1.6V to 5.25V.

Heat dissipation:

The junction to air thermal resistance $R_{\theta JA}$ of the LTC3528 is equal to $76^{\circ}\text{C}/\text{W}$ when the power PAD is soldered. The maximum operating junction temperature is 125°C . A margin of 25°C is taken. The converter is designed to work with a PCB temperature of -40°C to 85°C . The maximum dissipated power is

$$P_D = \frac{T_J - T_A}{R_{\theta JA}} = \frac{100 - 85}{76} = 0.2\text{W}.$$

Switching frequency

The switching frequency of the LTC3528 is 1MHz.

Design of inductor and capacitor

The same worksheet as for the 7.2V converter is used to find a good compromise between k and the size of the components. Results for $k = 0.84$, $\Delta v_{max} = 10\text{mV}$, and $\eta = 0.90$ are presented in Fig. 5.11. The coefficient k does not lie in the usually recommended range. To have a lower k, the inductance must be higher, and as a consequence, the inductor is bigger, which is not in our interest. The LTC3528 can be quite efficient with a quite high k because it enters in "burst mode" when the load is light. In this mode, the converter is active during a "burst" period, to charge the output capacitor; then the load slowly discharges the capacitor. The burst mode is illustrated in Fig. 5.12.

Forced values		
Name	Value	Unity
V_in_min	2,7000	[V]
V_in_max	4,2000	[V]
V_out	5,0000	[V]
I_out_max	0,2000	[A]
Efficiency	0,9000	[%]
Sw Frequ	1,00E+06	[Hz]
k	0,8760	no
DeltaV max	0,0100	[V]
Computed values		
Maximum Load	25,0000	[ohm]
Duty cycle max	0,5140	no
Duty cycle min	0,2440	no
Minimum L		
V_in (L_max)	3,7037	[V]
kept V_in (L_max)	3,7037	[V]
Duty cycle (L_max)	0,3333	no
L	4,70E-06	[H]
I_max	0,59	[A]
P_out	1	[W]
P_in	1,11	[W]
R_L (1%)	0,059049	[ohm]
Minimum C		
C	1,03E-05	[F]

Figure 5.11: Worksheet for 5V converter.

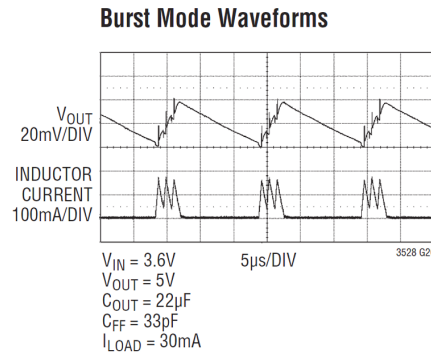


Figure 5.12: Burst mode operation (Source: LTC3528 datasheet).

The maximum inductor current is 0.59A. This current is acceptable for the switch, which can withstand 1A.

Inductor selection

The chosen inductor is the EPCOS B82472P6472M000. Its characteristics are given in table below.

The chosen model is the

Characteristics
Size: $7.3 \times 7.3 \times 4.5(\text{mm})$
$L = 4.7\mu H$
Magnetically shielded
Temperature range: up to 150°C
Automotive
$R_{max} = 33m\Omega$
Saturation current: 2A

Capacitor Selection:

One $10\mu F$ ceramic capacitors.

Design of feedback scaler

The internal reference of the control is 1.2V. The ratio RFBB / RFBA is thus 0.3158. If the resistances are too high, the feed-back input bias current ($I_{FB} < 1,00E - 07A$) could influence the output voltage.

The real components chosen have values of $RFBA = 100k\Omega$ and $RFBB = 31.6k\Omega$.

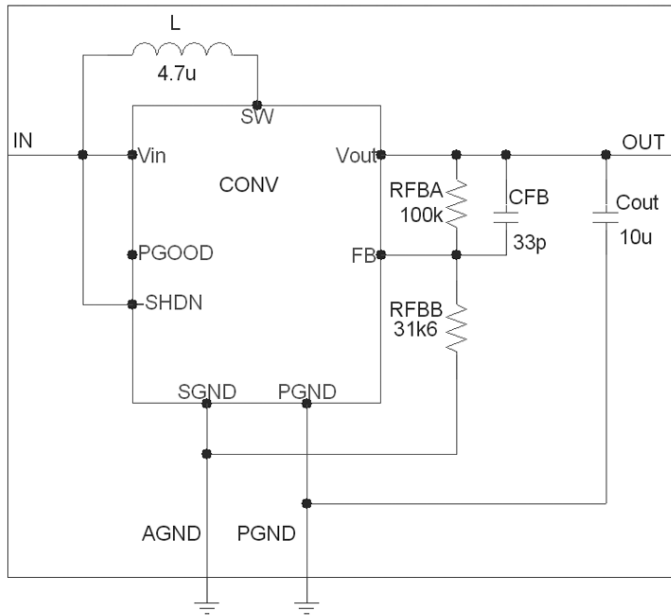


Figure 5.13: Schematics of 5V converter.

5.2.4 Design of 3.3V converter

Specifications

- Input voltage: 2.7V to 4.2V.
- Output voltage: 3.3V.
- Maximum output current: 200 mA.

The output voltage can be higher or lower than the input voltage. A buck-boost converter will be used. This is a converter able to take the configuration of a buck converter or of a boost converter, depending upon the input voltage.

Choice of control IC

The chosen control IC is the TPS63001. The TPS63001 can switch between boost or buck mode. There are two switches (each implemented by two field-effect transistors). A simplified schematics is shown in figure 5.14. When in Buck mode, the switch S2 stays in position 2 while the switch S1 is working at the switching frequency. For the Boost mode, S1 is kept in position 1 and S2 is working at the switching frequency. The switches and the control are included in the integrated circuit.

The advantages of this model are:

1. Very small size (3×3 mm).

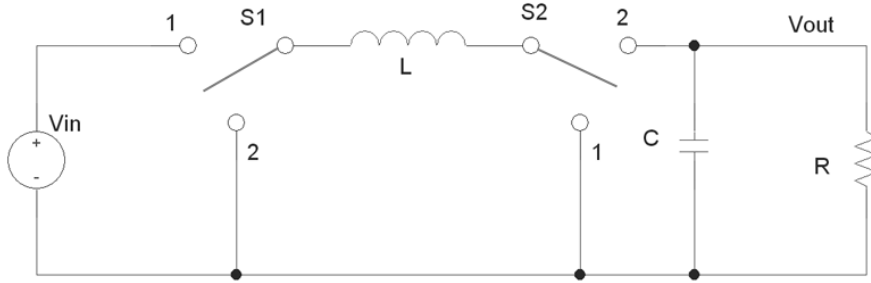


Figure 5.14: Simplified schematics of the 3.3V converter.

2. Switches are included.
3. High expected efficiency (more than 90%).
4. Power PAD and thermal shutdown.
5. There is a soft-start.

The choice of the control IC mainly depends on the properties of its internal switch. This switch must be able to:

1. withstand a current equal to I_{max} .
2. withstand a voltage of $V_{out} + V_{diode}$ (in boost mode).
3. dissipate the heat due to switching losses and ohmic resistance.

This is verified below.

Maximum current in the switch:

The switches are able to withstand 1.6A.

Maximum voltage on the switch:

The TPS61001 is designed for an output voltage of 3.3V.

Heat dissipation:

The junction to air thermal resistance $R_{\theta JA}$ of the TPS63001 is equal to $48.7^{\circ}\text{C}/\text{W}$ when the power PAD is soldered. The maximum operating junction temperature is 150°C . A margin of 25°C is taken. The converter is designed to work with a PCB temperature of -40°C to 85°C . The maximum dissipated power is

$$P_D = \frac{T_J - T_A}{R_{\theta JA}} = \frac{125 - 85}{45.7} = 0.82\text{W}.$$

Switching frequency

The switching frequency of the TPS63001 is between 1,250 and 1,500 kHz.

Design of inductor and capacitor

The components of the 3.3V converter must suit for the two operation modes, buck and boost. Two worksheets were used, one for the design of the boost mode (it is the same worksheet as for the other converters), and one for the design of the buck mode (it is a new worksheet).

For the buck mode, the inductance is computed using Eq. 5.9. The peak inductor current is found with Eq. 5.7. The desired series resistance and the output capacitor are also determined with Eqs. 5.10 and 5.13.

The inputs are $V_{in,Min}$, $V_{in,Max}$, V_{out} , $I_{out,Max}$, the expected efficiency η , the switching frequency f_s , k ($\Delta i_L/I_{av}$ max), and Δv_{max} .

The $V_{in,Min}$ for the buck mode is equal to the $V_{in,Max}$ for the boost mode but it is not necessarily 3.3V. For a buck converter with an efficiency of η , the $V_{in,Min}$ is equal to $\frac{V_{out}}{\eta}$. Similarly, for a boost converter with an efficiency of η , the $V_{in,Max}$ is equal to $\frac{V_{out}}{\eta}$.

Inductor selection

The chosen inductor is the EPCOS B82472P6472M000. It is the same model as for the 5V converter. The inductance is $4.7\mu H$. With this value, the k is equal to 0.429 in the boost mode and equal to 0.633 in the buck mode. Once again, the k is quite high but the converter works fine with a high k (the recommended value for L in the datasheet is $2.2\mu H$).

Capacitor selection

One $10\mu F$ ceramic capacitor will be used at the output.

The maximum inductor current is 0.34A. This current is acceptable for the switch, which is able to withstand 1.6A.

Design of other components

C_{by} and R_{by}

R_{by} and C_{by} are decoupling components. Values of respectively 100Ω and $0.1\mu F$ are recommended by the datasheet of the TPS63001.

Schottky diode

The present 3.3V converter and the EPS2 [2] will have to work in parallel. The behavior of these system must be studied. The engineering model will be equipped of a Schottky diode on the output of the 3.3V converter, before the feedback loop. A jumper will be placed in parallel to short-circuit the diode if needed. The same model of diode as in the 7.2V converter is used.

Forced values		
Name	Value	Unity
V_in_min	2,5000	[V]
V_in_max	3,4737	[V]
V_out	3,3000	[V]
I_out_max	0,2000	[A]
Efficiency	0,9500	[%]
Sw Frequ	1,25E+06	[Hz]
k	0,4290	no
DeltaV max	0,0045	[V]
Computed values		
Maximum Load	16,5000	[ohm]
Duty cycle max	0,2803	no
Duty cycle min	0,0000	no
Minimum L		
V_in (L_max)	2,3158	[V]
V_in (L_max) ok	2,5000	[V]
Duty cycle (L_max)	0,2803	no
L	4,70E-06	[H]
I_max	0,34	[A]
P_out	0,66	[W]
P_in	0,69	[W]
R_L (1%)	0,085464015	[ohm]
Minimum C		
C	9,97E-06	[F]

Figure 5.15: Worksheet for 3.3V converter in boost mode.

5.2.5 Remarks

If the HF amplifier is not supplied in 7.2V

The role of 7.2V converter is to supply the HF amplifier. The amplifier is still in an early state of development, and even if the maximum required power can be estimated, the required voltage is not really determined. The controller of the 7.2V converter, the TPS61087, has also been chosen because it is able to deliver a stabilized voltage between 5V and 18.5V. If the HF amplifier is not supplied with 7.2V, but has to be supplied in any voltage in the 5V to 18.5V range, the circuit will be easy to modify. As long as the TPS61087 is used, all the development steps of section 5.2.2 can be followed and adopted.

Values of the coefficient "k"

In this report, the coefficient k is the ratio between the current ripple and the average current in the inductor of a converter,

$$k = \frac{\Delta i_L}{I_{av}}$$

The literature about switching converters recommends using a k of 20% to 40% [16]. The

Forced values		
Name	Value	Unity
V_in_min	3,4737	[V]
V_in_max	4,2000	[V]
V_out	3,3000	[V]
I_out_max	0,2000	[A]
Efficiency	0,9500	[%]
Sw Frequ	1,25E+06	[Hz]
k	0,6330	no
DeltaV max	0,0013	[V]
Computed values		
Maximum Load	16,5000	[ohm]
Duty cycle max	1,0000	no
Duty cycle min	0,8271	no
Minimum L		
L	4,70E-06	[H]
I_max	0,21	[A]
P_out	0,66	[W]
P_in	0,69	[W]
R_L (1%)	0,165	[ohm]
Minimum C		
C	9,97E-06	[F]

Figure 5.16: Worksheet for 3.3V converter in buck mode.

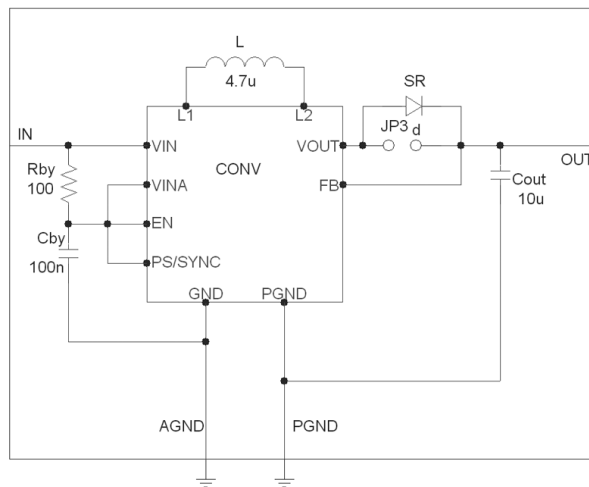


Figure 5.17: Schematics of 3.3V converter.

given reason is that a higher k would mean higher peak currents in inductors and semiconductor devices, and it would increase the size and cost of these components.

This is maybe true for high power devices, but in our case, the available inductors had saturation currents (or rated currents) much higher than the computed peak current. Con-

sequently, the k was chosen above 0.4 in our two converters. The more limiting factor was the series resistance, which grows quickly when the size of the inductor is decreased (the section of the wire is reduced).

5.3 Design of input filters

An undesirable feature of switch-mode power converters is their generation of conducted and radiated electromagnetic interference (EMI) on their input at the switching frequency and its harmonics. The power source and other systems supplied by the same power sources can be corrupted by EMI currents, if not filtered. Without filtering, EMI will be radiated by the input line and interfere with the operation of near equipments, especially radio equipments.

5.3.1 Type of filter

The datasheets of the converters used in section 5.2 (TPS63001, TPS61087, and LTC3528) recommend using one $4.7\mu F$ to $10\mu F$ ceramic capacitor close to the input of the converter. With the resistance of the source and the input line, this makes up a first-order low-pass filter. This may be sufficient in most of the usual applications for these converters, when they are directly connected to a battery.

In our application, the converters are connected to the batteries bus. The impedance of the bus seen from a converter is the impedance of the line plus the impedance of all the systems connected to this bus in parallel (two batteries, five solar panels, two other converters, the EPS2...). As a consequence, the impedance may be quite low and it is difficult to know the cut-off frequency of the input filter if it only consists in a capacitor.

Therefore, second-order low-pass filters will be used for the converter inputs. Second-order filters offer a better attenuation per decade of EMI and their cut-off frequencies can be chosen with precision.

5.3.2 Stability problem

As explained in Chapter 10 of [16], a converter is designed to have an input-to-output transfer function $G_{vg}(s)$ (the "audiosusceptibility") sufficiently small over a wide frequency range. The output voltage is regulated in spite of variations in the input voltage. The introduction of an input filter will change the dynamics of the converter, often in a manner that degrades the regulator performance. The audiosusceptibility is degraded and there are conditions under which the system may even go unstable.

The input power of a converter is more or less constant with the input voltage ($P_{in} = P_{out}/\eta$), thus one can write

$$P_{in} = V_{in}I_{in} \Rightarrow V_{in} = \frac{P_{in}}{I_{in}} \Rightarrow \frac{dV_{in}}{dI_{in}} = \frac{-P_{in}}{I_{in}^2} = \frac{-V_{in}}{I_{in}}. \quad (5.35)$$

Equation 5.35 is a simplification. In actuality, the control loop impacts the frequency response of the input impedance. As a consequence, the input impedance is not constant with frequency. The important thing to observe is that the slope of the voltage-current curve, which defines the dynamic impedance of the power supply, is negative (Fig. 5.18).

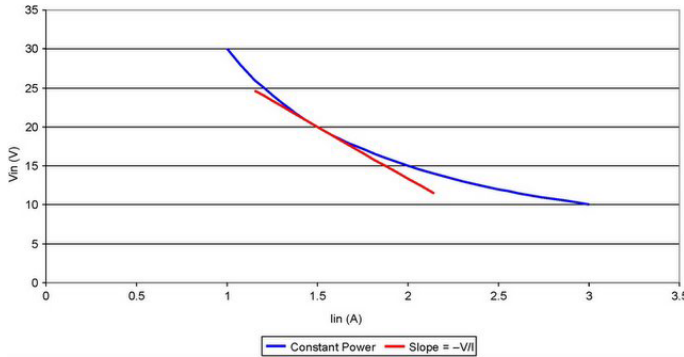


Figure 5.18: V-I curve of a converter input (from [24]).

If the source impedance and the dynamic input impedance of the converter have equal values but opposite signs at a given frequency, the voltage tends to infinity. The system is then unstable. The circuit corresponding to this situation is shown in Fig. 5.19.

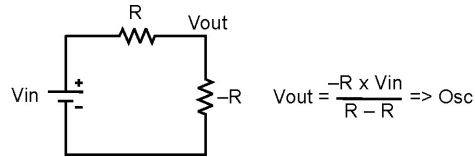


Figure 5.19: The negative impedance can result in oscillations (from [24]).

A good solution to have a stable system is to ensure that the magnitude of the output impedance of the source is always smaller than the magnitude of the input impedance of the converter. The impedance of the converter must be considered when it is minimal, i.e. with the lowest input voltage and the highest load.

Details on this stability problem are found in [24] and [16].

5.3.3 Middlebrook's criterion

The Middlebrook's extra element theorem can be employed to determine how the addition of an input filter affects the control-to-output transfer function [16]. The modified control-to-output transfer function can be expressed as follows

$$G_2 = G_1 \frac{1 + \frac{Z_o(s)}{Z_N(s)}}{1 - \frac{Z_o(s)}{Z_D(s)}},$$

where G_1 is the initial control-to-output transfer function and G_2 is the modified one, $Z_o(s)$ is the output impedance of the input filter, $Z_N(s)$ is the converter input impedance if the feedback controller operates ideally, and $Z_D(s)$ is the converter impedance in open-loop [16]. One can see that the control-to-output transfer function is not substantially affected by the addition of an input filter if the following inequalities are satisfied:

$$\|Z_o(s)\| \ll \|Z_N(s)\|, \quad (5.36)$$

$$\|Z_o(s)\| \ll \|Z_D(s)\|. \quad (5.37)$$

These inequalities give a maximum allowable output impedance of the input filter.

Formulas for $Z_N(s)$ and $Z_D(s)$ are available in Table 10.1, p. 382, of [16]). For example, for the boost converter, we have

$$Z_N(s) = -D'R^2 \left(1 - \frac{sL}{D'^2R} \right), \quad (5.38)$$

$$Z_D(s) = -D'R^2 \frac{\left(1 + \frac{sL}{D'^2R} + \frac{s^2LC}{D'^2} \right)}{1 + sRC}. \quad (5.39)$$

5.3.4 Comparison between Middlebrook's criterion ($Z_D(s)$ and $Z_N(s)$) and measured $Z_{in}(s)$

The first 7.2V converter prototype was following characterized by $L = 6.8\mu H$, $C = 20\mu F$, and $V_{out} = 7.2V$. The lowest impedance is obtained at $V_{in,Min}$ (here V_{in} is set to 3V, which corresponds to $D' = 0.354$) and maximum load (here $R = 17.2\Omega$).

Middlebrook

These characteristics where inserted in the Eqs. 5.38 and 5.39 implemented in Matlab. The resulting Bode diagram is shown on Fig. 5.20.

Measurement

The input impedance of the converter in the same conditions was experimentally measured. The complete description of the test can be found in our test report [1]. The plot of $Z_{in}(f)$ is shown on Fig. 5.21.

Conclusions

The shapes of the gain curves of measured $Z_{in}(f)$ and $Z_D(s)$ are similar. On the measured curve, the low gain under 1kHz is due to a measurement error; the real gain is between 5 and

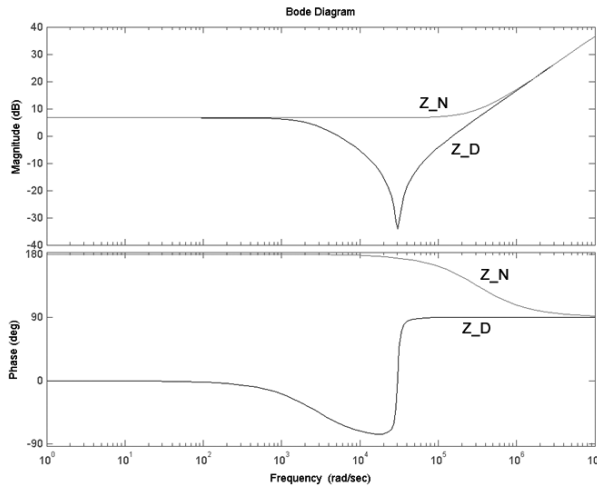


Figure 5.20: Computed Bode diagram of $Z_D(\omega)$ and $Z_N(\omega)$ for the 7.2V converter.

$10dB\Omega$. The most intriguing difference is that the minimum of the measured Z_{in} occurs at a frequency of 350kHz while the minimum of Z_D obtained with Eq. 5.39 is located at 30k rad/s (4.77kHz).

It is very unlikely that such a difference is due to a measurement error. One possible explanation is that the controller design and the switching frequency have an influence on the input impedance (Middlebrook's equations do not take them into account). No obvious explanation was found concerning this difference.

The input filter on the engineering model will be designed from the measured curves. The stability of the converters with these filters will be experimentally verified.

5.3.5 Measurements of the input impedance of the converters

Measurements on first prototype

The input impedance of the three converters was measured on the “breadboard” prototype. The measurements were made in the conditions under which the converters have the lowest $Z_{in}(f)$, i.e. for the maximum load and the minimum input voltage for the boost converters, and for the maximum load and maximum input voltage for the buck converter. We produced four measured plots, i.e. for

- the 3.3V converter with $V_{in} = 2.5V$ and $R = 36\Omega$ (Fig. 5.22).
- the 3.3V converter with $V_{in} = 4.2V$ and $R = 36\Omega$ (Fig. 5.23).
- the 5V converter with $V_{in} = 2.5V$ and $R = 24\Omega$ (Fig. 5.24).
- the 7.2V converter with $V_{in} = 3V$ and $R = 17.2\Omega$ (Fig. 5.25).

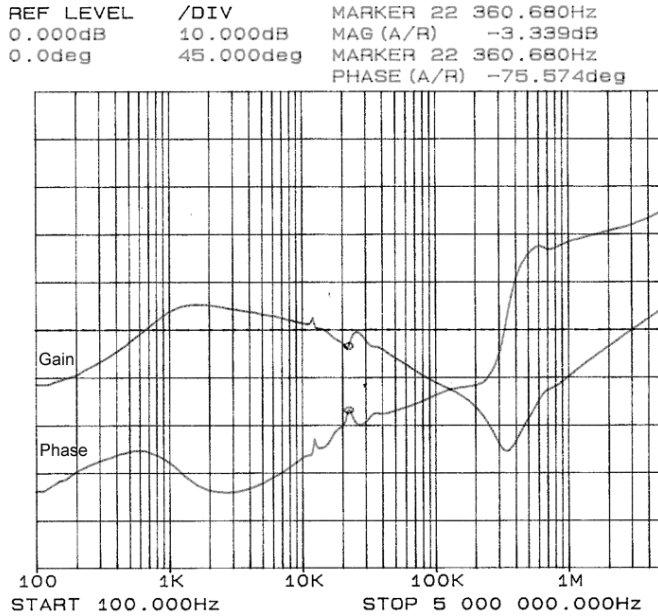


Figure 5.21: Measured Bode diagram of $Z_{in}(f)$.

However, some values of L and C used on the “breadboard” prototypes were modified while designing the engineering model (the engineering model uses the values given in this document). The plot measured on the breadboard model can be adapted to the situation of the engineering model.

Adaptation to new converters

The shape of a $Z_{in}(s)$ curve is composed of three main parts:

1. At low frequency, it is nearly constant. This part is essentially influenced by the load R.
2. At mid frequencies, the curve has a slope of -20dB/decade. This corresponds to the influence of C.
3. At high frequencies, the curve has a slope of +20dB/decade. There L has the more influence.

The impedance of a circuit composed of an inductor in series with a condensator and a resistor that are in parallel would have a similar shape ($Z_L(s) = sL$, $Z_C(s) = \frac{1}{sC}$, and $Z_R(s) = R$, where $Z_L(s)$ is the impedance of an inductor with a inductance L, $Z_C(s)$ the impedance of a capacitor with a capacitance C, and $Z_R(s)$ the impedance of a resistor with a resistance R). In the case of a converter, the shape of $Z_{in}(s)$ is determined by R, L, and C seen from the input through the converter. The observed curve is in fact $\alpha L + (\beta R // \gamma C)$ with α , β , and γ depending on the characteristics of the converter (Fig. 5.26).

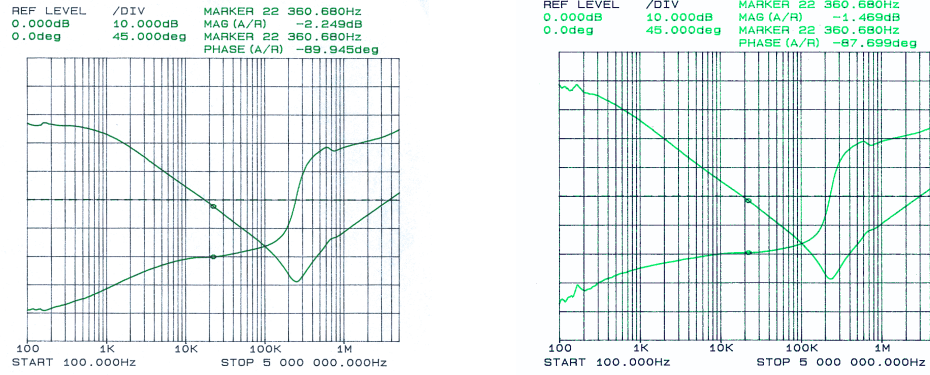


Figure 5.22: Z_{in} of 3.3V converter with $V_{in} = 2.5V$.
 Figure 5.23: Z_{in} of 3.3V converter with $V_{in} = 4.2V$.

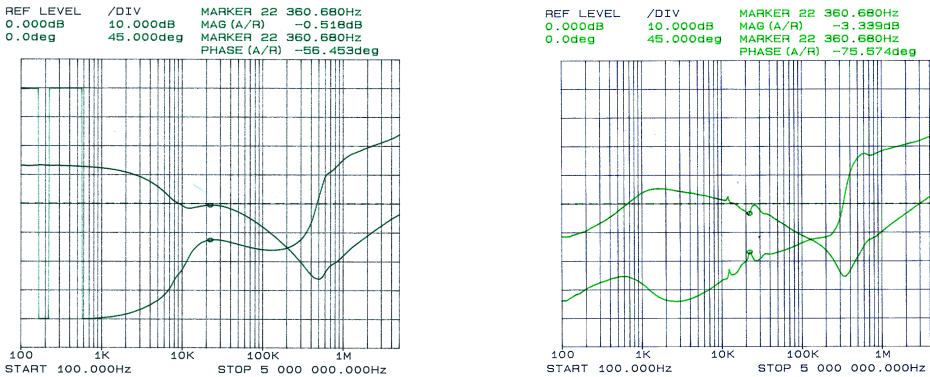


Figure 5.24: Z_{in} of 5V converter with $V_{in} = 2.5V$.
 Figure 5.25: Z_{in} of 7.2V converter with $V_{in} = 3V$.

As a consequence, if L, C, or R is modified, the new curve can be found by a translation of the corresponding part of the curve.

3.3V converter

L was $2.2\mu H$ (L1) and becomes $4.7\mu H$ (L2). $Z_L(s) = sL$, so we have $Z_{L2}(s) = \alpha Z_{L1}(s) = \alpha sL_1$ with $\alpha = 4.7/2.2 = +6.6dB$.

C was $20\mu F$ (C1) and becomes $10\mu F$ (C2). $Z_{C2}(s) = \frac{1}{sC^2} = \frac{1}{\gamma sC_1} = \frac{Z_{C1}(s)}{\gamma}$ with $\frac{1}{\gamma} = 20/10 = +6dB$.

5V converter

L is unchanged. C was $15\mu F$ (C1) and becomes $10\mu F$ (C2). $\frac{1}{\gamma} = 15/10 = +3.5dB$.

7.2V converter

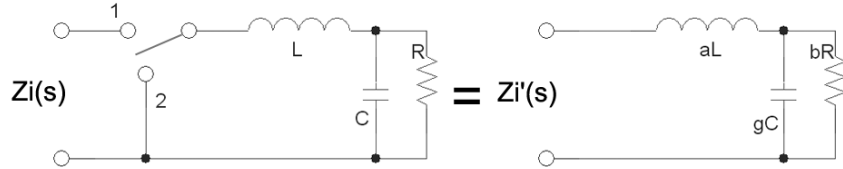


Figure 5.26: Equivalence between the input impedance of a converter and the input impedance of a LRC network.

L is unchanged. C was $20\mu F$ (C_1) and becomes $40\mu F$ (C_2). $\frac{1}{\gamma} = 20/40 = -6dB$.

Figures 5.22 to 5.25 show the results of translating the “old” magnitude curves to their new positions.

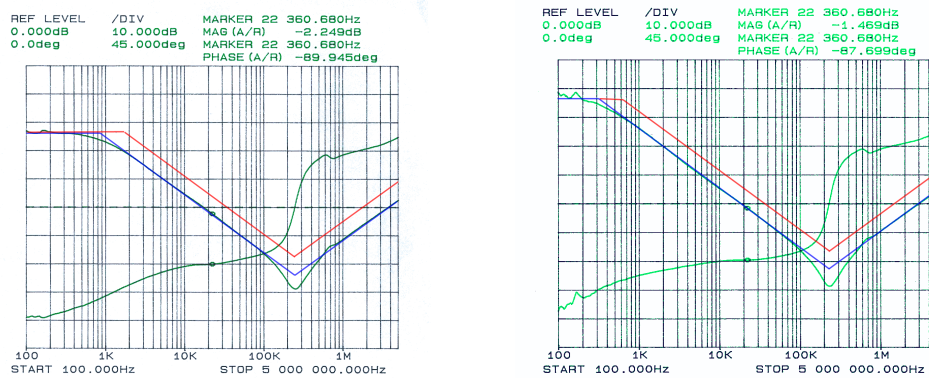


Figure 5.27: $\|Z_{in}\|$ of old (blue) and new Figure 5.28: $\|Z_{in}\|$ of old (blue) and new (red) 3.3V converter with $V_{in} = 2.5V$. (red) 3.3V converter with $V_{in} = 4.2V$.

5.3.6 Frequency design of the filters

The same filter will be used for the three converters. The filter must be designed so that its output impedance is lower than the input impedance of the converters. The 7.2V converter has the lowest $\|Z_{in}(s)\|$. The filter can be designed from the $\|Z_{in}(s)\|$ curve of the 7.2V converter.

A second-order low-pass filter is composed of a capacitor C_f and an inductor L_f connected as shown in Fig. 5.31. The output impedance of this filter is $Z_{out}(s) = Z_{Lf}(s)/Z_{Cf}(s)$. The shape of $\|Z_{out}\|$ is shown on Fig. 5.32. It is characterized by the resonant frequency f_f , the characteristic impedance R_{0f} , and the quality factor Q_f (infinite on this ideal case).

The values of f_f and R_{0f} are given by ([16])

$$f_f = \frac{1}{2\pi\sqrt{L_f C_f}}$$

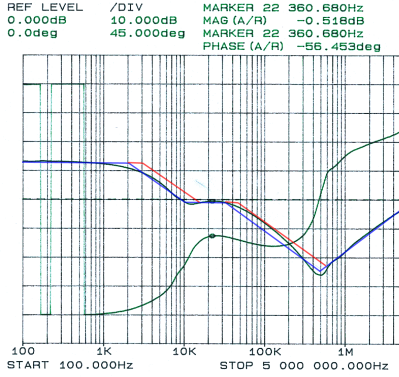


Figure 5.29: $\|Z_{in}\|$ of old (blue) and new (red) 5V converter with $V_{in} = 2.5V$.

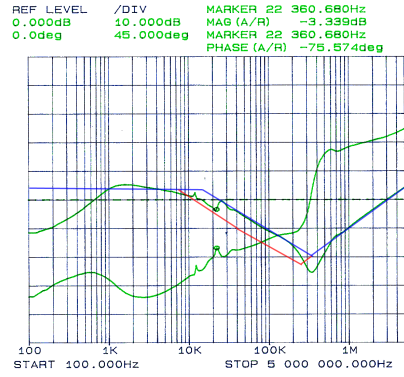


Figure 5.30: $\|Z_{in}\|$ of old (blue) and new (red) 7.2V converter with $V_{in} = 3V$.

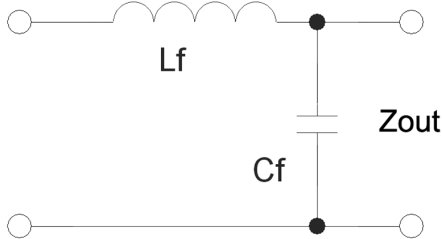


Figure 5.31: Schematics of a basic second-order low-pass filter.

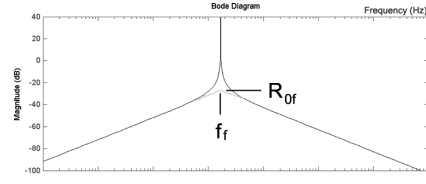


Figure 5.32: Output impedance of a basic second-order low-pass filter.

$$R_{0f} = \sqrt{\frac{L_f}{C_f}}$$

The design of the input filter can be seen as the placement of f_f and R_{0f} on the Bode diagram. A higher f_f corresponds to smaller electronic components, which is in our interest (but we must keep an eye on the desired attenuation at the switching frequency). R_{0f} cannot be too low otherwise the size of the capacitor becomes a concern.

There is a last obstacle to the good design of an input filter. As seen on Fig. 5.32, there is a peak at the resonant frequency, due to the high quality factor Q_f . Z_{out} can thus exceed the input impedance of the converter at f_f . To reduce Q_f , the filter must be damped. The damping can be done using a capacitor C_{fd} with a series resistance R_{fd} in parallel with the filter capacitor. Formulas to compute the optimal C_{fd} and R_{fd} can be found in [16]. A good value for C_{fd} is generally around $2.5 \times C_f$. In our case, R_{fd} will be found by looking at the Bode diagram of Z_{out} in Matlab.

From the Fig. 5.30, convenient $(f_f; R_{0f})$ pairs can be found. The criterion used is $R_{0f} = Z_{in}(f_f) - 15dB\Omega$, so that the output impedance of the filter is negligible compared to the input impedance of the converters. In Table 5.1, three $(f_f; R_{0f})$ pairs are compared. The attenuation at 1MHz corresponds to $-40 \log_{10}(f_f/1MHz)$. The corresponding L_f and C_f are given by

$$C_f = \frac{1}{2\pi f_f R_{0f}},$$

$$L_f = R_{0f}^2 C_f.$$

$(f_f; R_{0f})$ pair	C_f	L_f	Attenuation at 1MHz
$(10kHz; -18dB\Omega)$	$79.6\mu F$	$3.18\mu H$	80dB
$(20kHz; -20dB\Omega)$	$72.3\mu F$	$0.875\mu H$	68dB
$(30kHz; -22dB\Omega)$	$66.3\mu F$	$0.424\mu H$	61dB

Table 5.1: Comparison of three possible filters.

The filter with $f_f = 30kHz$ has the smallest components and offers an attenuation of 61dB. This filter was chosen.

The values of the real components will be $C_f = 66\mu F$ (three ceramic capacitors of $22\mu F$ in parallel), $L_f = 0.47\mu H$, $C_{fd} = 150\mu F$ (tantalum capacitor), and $R_{df} = 0.1\Omega$ (series resistance of the tantalum capacitor). The schematics of this filter is shown in figure 5.33 and the Bode diagram of its output impedance is shown in figure 5.34.

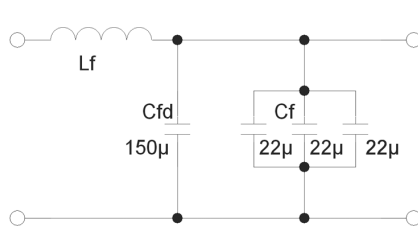


Figure 5.33: Schematics of the input filters of the converters of the EPS.

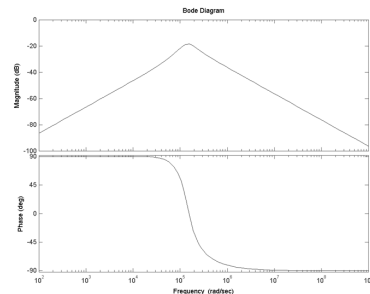


Figure 5.34: Output impedance of the input filters of the converters of the EPS.

5.4 Design of the dissipation system (shunt regulator)

The dissipation system must prevent the voltage on the batteries bus to get over 4.2V.

5.4.1 Choice of Design

Two kinds of solution were envisaged: a series regulator or a shunt regulator.

Series Regulator

A series regulator is inserted between the solar panels and the batteries bus (figure 5.35).

The drawbacks of this solution are:

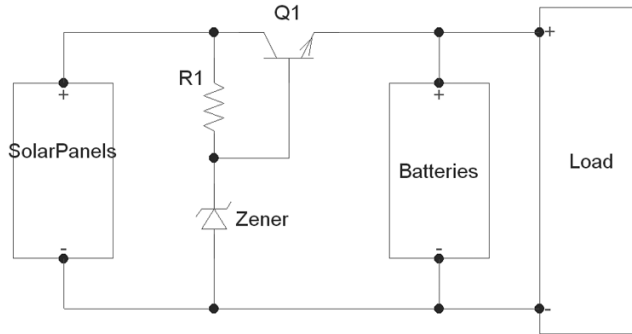


Figure 5.35: Series Regulator.

- There is always a voltage drop between the base and the emitter of the transistor. There will be power losses even if the batteries voltage is under 4.2V.
- All the exceeding power must be dissipated in the transistor.

Shunt Regulator

A shunt regulator is used in parallel with the solar panels.

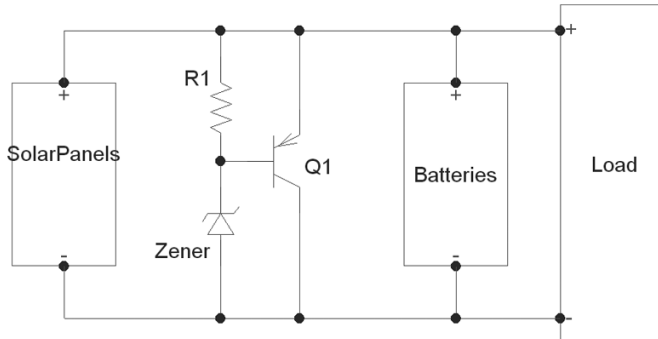


Figure 5.36: Shunt Regulator.

This solution does not suffer the same drawbacks. There is practically no power losses when the voltage of the bus is lower than 4.2V. A resistor can be inserted between the emitter and the ground and take a portion of the power to dissipate. This was the chosen solution.

5.4.2 First version

A first version of dissipation system was designed in [3]. The transistor was a field effect transistor. It was controlled by a logical comparator. The voltage on one input of the comparator was imposed by a reference. The other input was connected to a voltage scaler, measuring the bus voltage (figure 5.37).

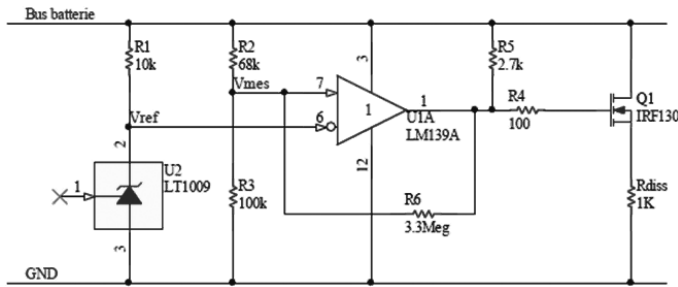


Figure 5.37: Schematics of the first dissipation system.

The advantage of this implementation is that nearby all the power can be dissipated in a resistor in series with the transistor. The disadvantage is that the transistor acts as a switch which can only be open or closed. When it is closed, the voltage of the batteries bus may suddenly drop and the control opens the switch. The circuit then enters in oscillation. To avoid this, a feed-back resistor is inserted on the comparator, introducing an hysteresis. This fixes a problem to bring another one: the dissipation system will partially discharge the batteries each time it is activated.

The circuit was tested and failed: the field effect transistor had a too high gate threshold voltage. Moreover, the oscillations occurred (test report: [1]).

It was discarded and a second version was designed.

5.4.3 Second version

This version is closer to the example of figure 5.36. A TL1431 is used instead of the Zener diode, for a better precision in the regulation. The TL1431 has three PIN: the cathode, the anode and the reference. The functional block diagram of the TL1431 is shown on figure 5.38.

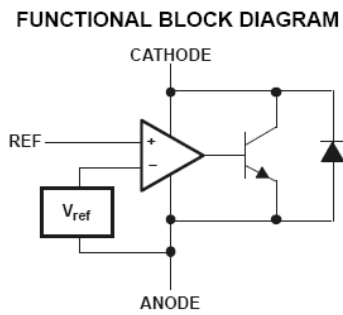


Figure 5.38: Functional block diagram of TL1431.

It looks similar to the first dissipation circuit, but it uses a operational amplifier instead of the comparator and a bipolar transistor instead of the FET. This is an analogical circuit. When it is activated, the circuit will find an equilibrium, and the amount of power dissipated in the shunt will exactly be the amount of exceeding power. The batteries will not be discharged by the circuit.

The PNP transistor is needed because the current in the TL1431 should not be higher than 100mA. A shunt resistor is inserted in the shunt branch but attention must be paid to the polarization of the transistor.

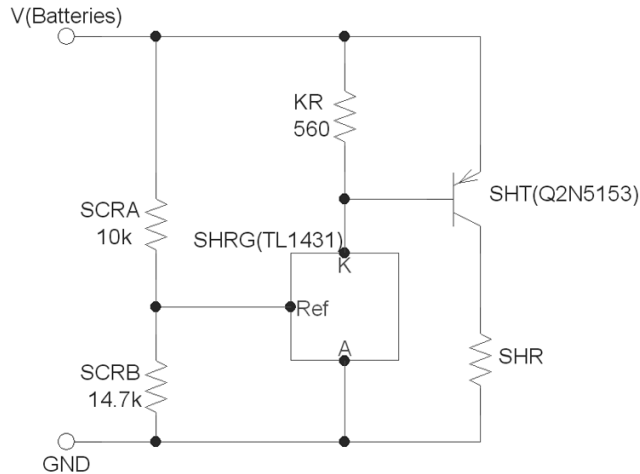


Figure 5.39: Schematics of the shunt regulator.

5.4.4 Components design

The solar panels output power may reach 5.5W. The shunt regulator must be able to dissipate this amount of power. 5.5W corresponds to a shunt current of around 1.3A at 4.2V. The power will be dissipated in the transistor and in the shunt resistor. The interest of the shunt resistor is that it can be located outside the EPS card. The planned solution is to place the shunt resistor on the face with no solar cells.

The shunt regulator is a critical system. A failure would cause the loss of the main power buss and thus the loss of the satellite. The TL1431 is available in space model. If the procurement of the space model was too difficult, military and automotive models may be suitable. A flight model PNP transistor has been provided by Thales ETCA: the Q2N5153.

$$\underline{R_{KR}}$$

The cathode current of the TL1431 (I_{KA}) must be inferior to 100mA. $I_{KA} = I_B + I_{KR}$, where I_B is the base current in the transistor and I_{KR} the current in the KR resistor. The minimal β of the transistor is 35, the maximal V_{EB} is 1.45V (for $I_C = 2.5A$) and the maximum I_C is 1.3A, thus

$$I_{KA} = I_B + I_{KR} < 100mA,$$

$$\frac{I_C}{\beta} + \frac{V_{EB}}{R_{KR}} < 100mA,$$

$$R_{KR} > \frac{1.45V}{100mA - \frac{1.3A}{35}} = 23.07\Omega.$$

The minimum cathode current for regulation is 1mA. When the regulation starts, the Emitter-Base voltage of the transistor V_{EB} is around 0.6V. If there is no base current ($I_B = 0$), the TL1431 is supplied through resistor KR:

$$I_{KR} > 1mA,$$

$$R_{KR} < \frac{V_{EB}}{1mA} = 600\Omega.$$

The chosen value for R_{KR} is 560Ω .

SCRA and SCRB

The intern reference of the TL1431 $V_I(\text{ref})$ is equal to 2.5V.

The ratio SCRB/SCRA is given by:

$$\frac{V_I(\text{ref})}{4.2V - V_I(\text{ref})} = 1.47.$$

The resistances must not be too high or the reference input current (up to $3\mu A$) can disrupt the regulation voltage. If they are too low, some power will be dissipated in the scaler.

The chosen values are $\text{SCRA} = 10k\Omega$ and $\text{SCRB} = 14.7k\Omega$.

SHR

For the regulation, the transistor must be in linear mode. The Emitter-Collector voltage must be superior to the Emitter-Collector saturation voltage ($V_{EC}(\text{sat}) = 0.75V$ when $I_C = 2.5A$, it will be less when $I_C = 1.3A$). We have

$$V_{EC} = 4.2V - I_C R_S H R > V_{EC}(\text{sat}),$$

$$R_S H R < \frac{4.2V - 0.75V}{1.3A} = 2.65\Omega.$$

A worksheet has been written to compute the dissipated power in the transistor and in the resistor as a function of the shunt current. Results are displayed on figure 5.40 for a shunt resistor of 2.35Ω (two resistors of 4.7Ω in parallel will be used). The maximum dissipated power in the transistor is 1.88W. Thermal simulations have been done in [7] and showed that the temperature can be kept under 85°C if a heat sink is used between the transistor and the structure.

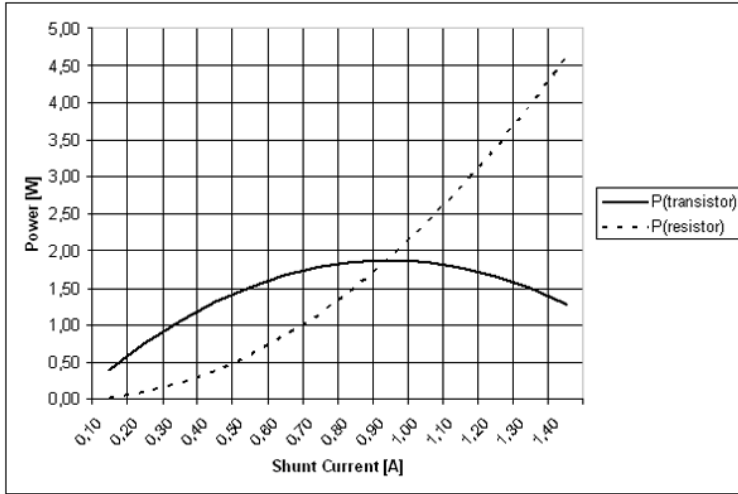


Figure 5.40: Dissipated power in the transistor and in the resistor.

5.5 Design of the protection circuits

5.5.1 Description

The protection circuit was chosen in [3]. It is the MAX890L. It can operate with an input voltage of 2.7 to 5.5V. It can thus be used for all systems supplied by 3.3V and 5V busses.

It is a current-limiting circuit. A threshold current (I_{thr}) can be chosen between 240mA and 1,200mA. The threshold depends on the value of the resistor R_{set} . It is possible to choose a threshold under 240mA, but the circuit will operate with less precision. When the current at the output becomes higher than the threshold, the MAX890L starts to decrease the output voltage. The voltage falls to zero when the output current reaches 1.5 times the threshold.

The circuit has a thermal shut-down. When the junction temperature exceeds 135°C, the switch turns off. It turns back on at 125°C. In case of high $\frac{dV_{DS}}{dt}$ on the output (short-circuit), the switch turns off too. It is then slowly tuned back on with the output current limited to $1.5 \times I_{thr}$.

The circuit provides a “*FAULT*” signal. It is an open-drain output that goes low when I_{thr} is reached or when the thermal shut-down is activated. There is a “*ON/OFF*” input. When this input is set to high, the power output is disconnected from the power input.

5.5.2 Components

The value of R_{set} depends on the desired I_{thr} . Here is the formula to choose R_{set} : $R_{set} = \frac{1,380}{I_{thr}}$. The protection circuit of the EPS has a R_{set} of $10k\Omega$ ($I_{thr} = 138mA$). It protects the measurement system and their total consumption is very low (less than 10mA).

A capacitor of $1\mu F$ is used on the input of the circuit and a capacitor of $0.1\mu F$ on the output. A pull-up resistor of $100k\Omega$ and a decoupling capacitor of $100pF$ are used on the “*ON/OFF*” input.

The schematics is shown on figure 5.41.

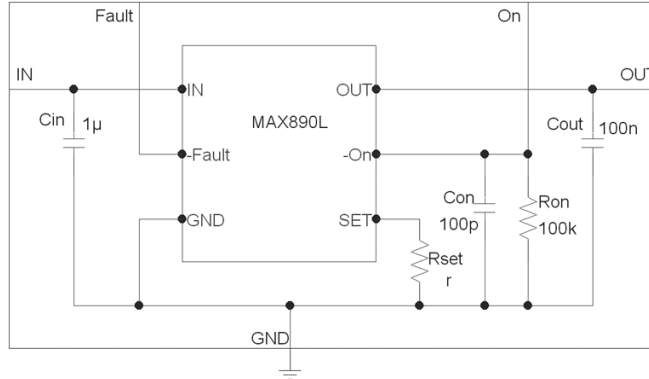


Figure 5.41: Schematics of the protection circuit.

A breadboard prototype was made. The tests of this prototype learnt us that the output voltage is decreasing when the output current exceeds I_{thr} (it was not specified in the datasheet).

5.6 Design of the antennas deployment circuit

5.6.1 Functionality

The role of the antenna deployment circuit on the EPS is to connect or disconnect a resistor to the batteries bus. The system is itself controlled by the OBC. The resistor is a thermo cutter the resistance of which is unknown. As it may require a large amount of power, the switch on the EPS will be designed to be able to deliver up to 10W in this resistor. The control signal is picked up on two PIN of the PC104 connector. The command voltage will be digital, with a low state at 0V and a high state at 3.3V. The antenna deployment is a critical function, so redundancy is desired. It is the reason why two independent control signals are provided.

5.6.2 Implementation

The converters may be unable to provide enough power. In addition, the system is supplied on the output of one converter, a trouble in this converter would paralyze the deployment system. This system will rather use the batteries bus. This means that the system is critical on two counts: it must work, or the satellite will be silent, and it must not have a short circuit, or the batteries will quickly be emptied.

Using two transistors in parallel will add redundancy to ensure that the system be activated, but doubles the risk to have a short circuit (if a heavy ion strikes one transistor). Using two transistors in series highly reduces the risk of short circuit, but increases the risk of a system malfunction.

There are two envisaged solutions:

1. The switch could be one single transistor with very high reliability, in other word, a flight model. This philosophy was adopted for the shunt regulator, as the problem was very similar. In this case the system is composed of one FET, one decoupling capacitor, one pull-down resistor and the thermo cutter. Both command lines are connected to the gate of the transistor. The schematics of this circuit is shown of the left of figure 5.42.
2. The switch could be composed of four transistors in quad-mount (two parallel branches of two transistors in series). In this way, there is redundancy against a risk of malfunction, and the risk of a short circuit is kept very low. The disadvantage is of course the required surface on the PCB. This solution will be useful if we can't find a space certified FET. The system would be composed of four FETs and the thermo cutter plus two capacitors and two resistors for the decoupling. Each branch is controlled by one control signal. Controlling two FET in series with the same voltage will not cause problems for this application (each transistor withstand the bus voltage and there is no critical requirements about the rise time). This is the circuit shown on the right of figure 5.42.

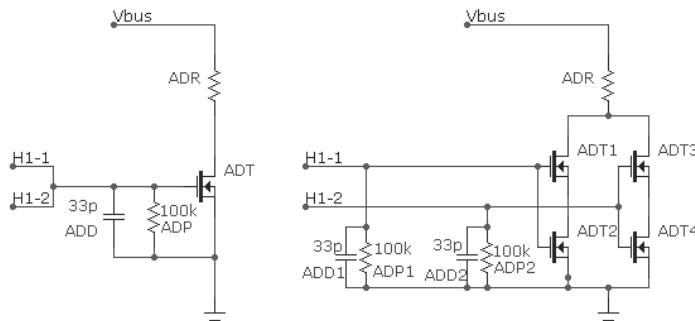


Figure 5.42: Propositions for the antennas deployment system.

5.6.3 Location

The deployment system (switch and decoupling) will be located on the EPS PCB. Doing so, it is close to the power source. The required surface is not a concern since there are few components. The thermo cutter is located near the antennas.

5.6.4 Components

No flight model for a low $V_g s$ FET has been found (investigations have been done at Thales Alenia Space to find such a component, without results).

A commercial model meets all requirements, the ROHM - RTR040N03TL. The quad-mount solution is thus adopted. It is a discrete component (if we use several transistors on one chip, there is a risk that a trouble affect all transistors).

Characteristics:
Gate-source threshold voltage ($V_{gs}(th)$): between 0.5 and 1.5V.
Drain-source on-state resistance: max. 66mohm ($V_{gs} = 2.5V$).
Total power dissipation: 1W (on a ceramic board).
Occupied Surface: $10mm^2$.
$V_{gs}(max)$: 12V.
$V_{ds}(max)$: 30.

The decoupling capacitors will be ceramic 100pF capacitors and the resistors will be 100k resistors.

5.7 Design of the battery heater

The function of the heater is to prevent the temperature of the batteries to drop under a determined temperature ($0^\circ C$). A simple and convenient heater consists in a heating resistor in contact with the batteries, in which the current flows when the temperature of the batteries drops under a chosen threshold (T_{th}).

As said in chapter 3, the system will be supplied by the batteries bus. A special attention must thus be given to the reliability.

The “switch” controlling this current can be a FET transistor. The transistor can be controlled by the OBC or by an independent system. In either case, the control voltage would be quite low (down to around 2.7V). We saw while designing the antennas deployment system that the available low $V_{gs}(th)$ MOSFET’s were commercial models. Then, the same solution is adopted to have a good reliability. Four transistors are mounted so that if one of them fails (stay opened or closed), the system is still operational.

5.7.1 Control by the OBC

If the system is controlled by the OBC, a PIN of the batteries connector (connector between the EPS and the batteries card) and a PIN of the PC104 port must be dedicated to the control signal (“BattH”) of the batteries heater. There is a temperature sensor on the batteries in the measurement system of the EPS. The OBC can retrieve the measurement of the temperature of the batteries through the I^2C data bus. The schematics of the circuit is shown on figure 5.43.

5.7.2 Independent control

The heater can also be controlled by an independent system. This solution was chosen on Swisscube because a failure of the OBC does not influence the heater. This is also the chosen solution for OUFTI-1, as explained in chapter 3.

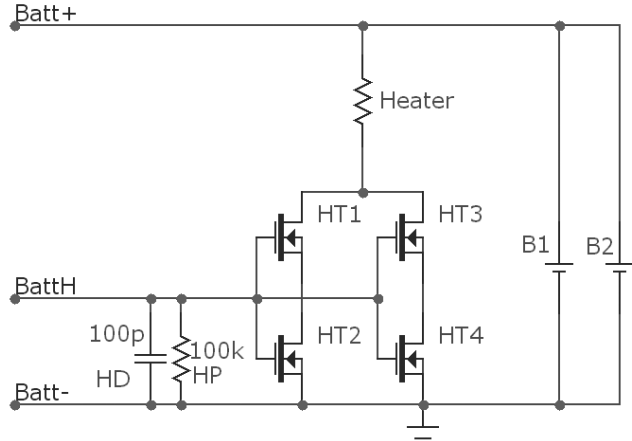


Figure 5.43: Schematics of the batteries heater circuit with a control by the OBC.

Here, an independent temperature probe is used. The same probe as in the measurement system can be used (LM94022). There are two logical inputs on the LM94022 that have to be set to chose the desired output voltage level, as shown on figure 5.44.

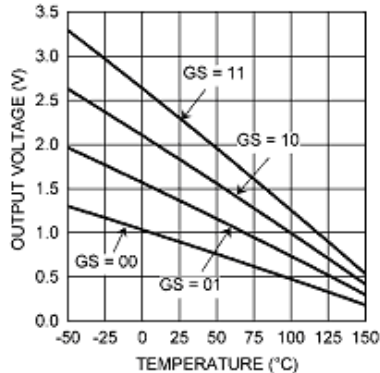


Figure 5.44: Output voltage of LM94022 as a function of T° and logical inputs.

The switch will be driven by a logical comparator that compares the output of the LM94022 with a voltage reference. A circuit using a logical comparator and where there is a feed-back loop is liable to enter in oscillation. The parry to this problem is to add an hysteresis. If there is enough distance between the heater and the temperature probe, the system will have an intrinsic hysteresis. A small electronical hysteresis will be added anyway.

The IC MAX9015 contains a logical comparator with hysteresis and a voltage reference (V_{ref}). Its output is a push-pull and thus able to drive the MOSFET's. The reference has a value of 1,236mV. The output voltage of the LM94022 has to be scaled. The schematics of the heater circuit with independent control is shown on figure 5.45.

The temperature threshold to activate the heater as well as the amount of dissipated power in the heater must be determined by thermal studies. Thermal simulations about the heater were done in [7] and the following values were chosen:

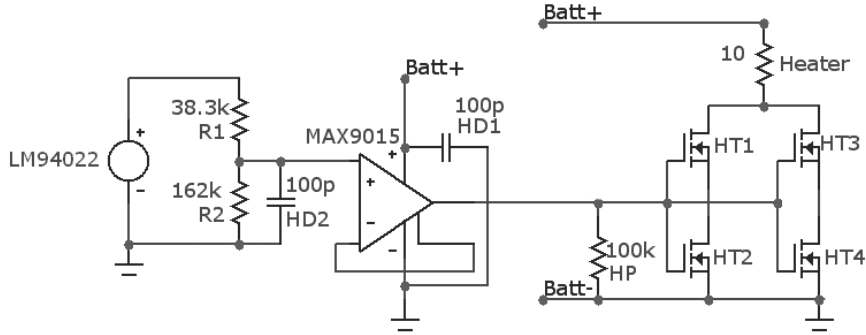


Figure 5.45: Schematics of the heater with independent control.

- Temperature threshold: 0°C .
- Dissipated power: $2 \times 250\text{mW}$ at 2.5V (there are two heaters of 250Ω in parallel).

At 0°C , the output of LM94022 is 1567mV (for GS = 01). The scaler ratio $R1/R2$ is then $331/1236$.

The scaler resistors R1 and R2 are chosen so that the input current of the comparator ($\pm 2\text{nA}$) is negligible compared to the current passing through the resistances. The current flowing through the resistance must itself be less than $30\mu\text{A}$ to have a good precision on the output of the LM94022. The precision of the resistors must be good (1% or better), and the size should be large enough to easily replace them (for calibrating). Suitable values for R1 and R2 are 42.2k and 158k .

Chosen models:

R1: TYCO ELECTRONICS RP73D2B42K2BTG. R2: TYCO ELECTRONICS RP73D2B158KBTG.
Size: “1206”. Precision: 0.1%. Temperature coefficient: $\pm 15\text{ppm}/^{\circ}\text{C}$.

A decoupling capacitor of 100pF is used in parallel with R2.

The output of the MAX9015 must be high when the temperature of batteries is under T_{th} . The output of the LM94022 is decreasing with temperature. As a consequence, it must be connected to the “+” input of the comparator while the reference is connected to the “-” input.

A decoupling capacitor of 100pF is connected on the V_c of the MAX9015.

5.8 Design of the measurement system

The design of the measurement circuits is the subject of the master thesis “Développement de l’infrastructure de mesure du nanosatellite OUFTI-1.” [10].

5.9 Components selection

This section explains some considerations that guided the choice of components.

5.9.1 Formats

Most components will be Surface Mounted Devices (SMD). There is a standard for the sizes of SMD resistors and capacitors. Most used values are show in the table 5.2.

0201	$0.60mm \times 0.30mm$
0201	$0.60mm \times 0.30mm$
0402	$1.00mm \times 0.50mm$
0603	$1.60mm \times 0.80mm$
0805	$2.00mm \times 1.25mm$
1206	$3.20mm \times 1.60mm$
1210	$3.20mm \times 2.50mm$

Table 5.2: Examples of standard SMD formats.

For the realization of a PCB, formats of resistors and capacitors are generally harmonized: only one or two formats are used. In our case, the used formats are 0805 and 1210. Most of high-capacity ceramic capacitors are available in the 1210 format. The 0805 format is used for smaller components, but is still large enough to allow manual modifications on the prototypes.

5.9.2 Capacitors

In most systems, the capacitors are the components with the higher failure rate. The choice of reliable capacitors is thus especially important.

5.9.3 Dielectric

Capacitor dielectrics were classified by the Electronic Industries Association (EIA) in function of the relative variation of their capacity in a given temperature range. Most used capacitor classes are shown in the table 5.3. It is composed of a prefix, indicating the temperature range, and of a suffix, indicating the relative variation of capacity in this range.

Most popular dielectrics are X5R and X7R. On the EPS of OUFTI-1, X7R capacitors will be chosen (this corresponds to a variation of 15% of capacity in the temperature range of -55°C to 125°C). They not only have one of the lowest variation of capacity with temperature, but the parasitic inductance of the capacitor is very low (The inductance has no influence under 10MHz).

Prefix	Temperature range
X7	-55 to 125°C
X5	-55 to 85°C
Y5	-30 to 85°C
Z5	10 to 85°C
Suffix	Relative variation of capacity
D	3.3%
E	4.7%
F	7.5%
P	10%
R	15%
S	22%
T	+22%, -33%
U	+22%, -56%
V	+22%, -82%

Table 5.3: Prefixes and suffixes used by EIA to classify capacitor dielectrics.

5.9.4 Rated voltage

The rated voltage of ceramic capacitors is generally given at ambient temperature. At a temperature of 125°C, the rated voltage can lose 50% of its value. A good caution rule is to chose capacitor with a rated voltage that is twice the voltage they will be submitted to.

5.9.5 Bending strength

The EPS card could bend under the effect of vibrations and accelerations during launch, and under the effect of temperature gradients. Small size high-capacity ceramic capacitors are sensible to mechanical deformation. Some models are designed to have a better bending strength: the automotive and “flexible termination” models. The capacitors of the EPS were chosen among automotive and “flexible termination” models.

5.10 Schematics of the EPS

The complete schematics of the engineering model of the EPS card are shown in the Appendix D. They include connectors, jumpers, tests points and the deployment switch (switch which disconnects the batteries during launch).

Chapter 6

Prototypes of the EPS

6.1 Introduction

The initial development plan of the subsystems cards of OUFTI-1 included three phases concerning the realization and tests of prototypes: the breadboards model, the engineering model, and the flight model.

- Phase 1: The breadboards model.

The different modules of a subsystem are made on breadboards. This allows to know the electrical components and test if the modules work fine independently. Several prototypes were made during the internship of Philippe Ledent at Thales Alenia Space: one prototype of the first dissipation system, one PCB with the prototypes of the three DC/DC converters. Two prototypes were made during this work: the prototype of the second dissipation system and the prototype of the protection circuit. The breadboards models were tested during the internship of the author. Most important tests and results are reported in [1].

- Phase 2: The engineering model.

The engineering model is an on-scale PCB prototype. It is supposed to be nearly identical to flight model but it is only devoted to tests. The engineering model can include more test points or jumpers than the flight model. The engineering model of the EPS was made during this work. The realization of the engineering model will be detailed in this chapter. The tests on the engineering model are reported in [1] too.

- Phase 3: The flight model.

The flight model is the model that will be sent in space. It will be produced next year, when the engineering model is fully validated.

6.2 The breadboards model

This sections presents the prototypes on breadboard made during this work: the second dissipation system and the protection circuit.

6.2.1 The second dissipation system

The second dissipation system has been designed in section 5.4. A prototype was made on breadboard, based on this design. A picture of the prototype is shown in the Appendix C.

Terminals

The terminals are:

- Vbus: it represents the batteries bus.
- GND: the ground.
- Base: connected to the base of the transistor for measurements.
- Collector: connected to the collector of the transistor.

Components

The transistor is the model that will be used on the flight model. It is in close contact with a large heat dissipater (the transistor may have to dissipate up to 2W of power).

The TL1431 is a old plastic-case model (LP package).

The shunt resistor is no included on the breadboard. It must be connected between the “collector” and the “GND” terminals. If the circuit is used without the shunt resistor, the transistor cannot play its role and the shunt current will entirely pass through the TL1431. The maximum current in the TL1431 is 100mA.

The resistors are axial leaded components.

6.2.2 The protection circuit

A prototype of the protection circuit (presented in section 5.5) was made on breadboard. A picture of the prototype is shown in the Appendix.

Terminals

The terminals are:

- In: there are two rows of pins, the upper pins for input (+) and the lower pins for input (-).
- Out: there are two rows of pins, the upper pins for output (+) and the lower pins for output (-).
- On: this pin is connected to the “ $\overline{ON/OFF}$ ” input.
- Fault: this pin is connected to the “ \overline{FAULT} ” output.

- Rs: there are three pins for Rs (R_{set}).

Components

The MAX890L is the same model as planed for the flight model. Capacitors and resistors are leaded components.

For Rs, two potentiometers were used in series, one of $0\text{to}100\Omega$ and one of $0\text{to}10k\Omega$. Access pins were soldered on the terminals of each potentiometer.

There is a pull-up resistor on the “ $\overline{ON/OFF}$ ” input. The corresponding pin must be connected to ground to activate the circuit.

There is a pull-up resistor on the “ \overline{FAULT} ” output.

Two LED were included in the circuit: one between the In(+) and the “ $\overline{ON/OFF}$ ” (it is on when the circuit is on), and one between the In(+) and the “ \overline{FAULT} ” (it is on when the circuit is in fault mode).

6.3 The engineering model

The engineering model is a PCB in the PC104 standard, the real size of the PCB in the CubeSat. The design of the engineering model is supposed to be close to the design of the flight model. The engineering model integrates all the so far developed systems. It also can integrate features devoted to tests, e.g. jumpers and test points.

There are several reasons to make a real-scale prototype:

- The electronical behavior of a circuit can be influenced by geometrical characteristics, such as the distance between components. Some measurements will only make sense on a real scale prototype.
- Mechanical tests can be performed.
- The on-scale model is the only way to know with precision the surface occupied by the circuits.

A picture of the engineering model can be found in the Appendix C.

6.3.1 Included systems and interfaces

The engineering model of the EPS card was produced during this work. The following systems were included in the design:

- The dissipation system.
- The 3.3V, 5V, and 7.2V converters with their input filters.

- The antenna deployment system.
- Sensors and ADC for the measurement of the housekeeping parameters of EPS and the temperatures of the faces.
- The protection circuit for the measurement system.

The engineering model has the following interfaces:

- Main PC104 connector of 4×26 pins. The pins attribution was managed by the OBC team [9].
- Five 2-pins connectors for the solar panels (Schottky rectifiers are included on the PCB).
- One 4-pins connector for the batteries card.
- Two 2-pins connectors for the shunt resistances of the dissipation system.
- One 2-pins connector for the thermo-cutter of the antennas deployment system.
- Nine 3-pins connectors for the temperatures probes.

The card also include tests points and jumpers.

- Four jumpers on each DC/DC converter:
 - between the batteries bus and the (+) input of the input filter,
 - between the (+) output of the input filter and the (+) input of the converter,
 - between the (+) output of the converter and the corresponding power bus,
 - and in the feed-back loop (to open the loop, for tests).
- One jumper to short-cut a Schottky rectifier on the output of the 3.3V (for the tests with EPS2).
- One jumper between the batteries bus and the connector to the batteries card.
- One jumper between the batteries bus and the dissipation system.
- One jumper between the 3.3V bus and the protection circuit of measurement system.

The engineering model of the batteries card was not concretized yet. The batteries card will have to include: the batteries, the PCM's, the USB charger, and the batteries heater.

6.3.2 Implementation

The implementation of the EPS is a complex work.

The EPS card holds a lot of circuits and connectors. The density of components per unity of surface will be high. A multi-layer PCB is required. There are very sensible measurements circuits and noisy DC/DC converters on the same card, which can make the layout more complex. The PCB also have to make the heat circulation from the transistor of the dissipation system to “cold points” easier.

We took the decision to subcontract the realization of the engineering model PCB. The subcontractor was Deltatec.

Deltatec

Deltatec is a small company based in Ans near Liège. The company is specialized in electronics, hardware and software. They have an experience in the production of space-certified PCB's as they were one of the subcontractors of Thales Alenia Space.

Documents provided to Deltatec

A complete document was written for Deltatec. This document included:

1. The complete electrical schematics of the engineering model of the EPS card.
2. The complete list a used components, with manufacturer's reference and the command code of a distributor. This list can be found in the Appendix.
3. The datasheets of used components.
4. A quick presentation of the EPS.
5. Mechanical, electrical and thermal specifications for the EPS card (mechanical and thermal specifications were written with the MECH and THER teams).

Work done by Deltatec

Deltatec had to make the layout of the card. The company had to order the components, subcontract the manufacturing of the PCB and was responsible of the assembly of the components on the PCB.

Final product

The final product of Deltatec was two complete cards (PCB with soldered components and PC104 connector) and tree empty cards (only PCB with layout and PC104 port). No electrical tests were made by Deltatec.

6.3.3 Tests

The engineering model of the EPS card was tested. The complete description and the results of the most important tests can be found in the test report [1]. All the systems of the engineering model of the EPS card except the measurement system were tested, with temperature range of -30°C to 70°C. The results were satisfying, except the 7.2V converter. The 7.2V converter produces a stabilized voltage of 7.2V and is stable, but a gain margin of 1 dB was measured under particular conditions.

Chapter 7

Miscellaneous activities, presentations and publications

7.1 Publications

1. Document including schematics, list of components, datasheets and specifications (electrical, mechanical and thermal) for the production of the engineering model of the EPS by Deltatec.
2. Document about the choice of components for OUFTI-1.
3. Document explaining how to integrate the behavior of the EPS into an operational simulator of OUFTI-1 (this simulator is presented in [6]).
4. Progress reports for the ESA.
5. (...)

7.2 Presentations

1. Presentation to high-school students - Posters and demos, as part of “L’Espace j’en rêve”, EuroSpace Center, Redu, Belgium, 1 Oct. 2008.
2. Public presentation, “The first nanosatellite developed at the University of Liège”, Space Days, Liège, Belgium, 7 Oct. 2008.
3. Presentation to other CubeSat teams, ESA Second European CubeSat Workshop, ESA/ESTEC, Noordwijk, The Netherlands, 20-22 Jan. 2009.
4. Presentation to other CubeSat teams, 6th Annual CubeSat Developer’s Workshop, California Polytechnic State University, San Luis Obispo, 22-25 Apr. 2009

7.3 Activities

As OUFTI-1 is designed for communications in D-STAR, an amateur-radio communication protocol, the author acquired the “HAREC” ham-radio license, which allows to use the ham-radio frequencies for radio communications.

Chapter 8

Conclusions

The work described here corresponds to the second phase of work on the development of the Electrical Power System of OUFTI-1. The objective was to carry the project forward as far as possible. (The first phase had been carried out by Philippe Ledent during his stay at Thales during the summer 2008.)

8.1 Accomplished work

8.1.1 Architecture

The architecture of the EPS as well as interaction between components are now established.

The batteries are connected to the main power bus (“batteries bus”). The voltage of the batteries bus is determined by the state of charge of the batteries. The batteries will be protected against under-voltage and over-currents by the protection circuit module from the manufacturer. They will be protected against over-voltage by the dissipation system. Finally, they will be protected against the cold by the batteries heater.

The solar cells of each face of the CubeSat are connected in series and protected against reverse-bias current by a Schottky rectifier. This forms a solar panel. Solar panels are connected to the batteries bus without maximum power point tracking (MPPT) system. A solar panel is characterized by an I-V curve. The produced power is thus determined by the voltage of the batteries bus.

The power conditioning unit converts power from the batteries bus and provides three stabilized voltage power busses to supply the subsystems of the CubeSat. The protection circuit (over-current protection) of each subsystems is located on this subsystem’s electronic board.

The antennas deployment circuit is located on the EPS and is supplied from the batteries bus.

The power budget was computed and there is enough power to supply the satellite and allow D-STAR and AX.25 communications.

8.1.2 Design

A model of Li-Po battery from KOKAM was selected. Batteries are delivered with a battery protection circuit, which we will use. The solar cells are the new 30% efficiency solar cells from AzurSpace.

The dissipation system, the battery heater, the three DC/DC converters, the input filters of the converters, the antenna deployment system, and the protection circuit were completely designed as part of our work (electrical schematics and components selection).

The design procedures were explained in detail to make the development of our future CubeSats easier.

8.1.3 Implementation and tests

Breadboard prototypes of the dissipation system and the protection circuit were made and tested (tests are reported in [1]). (The breadboard prototype of the converters and the first dissipation system were made by Philippe Ledent.)

The engineering model of the EPS electronic card was made. The PCB routing and manufacturing were made by Deltatec, our subcontractor. The engineering model includes the dissipation system, the three DC/DC converters, the input filters of the converters, the antenna deployment system, the measurement system (designed in [10]), and the protection circuit for the measurement system. The circuits of the engineering model were tested without the batteries and solar panels, with a temperature range of -30°C to 70°C (tests are reported in [1]).

8.2 Future work

This is a non-exhaustive list of work that remains to be done.

- Improve the design of the 7.2V converter to upgrade the frequency stability of the converter (optional).
- Measure the I-V curve of the solar panels and compare the result with the Matlab model.
- Make the engineering model of the batteries electronic card.
- Test the batteries heater.
- Test the protection circuit module (PCM).
- Test the complete engineering model.
- Test the compatibility between the EPS and the EPS2 when connecting the 3.3V outputs together.
- Test the EPS with all other subsystems, both in the laboratory and in appropriate environmental conditions.

Bibliography

- [1] Pierre Thirion, *Test of prototypes of the EPS of student nanosatellite OUFTI-1*, Internship Report, University of Liège, Liège, Belgium, 2009.
- [2] Philippe Ledent, *Design and Implementation of On-board Digitally Controlled Electrical Power Supply of Student Nanosatellite OUFTI-1 of University of Liege*, Master's Thesis, University of Liège, Liège, Belgium, 2009.
- [3] Philippe Ledent, *Architecture et design de l'EPS de OUFTI-1*, Internship Report, University of Liege, Liège, Belgium, 2009.
- [4] Stephanie Galli, *Mission Design for the CubeSat OUFTI-1*, Master's Thesis, University of Liège, Liège, Belgium, 2008.
- [5] Gauthier Pierlot, *Oufti-1: structural integrity, system configuration and vibration testing.*, Master's Thesis, University of Liège, Liège, Belgium, 2009.
- [6] Vincent Beukelaers, *From mission analysis to space flight simulation of the OUFTI-1 nano-satellite*, Master's Thesis, University of Liège, Liège, Belgium, 2009.
- [7] Lionel Jacques, *Thermal Design of the OUFTI-1 nanosatellite*, Master's Thesis, University of Liège, Liège, Belgium, 2009.
- [8] François Mahy, *Design and Implementation of On-board Telecommunication System of Student Nanosatellite OUFTI-1 of University of Liège*, Master's Thesis, University of Liège, Liège, Belgium, 2009.
- [9] Damien Teney, *Design and Implementation of On-Board Computer of Student Nanosatellite OUFTI-1 of University of Liège*, Master's Thesis, University of Liège, Liège, Belgium, 2009.
- [10] Nicolas Evrard, *Développement de l'infrastructure de mesure du nanosatellite OUFTI-1.*, Master's Thesis, Liege: Hemes-Gramme Institute, Academic year 2008-2009.
- [11] Cal Poly State University, *Cubesat Community Website*, <http://cubesat.atl.calpoly.edu/>, consulted in may 2009.
- [12] Cal Poly State University, *CubeSat Design Specification*, Revision 11, 11/02/2008.
- [13] Ryan Connolly, "The P-POD Payload Planner's Guide", 2000
- [14] Edouard Perez, *VEGA launch vehicle User's Manual*, ARIANESPACE, March, 2006.

- [15] Fabien Jordan, *Phase B Electrical Power System (EPS)*, Report of Diploma, Yverdon, 19/12/2006.
- [16] Robert W. Erickson, *Fundamentals of Power Electronics*, second edition, Kluwer Academic Publishers, January 2001, ISBN-10: 0792372700, ISBN-13: 978-0792372707.
- [17] M.R. Patel, *Spacecraft power systems*, CRC Press, 2005.
- [18] James R. Wertz and Wiley J. Larson, “Space Mission Analysis and Design”, 1999
- [19] Varta Microbattery GmbH, *VARTA PoLiFlex® Batteries Superior Polymer Technology*, Hanbook, February 2008.
- [20] KOKAM, *SPECIFICATION FOR SLPB554374H*, Datasheet, QA-070329 .
- [21] KOKAM, *Protection Circuit Module Specification MODEL : SKP0101-010304-307R5-1*, Datasheet, rev 1.0 16Jun2006.
- [22] PUMPKIN, *CubeSat Kit. FM430 Flight Module*, Datasheet, Hardeware Revision C, Document revision J, San Francisco, USA, June 2008.
- [23] AzurSpace, *30 % BOL Efficiency Solar Cell*, Weight_reduced_III-V_TJ_Cells.ppt.
- [24] Robert Kollman, “Power Tip #3: Damping the input filter, part 1” in *Power Management DesignLine*, <http://www.powermanagementdesignline.com/howto/210500098>, 09/04/2008.
- [25] Evelyne Simon, “Evaluation of Lithium Polymer Batteries” for *NASA Battery Workshop*, presentation available at http://batteryworkshop.msfc.nasa.gov/presentations/ThuAM_01_Evaluation_Lithium_Polymer_Bat 2005.

Appendix A

Matlab code for the I-V curves of solar panels

The first function gives the current in one solar cell as a function of the voltage (in V), the insolation G (with $G_{nom} = 1350W/m^2$ as unity), and the temperature (in °C).

```
function I = Cell_GaAs(V,G,TaC)
%Code produced by the team from the CubeSat SwissCube
%and modified by Philippe Ledent (OUFTI-1) (september 2008)
%               Pierre Thirion (OUFTI-1) (april 2009)
%
%Model of 30% efficiency solar cell from AzurSpace : I=f(V,T)
%Use of function : I = Cell_GaAs(V,G,TaC)
%V = Voltage on cell terminals [V]
%G = relative insolation [-] (G=1 => 1367 W/m^2)
%TaC = temperature of the cell in operation [Celsius]

%Boltzmann constant
k = 1.38e-23;
%Electric charge
q = 1.60e-19;
%Quality factor of the diode (1<n<2)
n = 1.5;
%Band gap voltage (1.12eV < Vg < 1.757eV)
Vg = 1.75;

%Reference values
Tref = 273 + 28; %temperature
Voc_Tref = 2.716; %open circuit voltage (G=1 et T=Tref)
Isc_Tref = 0.52815; %short circuit current (G=1 et T=Tref)

%Temperature of the cell in operation
```

```

TaK = 273 + TaC;
%Photo-current thermal coefficient
K0 = 2.72e-4/Isc_Tref;
%Photo-current (G=1 et T=Tref)
Iph = Isc_Tref * G * (1 + K0*(TaK - Tref));
%Diode saturation current (T=Tref)
Id_Tref = Isc_Tref / (exp(q*Voc_Tref/(n*k*Tref))-1);
%Diode saturation current (T=Tak)
Id = Id_Tref * (TaK/Tref)^(3/n) * exp(-(Vg * q/(n*k))*(1/TaK - 1/Tref));
%Calculation of serie resistance Rs
Vpmax_Tref = 2.427; %voltage at maximum power for T=Tref
Ipmax_Tref = 0.529; %current at maximum power for T=Tref
Rs = (Voc_Tref-Vpmax_Tref)/Ipmax_Tref;

%Iterative calculation of Isc
I = zeros(size(V));
for i=1:10 \%number of iteration = 10
for j=1:length(V);
I(j) = I(j) - (Iph - I(j) - Id*(exp(q*(V(j)+I(j)*Rs)/(n*k*Tref)) -1))/...
(-1 - (Id*(exp(q*(V(j)+I(j)*Rs)/(n*k*Tref)) -1))*q*Rs/(n*k*Tref));
end
end

```

The second function gives the voltage at the terminal of the used Schottky diode as a function of the current flowing in the diode.

```

vmax = 3.5;
function vv = v_diode(vi)
% by Pierre Thirion
% Use of function : V = v_diode(I)
% V = Voltage on diode terminals [V]
% V is computed by linear interpolation, on the basis of real measurements
% of the I-V curve of the diode.
% I = Current in the diode [A]

% mesures (except the first)
d_v = [0 0.141 0.213 0.227 0.24 0.25 0.26 0.27 0.28
       0.3 0.32 0.34 0.36 0.38 0.39 0.4 0.41 0.42 0.44 0.46
       0.48 0.5 0.52 0.54 0.56 0.58] ;
d_i = [0 0.00001 0.00002 0.00003 0.0005 0.00007 0.0001 0.00017 0.00023
       0.00047 0.00095 0.00206 0.0036 0.0095 0.015 0.021 0.031 0.04 0.072 0.122
       0.184 0.27 0.358 0.46 0.605 0.9] ;

vv = zeros(size(vi));

for k = 1:(length(vi)-1)

```

```

i = vi(k);
dii = (d_i - i);
co = 0;
for j = 1:(length(dii)-1)
    if ((dii(j) <= 0) && (dii(j+1) > 0))
        co = j;
    end
end
% linear interpolation
if (co == 0)
else
    a = (i - d_i(co+1)) / (d_i(co) - d_i(co+1));
    v = d_v(co)*a + d_v(co+1)*(1-a);
end
vv(k) = v;
end

```

The following code gives an exemple of the use of the above functions to plot to I-V and P-V curves of a solar cell under full insolation and at a temperature of 28°C.

```

v = [0:0.05:vmax];

ia = Cell_GaAs(v, 1, 25);
da = v_diode(ia);
va = 2*v-da;

figure;
plot(va,ia)

AXIS([0 2*vmax 0 0.6])
GRID ON
XLABEL('Voltage [V]')
YLABEL('Current [A]')

figure;

pa = ia.*va;

plot(va,pa)

AXIS([0 2*vmax 0 3])
GRID ON
XLABEL('Voltage [V]')
YLABEL('Power [W]')

```

Appendix B

Power budget worksheet

In this example, the power budget is computed for an HF amplifier with an efficiency of 30%.

<u>Power Budget</u>					
Subsystem	Mode	Base consumption			
		On 3,3V [mA]	On 5V [mA]	On 7,2V[mA]	On batt. [mW]
EPS1	On	0	0	0	22
	On+heater	0	0	0	500
EPS2	Off	0	0	0	0
	Supply	0	0	0	300
OBC1	Test	0	0	0	660
	On	0	2	0	0
OBC2	On	3	0	0	0
	On	5	0	0	0
Meas. System	RX	20	0	0	0
	RX+TX	35	0	347	0
Beacon	On	16	0	46	0
	Total	79	2	393	1482

<u>Converters</u>			
Voltage [V]	3,3	5	7,2
Efficiency (%)	90	70	85

Subsystem	Mode	Real instantaneous consumption [mW]			
		On 3,3V	On 5V	On 7,2V	On batt. bus
EPS1	On	0,00	0,00	0,00	22,00
	On+heater	0,00	0,00	0,00	500,00
EPS2	Off	0,00	0,00	0,00	0,00
	Supply	0,00	0,00	0,00	300,00
OBC1	Test	0,00	0,00	0,00	660,00
	On	0,00	14,29	0,00	0,00
OBC2	On	11,00	0,00	0,00	0,00
	On	18,33	0,00	0,00	0,00
Meas. System	RX	73,33	0,00	0,00	0,00
	RX+TX	128,33	0,00	2939,29	0,00
Beacon	On	58,67	0,00	389,65	0,00

Cold Case

Orbit duration [hour]	Sunlight duration [hour]	Eclipse duration [hour]
1,72	1,10	0,62

Subsystem	Mode	Time share (%)	Mean Instantaneous Consumption			Subtotal
			On 3,3V	On 5V	On 7,2V	
EPS1	On	66	0,00	0,00	0,00	14,52
	On+heater	34	0,00	0,00	0,00	170,00
EPS2	Off	0	0,00	0,00	0,00	0,00
	Supply	99	0,00	0,00	0,00	297,00
OBC1	Test	1	0,00	0,00	0,00	6,60
	On	100	0,00	14,29	0,00	0,00
OBC2	On	100	11,00	0,00	0,00	11,00
	Meas. System	On	100	18,33	0,00	0,00
COM	RX	95	69,67	0,00	0,00	0,00
	RX+TX	5	6,42	0,00	146,96	0,00
Beacon	On	100	58,67	0,00	389,65	0,00
						448,31
Cons. Pwr /orbit [mWh]			Cons. Pwr during sun [mWh]		Cons. Pwr during ecl. [mWh]	
2069,33			1326,44		742,89	

Single solar panel input ($\Gamma = 5^\circ \text{C}$)			
Voltage [V]	3,0	3,7	4,2
Power [mW]	1500,0	1900,0	2200,0
	Solar Panels input [mW]		
1,27	1905,0	2413,0	2794,0
	Solar Panels input /orbit [mWh]		
2100,3	2660,4	3080,4	

Mean Case

Orbit duration [hour]	Sunlight duration [hour]	Eclipse duration [hour]
1,72	1,30	0,42

Subsystem	Mode	Time share (%)	Mean instantaneous Consumption			Subtotal
			On 3,3V	On 5V	On 7,2V	
EPS1	On	90	0,00	0,00	0,00	19,80
	On+heater	10	0,00	0,00	0,00	50,00
	Off	0	0,00	0,00	0,00	0,00
	Supply	99	0,00	0,00	0,00	297,00
EPS2	Test	1	0,00	0,00	0,00	6,60
	On	100	0,00	14,29	0,00	0,00
	On	100	11,00	0,00	0,00	11,00
	Supply	100	18,33	0,00	0,00	18,33
OBC1	On	69	50,60	0,00	0,00	0,00
	RX	31	39,78	0,00	911,18	0,00
	RX+TX	100	58,67	0,00	389,65	0,00
	On					448,31
Beacon						

Cons. Pwr./orbit [mWh]	Cons. Pwr. during sun [mWh]	Cons. Pwr. during ecl. [mWh]
3211,06	2433,99	777,08

Single solar panel input ($T = 15^\circ C$)			
Voltage [V]	3,0	3,7	4,2
Power [mW]	1550,0	1950,0	2150,0
	Solar Panels input [mW]		
1,27	1968,5	2476,5	2730,5
	Solar Panels input /orbit [mWh]		
	2566,5	3228,8	3559,9

Hot Case

Orbit duration [hour]	Sunlight duration [hour]	Eclipse duration [hour]
1,72	1,72	0,00

Subsystem	Mode	Time share (%)	Mean Instantaneous Consumption			Subtotal
			On 3,3V	On 5V	On 7,2V	
EPS1	On	100	0,00	0,00	0,00	22,00
	On+heater	0	0,00	0,00	0,00	0,00
EPS2	Off	0	0,00	0,00	0,00	0,00
	Supply	99	0,00	0,00	0,00	297,00
	Test	1	0,00	0,00	0,00	6,60
OBC1	On	100	0,00	14,29	0,00	0,00
OBC2	On	100	11,00	0,00	0,00	11,00
Meas. System	On	100	18,33	0,00	0,00	18,33
COM	RX	67	49,13	0,00	0,00	0,00
	RX+TX	33	42,35	0,00	969,97	1061,45
Beacon	On	100	58,67	0,00	389,65	448,31

Cons. Pwr /orbit [mWh]	Cons. Pwr during sun [mWh]	Cons. Pwr during ecl. [mWh]
3231,85	3231,85	0,00

Single solar panel input ($T = 45^\circ C$)			
Voltage [V]	3,0	3,7	4,2
Power [mW]	1500,0	1900,0	2000,0
	Solar Panels input [mW]		
1,27	1905,0	2413,0	2540,0
	Solar Panels input /orbit [mWh]		
	3276,6	4150,4	4368,8

Appendix C

Pictures of the prototypes

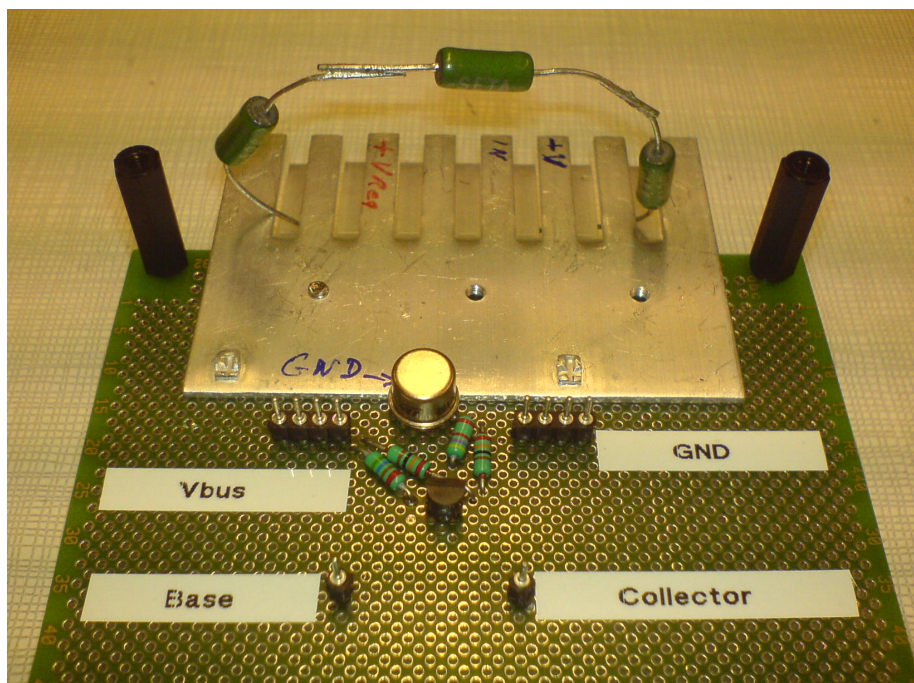


Figure C.1: Prototype of the shunt regulator.

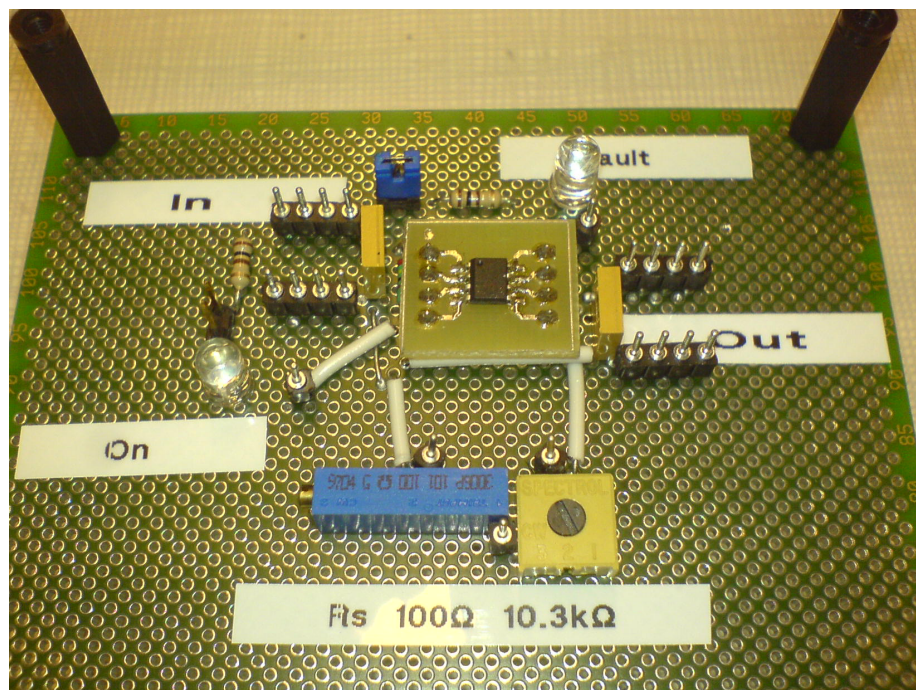


Figure C.2: Prototype of the protection circuit.

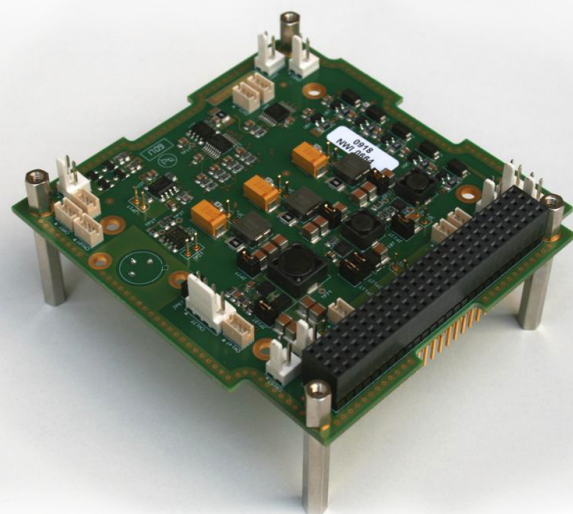


Figure C.3: Engineering model of the EPS card.

Appendix D

Schematics of the engineering model of the EPS

The latest schematics of the engineering model of the EPS were edited by Deltatec. Remark: there is one mistake in the schematics of the dissipation system (shunt regulator). The Emitter and the Collector of the transistor are inverted.



Rue Gilles Magnée 92/6
B-4430 ANS
BELGIUM

TEL : (32) 4 239 78 80
FAX : (32) 4 239 78 89
e-mail : main@deltatec.be

CUSTOMER :

ULG

PROJECT :

PROJECT NUMBER : 521

PROJECT NAME : OUFTI 1

PROJECT PART : EPS1

REFERENCE :

DOCUMENT ID : 20597

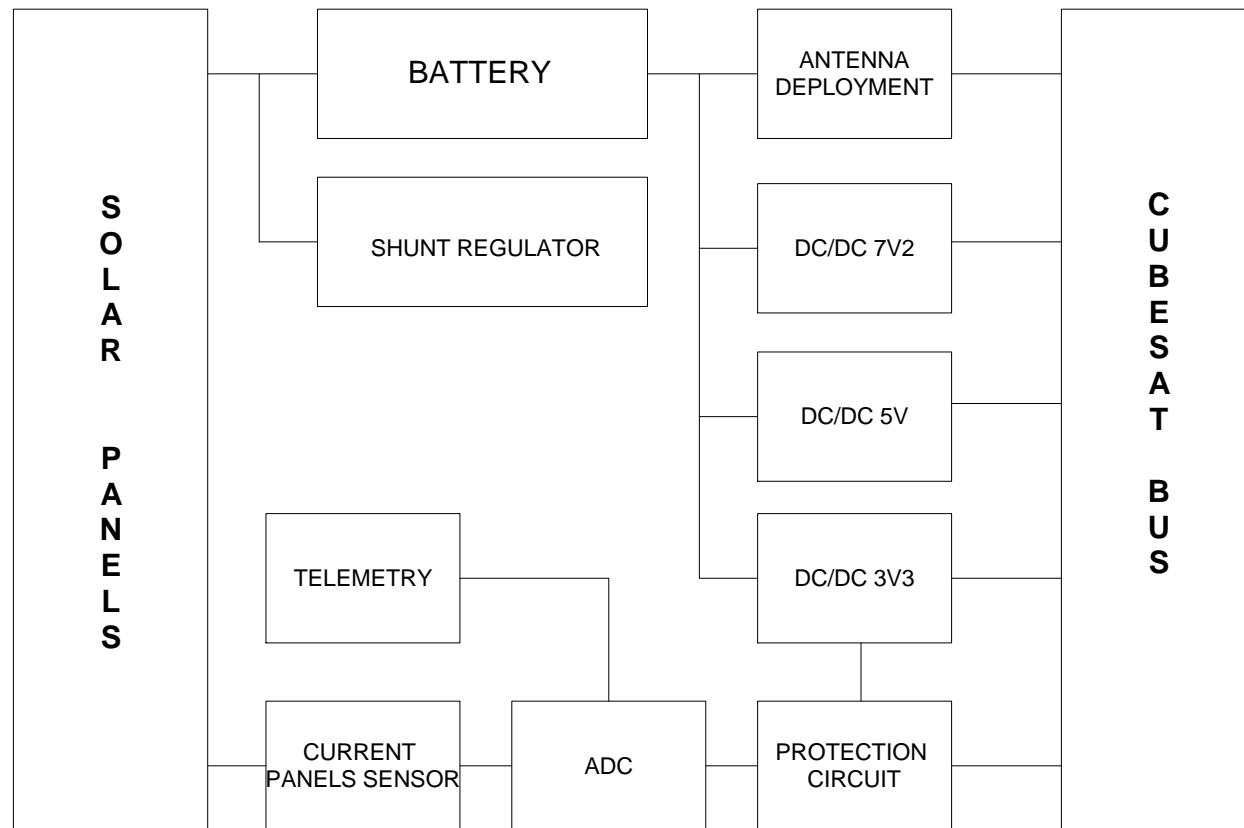
REVISION : 1.0

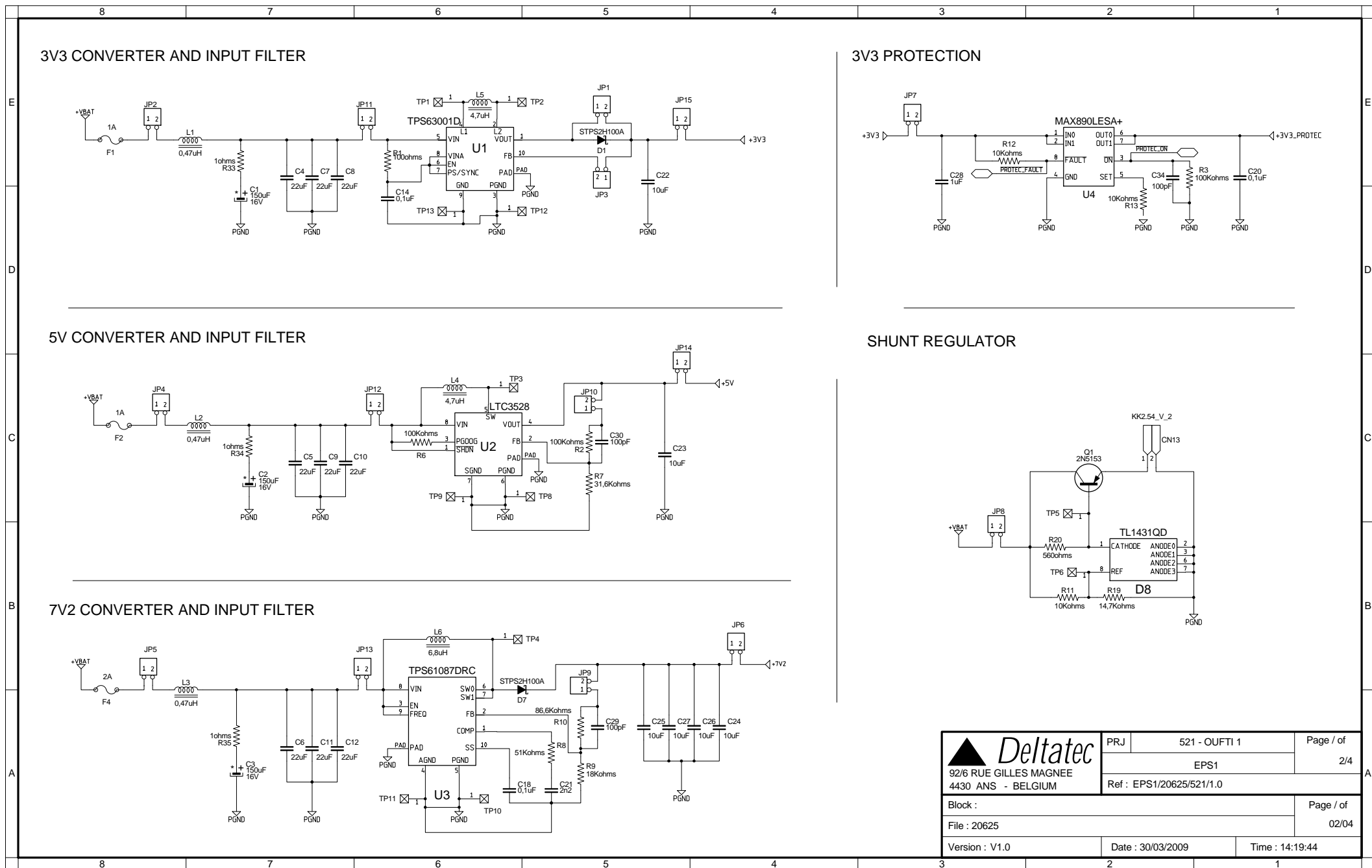
REDRAW : 0

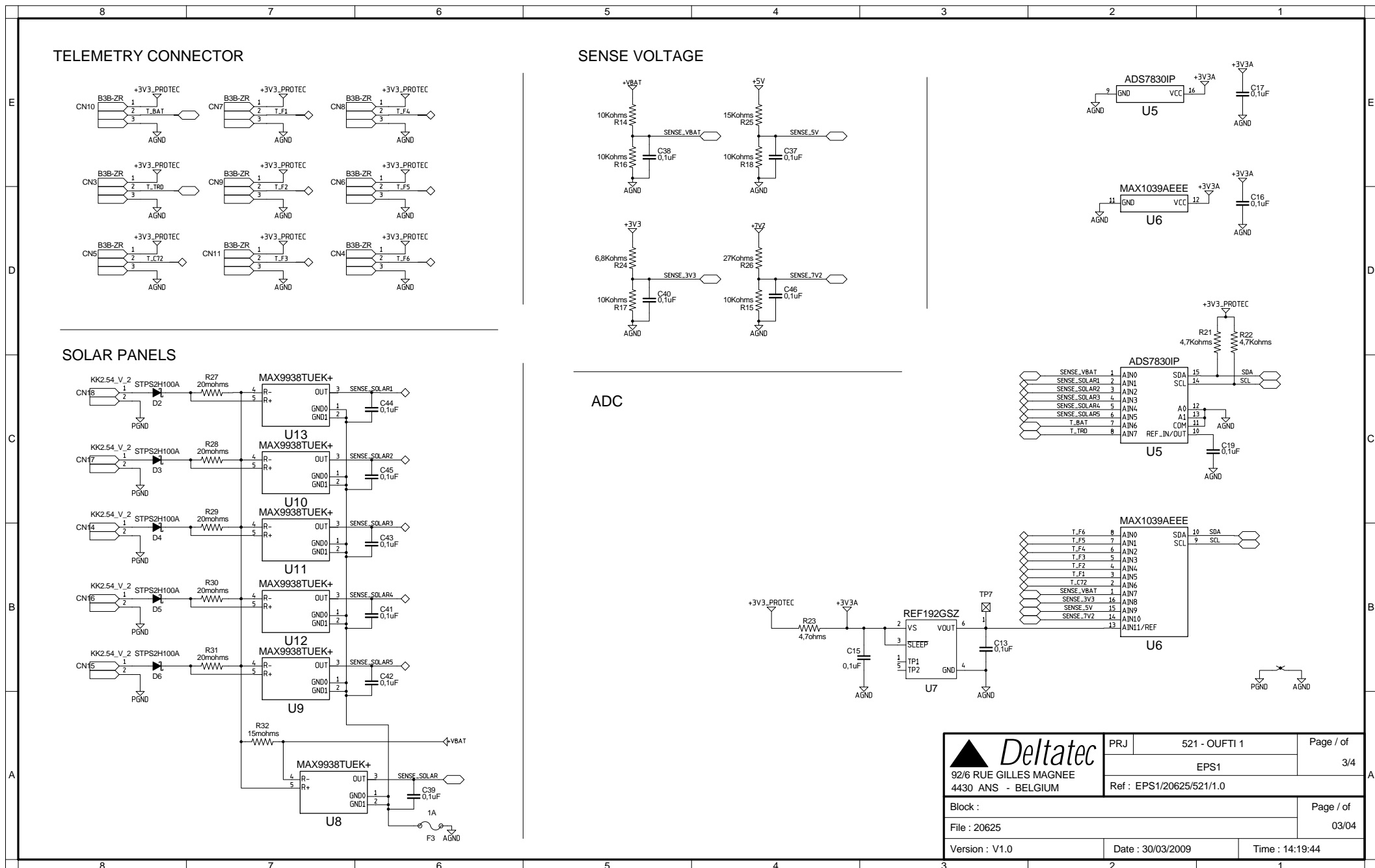
DATE : 30/03/2009

SHEET COUNT : 4

DESIGN TOP LEVEL :

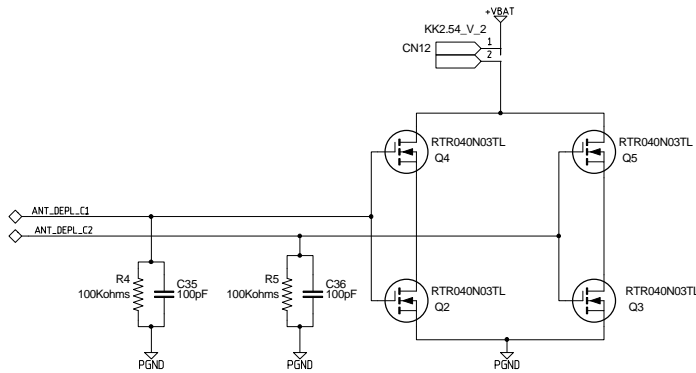




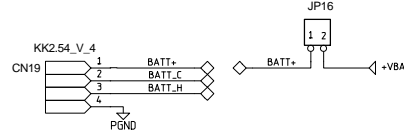


8 7 6 5 4 3 2 1

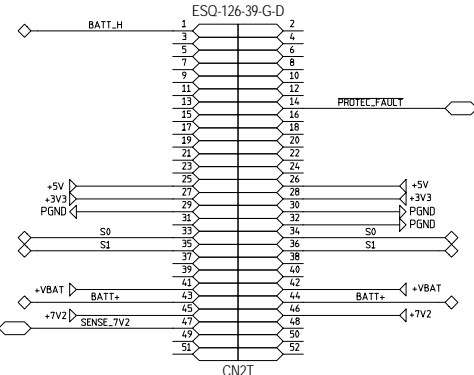
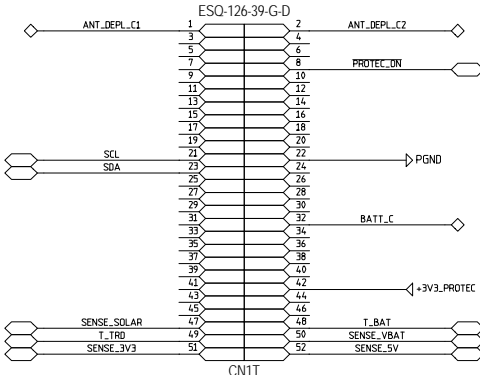
E ANTENNA DEPLOYMENT CIRCUIT



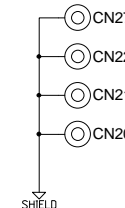
E BATTERY CONNECTOR



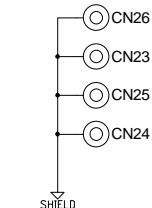
C CUBSAT BUS



C BATTERY FIXATION



B PC104 HOLES



8 7 6 5 4 3 2 1